A Critical Reexamination of Some Assumptions and Implications of Cable Theory in Neurobiology

Thesis by

Gary R. Holt

In Partial Fulfillment of the Requirements

for the Degree of

Doctor of Philosophy

California Institute of Technology

Pasadena, California

1998

(Submitted 12 December, 1997)

© 1998
Gary R. Holt
All Rights Reserved

Acknowledgements

I thank God for helping me through the last $n + 1$ years, and for giving hope through his precious promises.

I also want to thank those whom God has brought into my life:

— Christof Koch, my advisor, for support and advice on research and academic life;

— Rodney Douglas, for warmly inviting me to his lab, and for contributing lots of ideas;

— Bashir Ahmed, Neil Berman, and Kevan Martin for some of the intracellular cortical data presented in various plots in chapter 5 and appendix B;

— The Sloan Foundation and the Office of Naval Research for financial support;

— David Kewley for helpful discussions about the extracellular fields of cortical neurons;

— Yong-Nam Jun for a few references when I began the analysis of ephaptic interaction;

— Mike Holst for donating his Poisson equation solver to me, and for taking time to explain it;

— Various people on the net who devoted huge amounts of time to making free software (perl, gcc, and lots of other utilities) work reliably and explaining it;

— My parents and grandparents, for their prayers and support in a variety of other ways;

— My friends in the Caltech Christian Fellowship for prayers and encouragement.

Abstract

Linear cable theory lies at the core of our understanding of how an individual neuron works. Cable theory usually assumes that neurons do not interact significantly except at specific, anatomically specialized locations (synapses and gap junctions). An analysis of the extracellular electrical fields shows that spikes in one neuron could cause a depolarization of several mV in a dendrite or axon passing by its initial segment. This is somewhat larger than typical chemical synapses; such ephaptic interactions could possibly play a role in controlling action potential failure at branch points.

Applying conclusions of linear cable theory to nonlinear spiking neurons has led to incorrect ideas about neural function. For example, in linear cable theory changing the membrane conductance can be used to scale the amplitude of EPSPs. Shunting inhibition has therefore been repeatedly proposed as a mechanism for division or normalization. This mechanism does not work if the neuron is spiking, i.e., when the output is firing rate rather than EPSP amplitude. When a neuron spikes, its time-averaged voltage does not increase much even if the firing rate goes up; therefore current through a shunt resistance is independent of firing rate, and shunting inhibition acts subtractively rather than divisively.

Cable theory also predicts that EPSPs are low-pass filtered by the membrane resistance and capacitance, and investigators have therefore assumed that the membrane time constant determines how fast a neuron can respond. Agin, because of the spiking mechanism, the membrane potential never reaches steady state, so the time constant is not obviously relevant. The dynamics of firing rates may be better described by currents than voltages.

Applying this principle to the dynamics of simple feedback networks shows that a key factor in the response time of a network is the adaptation current. Without adaptation, the network time constant can be long because it is the gain of the network multiplied by the synaptic time constants. Adaptation can cancel out the long tails of synaptic current, significantly speeding up response times. Recurrent inhibition has a similar effect.

Another key factor determining input current is synaptic depression and facilitation. Recurrent networks are especially sensitive to synaptic depression because of the feedback; within a very short period of time the network behaves like a feedforward network because the recurrent synapses have been depressed away. However, facilitation and depression can act together to provide a log-exponential transform, allowing subtractive inhibition at one stage to have a divisive effect at another.

Contents

List of Figures

List of Tables

Part I

Foundations of Cable Theory

The wide world is all about you: you can fence yourselves in, but you cannot for ever fence it out.

— J. R. R. Tolkien

Chapter 1 Introduction

1.1 What is a neuron supposed to do?

After a century of work, our knowledge of the phenomenology of neural function is staggering. Hundreds of different brain areas have been mapped out in various species. Neurons in these regions have been classified, subclassified, and reclassified based on anatomical details, connectivity, response properties, and the channels, neuropeptides, and other markers they express. Hundreds of channels have been quantitatively characterized, and the regulation and gating mechanisms are beginning to be understood. Every issue of neuroscience journals reports identification of several new proteins related to vital functions such as synaptic transmission, neurotransmitter synthesis, or various metabolic functions of neurons.

Despite this wealth of descriptive data, we still do not have a grasp on how exactly these thousands of proteins are supposed to accomplish computation. For example, how is it that cells in primary visual cortex respond only to stimuli of a certain orientation? Primary visual cortex is probably the most intensively studied piece of the brain, and orientation-selective responses are the most obvious characteristic of the cells. Yet despite thirty years of intensive study, and even a Nobel prize in the field, the mechanism of orientation selectivity is still hotly debated. We cannot answer with certainty even the most basic questions: How important is inhibition in determining orientation selectivity? Is recurrence important? Are dendritic nonlinearities important? In short, what is it about the neurons or the network that actually gives it orientation selectivity?

At least part of the reason for such confusion is an inadequate understanding of the basic biophysics. Contradictory simplified models of neurons have been used to understand the same functions. As an extreme example, neurons are sometimes regarded as high-pass filters (coincidence detectors; McCulloch and Pitts, 1943; Abeles, 1982; Softky, 1995), sometimes as low-pass filters (Hopfield, 1984; Carandini *et al.*, 1996b), and sometimes as more complicated kinds of filters. Of course the results are different. In some cases, as I will show in chapters 4 and 5, untested assumptions and simplifications have led to incorrect theories of the operation of cortical neurons. Difficult experiments to test these theories have been performed, experiments which never needed to be done if the fundamentals had been more carefully thought through.

To address this problem, this thesis reanalyzes a few of the premises and conclusions from biophysical analyses of neurons. First, I examine in detail the assumptions behind cable theory

and compartmental modeling, especially the assumption that neurons communicate only through anatomical specializations like gap junctions or synapses. Models usually assume that if synaptic inputs are completely specified, then the output of the neuron is also determined. The goal of biophysical modeling has been to calculate and to understand how this output depends on the synaptic input. The primary mathematical framework, one-dimensional cable theory, assumes that ion concentrations and extracellular potentials do not change appreciably because of the activity of neighboring cells.

Is the extracellular environment sufficiently constant that we can make this approximation? Only a small fraction (usually about 20%) of the space in the brain is actually extracellular (Nicholson, 1995; Syková, 1997). At the narrowest, there is only about 20 nm between one cell membrane and the membrane of its neighbor (Van Harreveld, 1966, 1972). Because of the small size of the extracellular space, there has been speculation over the years that some of the assumptions of cable theory might break down. In fact, I show in chapter 2 that they may break down near cell bodies of cortical neurons. A single spike from a cortical neuron is accompanied by an extracellular potential of 3 mV or more near the cell body. This field potential can have a substantial effect on nearby neural elements, in some cases much stronger than the effect of a typical synapse. It is possible that such effects could play at least a small role in some kinds of computation.

The second part of this thesis also analyzes the effect of a spike from a neuron, but this time on the neuron itself. Surprisingly, although action potentials are the most obvious behavior of neurons, they have been overlooked in many simplified neural models. There have been a number of studies which assume that the output of the neuron is the membrane voltage, rather than the firing rate. Over the last thirty years, many people have calculated what factors influence the membrane voltage—the shape of the dendritic tree, the various active conductances in the dendrites, the conductance of the cell—while ignoring the largest effect on the membrane voltage, the action potential and subsequent repolarization. Not only crude non-spiking models of neurons, such as variants on the Hopfield point neuron model, are affected by this oversight. Even sophisticated compartmental models and analytic work often assumes that the output of the neuron is directly proportional to what the voltage at the soma would be if there were no spiking mechanism.

In a non-spiking neuron, shunting inhibition (inhibition with a reversal potential near the "resting potential" of the neuron) has a divisive effect on the membrane potential of the neuron, so it has been postulated as a mechanism for division or normalization. In a spiking neuron, however, I found that it has a subtractive effect (chapter 4). In a non-spiking neuron, the rate of membrane potential change is governed by the time constant of the cell; the time constant is a measure of how quickly the cell approaches steady state, and so it has been used as a measure of the rate at which a neuron can respond. But a spiking cell has no steady state, and in fact the membrane time constant is

not a useful measure of response time; instead, other factors such as synaptic time constants and adaptation conductances determine the dynamics of firing (chapter 5).

The third part of this thesis builds on the observation that synaptic time constants and adaptation control the firing rate of an individual cell, and extends this to recurrent networks. Cortical feedback is thought by some to be essential in the response of cortical cells (Douglas and Martin, 1991). However, recurrence greatly amplifies the effects of any delays in feedback, and recurrent systems can have unreasonably slow response times. In chapter 6, I analyze how spike frequency adaptation can substantially speed up the response of a recurrent system so that it is little slower than a feedforward system. Recurrence also greatly amplifies the effect of nonlinearities in the feedback. Synaptic depression and facilitation can therefore have a profound impact on the operation of these circuits (chapter 7).

What is a neuron supposed to do? We are still a long way from answering this question. This thesis rules out some incorrect answers, and begins to examine other factors such as synaptic depression and ephaptic transmission which may possibly play a larger role than we expected.

1.2 Assumptions and derivation of the cable equation

Most models of neurons are based on the idea that the neural membrane is a leaky capacitor. For "neurons" which do not have any spatial extent, this takes the form of a simple RC circuit (e.g., Hopfield, 1984; Carandini *et al.*, 1996b; see section 1.3 and figure 1.4), possibly with a spiking mechanism (the integrate-and-fire neuron; Lapicque, 1907). Point neurons are simple because there is only one voltage to account for, and therefore are widely used in modeling. For some properties of neurons, however, variations of voltage with location can be important. In this case, neurons must be described by the cable equation, a partial differential equation that takes into account the capacitance and leakiness of the neural membrane and the finite resistance of the intracellular space.

Since several parts of this thesis deal with violations of various assumptions of cable theory, it is helpful to set them down explicitly in some detail. Cable theory in neurobiology has a long history, having first been applied to neurons in 1863 by Matteucci and a decade later by Hermann, and subsequently elaborated by many investigators (see Rall, 1977 for a historical overview). In its most general form, the "core conductor" model, a long thin electrically conducting core is surrounded by a membrane. The core cross section is sufficiently small that it can be treated as one-dimensional. Usually, the membrane is surrounded by extracellular space which is assumed to be isopotential (grounded). However, an effectively one-dimensional extracellular space surrounding the cable is sometimes considered by making a minor modification to the equation, and this is the form we will derive here. The assumptions in the derivation are:

1. **Magnetic fields are negligible.** The magnetic field makes a difference of about one part in 10^9 (Rosenfalck, 1969) because the currents involved are not large.

2. **Ion concentrations and fluxes may be treated as continuous variables, ignoring stochastic effects.** This is generally a good assumption. For example, although extracellular clefts can be extremely narrow (e.g., 20 nm at the narrowest), there are still 36,000 potassium ions per square micron in such a cleft. All other relevant ions have higher concentrations (except intracellular calcium), so effects due to a finite number of ions are not likely to be important.

   A more important source of stochastic variations in ion flux is random channel openings. There may be only 3–4 channels per square micron of membrane (e.g., see Colbert and Johnston, 1996). Random variations in channel openings might even cause spontaneous action potentials in very small structures such as dendritic spines (Strassberg and DeFelice, 1993; Chow and White, 1996). This may explain why very small axons are not myelinated (Franciolini, 1987).

   However, most structures of interest are not so small. When we assume that ion concentrations and fluxes are continuous variables, then ionic flow in the extracellular fluid and through membranes is well modeled by the Nernst–Planck equation for electrodiffusion (see Hille, 1977):

$$\mathbf{J}_i = -D_i n_i \left(\frac{F z_i}{RT} \nabla \phi + \frac{\nabla n_i}{n_i} \right), \tag{1.1}$$

   where $\mathbf{J}_i$ is the flux of ions of species i, D_i is the diffusion coefficient, n_i is the concentration, ϕ is the potential, z_i is the valence, and $RT/F = kT/e \approx 27$ mV measures how electrical potential trades off against thermal energy.

   This equation must be coupled with several others that describe how J_i influences ϕ and n_i. First, the total amount of any species remains constant, so

$$\frac{\partial n_i}{\partial t} = -\nabla \cdot \mathbf{J}_i. \tag{1.2}$$

   Second, the flow of ions alters ϕ by changing the local charge density ρ:

$$\frac{\partial \rho}{\partial t} = -F \sum_i z_i \frac{\partial n_i}{\partial t}. \tag{1.3}$$

   The charge density affects the potential through Gauss's law,

$$\epsilon \nabla^2 \phi = -\rho \tag{1.4}$$

where ϵ is the permittivity.

3. **The extracellular and intracellular space can be treated as if it were homogeneous, rather than modeling all membranes explicitly.** Intracellular space in most neurons has numerous membranes, including various vesicles and the endoplasmic reticulum. Extracellular space is densely packed with dendrites, axons, and glia. It would be difficult to make any general statements unless it is possible to ignore the complex geometry of the space. Fortunately, the distance scale of electrical potential variations is usually much larger than such inhomogeneities. It is therefore a good approximation to replace the potential by its average over some small volume, and adjust the dielectric constant appropriately. See appendix A for an explicit test of this idea for an array of parallel axons.

   As a result, only the plasma membrane of the cell being studied needs to be explicitly modeled, and the extracellular and intracellular space can be replaced by homogeneous resistive fluids.

4. **Extracellular and intracellular ion concentrations do not change appreciably.** This assumption is examined critically for extracellular potassium in chapter 3. This assumption has been examined for the intracellular space by Qian and Sejnowski (1989, 1990) and found to hold everywhere except in very small structures like dendritic spines.

   If ion concentrations are roughly constant, the Nernst potentials for the various ions are well-defined, and flow through ion channels can be expressed as $I_i = g_i(E_i - V_m)$, where g is possibly voltage-dependent.

   Also, the diffusion term in equation 1.1 can be neglected. Combining the flux of all ions into a total flux of charge $\mathbf{J} = F\sigma z_i \mathbf{J}_i$, equations 1.1–1.3 become

$$\mathbf{J} = -\sigma \nabla \phi \tag{1.5}$$

$$\frac{\partial \rho}{\partial t} = -\nabla \cdot \mathbf{J} \tag{1.6}$$

   where

$$\sigma = \frac{F^2}{RT} \sum_i z_i D_i n_i \tag{1.7}$$

   is the conductivity.

5. **The intra- and extra-cellular fluids are electrically neutral.** Equation 1.4 can be

combined with equations 1.5–1.6 to obtain

$$\frac{\partial \rho}{\partial t} = -\frac{\sigma}{\epsilon}\rho \tag{1.8}$$

which indicates that the system relaxes to electroneutrality with a time constant of ϵ/σ_e. σ for extracellular space is about 0.3 μS/μm (300 Ω-cm; see, e.g., Ranck, 1963 for empirical measurements; this can also be calculated directly from equation 1.7 using diffusion coefficients adjusted for tortuosity, as in section 3.4 on page 53). Taking into account the dielectric constant of water, and the effect of all the membranes in the extracellular space, the permittivity of tissue is about 10^5 times the permittivity of empty space in the relevant frequency range (Rosenfalck, 1969), so the time constant will be about 3 μs.

To a good approximation, then, the charge density ρ is always 0 on the time scales we are interested in.[1] This is an important simplification; it means that the capacitive effects of inactive membranes can be ignored because very little current crosses them. Both the extracellular and intracellular space are almost purely resistive, and therefore the potential is an instantaneous function of the transmembrane current. In other words, the only time dependence is in the membrane of the cells producing the extracellular potential (in the activation and inactivation of conductances and in the capacitance); other membranes play a negligible role.

When we set $\rho = 0$ and $\partial\rho/\partial t = 0$, equations 1.5 and 1.6 turn into Laplace's equation,

$$\nabla \cdot (\sigma \nabla \phi) = 0 \tag{1.9}$$

with the boundary conditions

$$\sigma \nabla \phi \cdot \mathbf{n} = J_m, \tag{1.10}$$

where $\mathbf{n}$ is the normal to the membrane and J_m is the transmembrane current per area (Rall, 1969).

6. **The intracellular space can be treated as one-dimensional.** In other words, the radial voltage drop is negligible compared to the longitudinal voltage drop on the relevant distance scale; essentially all the current flow is axial. A mathematical analysis is too lengthy to present here, but this assumption has been studied in detail (Clark and Plonsey, 1966; Rall, 1969) and found to be true in almost any practical case.

[1] The same conclusion can also be reached from the phase of complex impedance measurements at relevant frequencies (e.g., Plonsey, 1969).

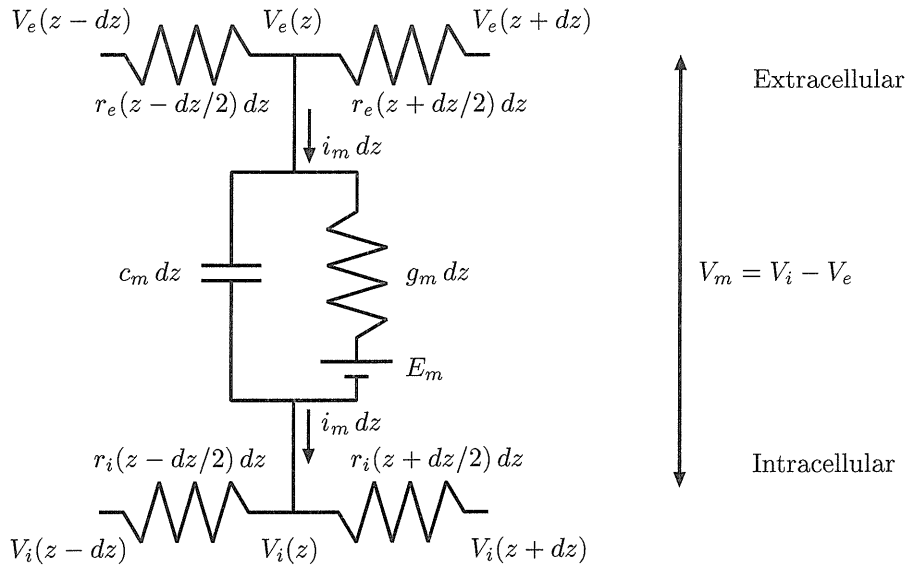

Figure 1.1: Schematic for the core-conductor model including a one dimensional extracellular space.

This reduces equation 1.9 to a one dimensional PDE. However, it is often more intuitive to think in terms of equivalent circuits; a one dimensional intracellular space is properly described by the bottom half of the circuit in figure 1.1. Summing the currents into the bottom node gives

$$\frac{V_i(z-dz)-V_i(z)}{r_i\,dz} + i_m\,dz + \frac{V_i(z+dz)-V_i(z)}{r_i\,dz} = 0, \tag{1.11}$$

where V_i is the intracellular potential, i_m is the current through the membrane into the cell per unit length, $r_i = \pi a^2/\sigma_i$ is the resistance per unit length of cytoplasm, a is the radius of the axon, and σ_i is the intracellular resistivity. After simplifying,

$$\frac{\partial^2 V_i}{\partial z^2} = -r_i i_m. \tag{1.12}$$

7. **No other neurons inject current into the extracellular space.** This assumption will be analyzed in detail in chapter 2. This implies that neurons' electrical activity are entirely independent of each other: there is no cross talk. The extracellular potential is either 0 or due solely to the neuron being considered.

8. **The extracellular space can be treated as either one-dimensional or isopotential (grounded).** The validity of a one-dimensional extracellular space model will be analyzed in detail in section 2.2.2. It is equivalent to assuming that most of the extracellular current is

flowing radially rather than axially. Physically, this means that the cable is surrounded by a non-conducting sheath with a radius not too much larger than the cable itself. This is the case, for example, if an axon is removed from the animal and placed into oil with only a thin layer of water around it, as was commonly done in the early days of neurophysiology. It also may be a good approximation for axons in peripheral nerve because of the connective tissue surrounding the fibers.

Summing the currents into the top node of figure 1.1,

$$\frac{\partial^2 V_e}{\partial z^2} = r_e i_m \tag{1.13}$$

where $r_e = (\pi b^2 - \pi a^2)/\sigma_e$ is the resistance per unit length of the extracellular space, b is the radius of the sheath surrounding the neuron, and σ_e is the extracellular resistivity.

The large volumes in the central nervous system cannot be modeled as one-dimensional, because the extracellular current flow is not mostly axial (see section 2.2.1). In this case, Laplace's equation (equation 1.9 must be solved. However, field potentials are usually small in comparison with the transmembrane potentials (on the order of tens of microvolts). For this reason, the extracellular potential is usually set to 0 (i.e., $r_e = 0$).

9. **The membrane can be modeled by a capacitor in parallel with a conductance** as shown in figure 1.1. If there is more than one conductance in the membrane, then $g_m = \sum g_i$ and $E_m = (\sum g_i E_i)/\sum g_i$, where E_i is the Nernst potential for each species of ion.

   As long as the g_i have a suitable voltage dependence, this will always be the case; however, analytic results from cable theory are only useful if g_i does not depend strongly on voltage or time. This is often approximately true in neurons when the membrane potential is not close to threshold. When neurons are firing then g_i cannot be considered approximately constant, and the predictions of linear cable theory break down. While it may seem obvious, neglect of this fact has led to some important misconceptions (chapters 4 and 5).

   From figure 1.1,

$$i_m = g_m(V_m - E_m) + c_m \frac{\partial V_m}{\partial t}. \tag{1.14}$$

The neuron may be accurately modeled by cable theory if and only if these assumptions hold. Adding equations 1.12 and 1.13 gives

$$(r_e + r_i) i_m = \frac{\partial^2 V_i}{\partial z^2} - \frac{\partial^2 V_e}{\partial z^2} = \frac{\partial^2 V_m}{\partial z^2}. \tag{1.15}$$

Substituting this into equation 1.14 gives the full cable equation:

$$\frac{1}{r_e + r_i}\frac{\partial^2 V_m}{\partial z^2} = g_m(V_m - E_m) + c_m\frac{\partial V_m}{\partial t} \tag{1.16}$$

or

$$\lambda^2\frac{\partial^2 V_m}{\partial z^2} = V_m - E_m + \tau\frac{\partial V_m}{\partial t} \tag{1.17}$$

where $\lambda^2 = 1/g_m(r_e + r_i)$ and $\tau = c_m/g_m$.

The effect of the extracellular space, with these assumptions, is merely to increase the effective intracellular resistance, i.e., to change r_i into $r_i + r_e$. This is because the axial intracellular currents are equal and opposite to the axial extracellular currents.

Near a cell body, extracellular fields may be several mV. When considering axons and dendrites passing near the cell body of another cell, assumptions 7 and 8 are violated, and the extracellular fields must be explicitly taken into account. I show that axons and dendrites passing near the cell body feel a depolarization approximately equal to the amplitude of the extracellular potential (chapter 2).

1.3 Implications of cable theory

Some early researchers such as Lorente de Nó (1947b) argued on the basis of extracellular records that active propagation of impulses in dendrites was important for function. Intracellular work in motoneurons, however, showed that if dendrites are active, their threshold for impulse generation is certainly much higher than the axon and soma (Fuortes *et al.*, 1957; Coombs *et al.*, 1957a, 1957b), and many properties of the dendrites could be well accounted for by passive cable theory (Rall, 1977). The classic conception of a neuron, as developed by Eccles, Rall, and others, is that dendrites sum up and smooth synaptic inputs, and deliver the results as an EPSP to the soma. The soma, it is assumed, converts the EPSP into a firing rate. A great deal of experimental and theoretical work has gone into measuring how various manipulations affect the amplitude of the somatic EPSP.

How does the soma convert EPSPs into firing rates? This is a much more subtle question than it appears at first sight. Before the origins of the action potential were well understood, it was not appreciated how significantly the action potential itself affects the membrane potential. For example, when studying the stretch receptor in a muscle, Katz (1950) noted that in response to a steady stimulus there was "a local preliminary depolarization which re-develops after each discharge and which varies with the strength of the stimulus." Today, after years of compartmental

This figure has been censored for copyright reasons.

Figure 1.2: The slow potential theory. Taken from Stevens (1966), figure 4-1. Used completely without permission.

models and theoretical analysis of the cable equation, it seems that the best way to understand this depolarization is as an effect of a transmembrane current (see below). But since the current could not be measured directly at the time, the earlier physiologists tended to regard the observable voltage change as the fundamental quantity, which they sometimes called a *generator potential* (Granit, 1947, 1955; Granit *et al.*, 1963). In this example, Katz (1950) disabled spiking pharmacologically in muscle stretch receptors and measured the amplitude of the generator potential. He found that it was proportional to the firing rate for the same stimulus without local anesthesia, and concluded that "the local spindle potential appears to be an essential link between the input and output of the sense organ...."

The same idea is carried somewhat further by the classic textbook of Stevens (1966). The *slow potential theory* (figure 1.2) is the idea that "an above-threshold depolarization whose magnitude changes relatively slowly" is faithfully encoded in the firing frequency of the cell. Temporal summation in the dendrites of a postsynaptic cell will yield a depolarization proportional to the frequency. As a result, "nerve impulse frequency appears to be translated back into a depolarization similar to the one which originally generated the axonal nerve impulses."

Regarding the depolarization as the cause of the spikes, as Katz and other early investigators did, is certainly correct as far as it goes, since clearly if there is no depolarization there will be no spikes. However, treating the generator potential as if it is a real potential can be misleading. When spikes are disabled, the generator potential is a long slow depolarization, as shown schematically

in figure 1.3A. When spikes are not disabled, the observed potential is *not* a set of spikes riding on top of the unaltered generator potential (shown in dotted lines), as would be expected from a model which first computes the generator potential and then computes a firing rate. Instead, at the spike initiation zone the depolarization is chopped off by each spike and begins anew after the spike repolarizes (figure 1.3B). That was why the physiologists had to disable spikes to see the generator potential. There is no place in the neuron where the membrane potential is equal to the generator potential[2].

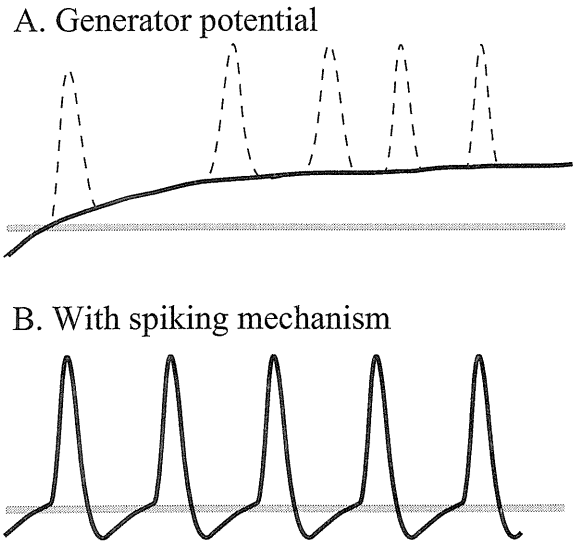

Figure 1.3: A schematic of the membrane voltage with spikes disabled (the generator potential; **A**) and with spikes enabled (**B**). When spikes are enabled, the membrane potential is not the generator potential with spikes riding on top of it (dotted lines in A); the potential is truncated at threshold (grey lines) and begins anew after each spike.

It may seem uncharitable to quibble with the best physiologists in the world about one of their ideas that after a half century of intensive research looks a trifle naive. The reason for examining it in some depth is that although we do not often use the term "generator potential" any more, many modern modeling and experimental efforts are based on exactly the same idea. This idea leads to some important misconceptions about neural function.

Consider, for example, the recent model of Carandini and Heeger (1994) and Carandini *et al.* (1996b, 1997) in figure 1.4. This model has been quite popular for explaining some features of normalization in cortex, and in fact has set experimentalists looking to confirm its biophysical prediction of a large conductance change. It explicitly computes an above-threshold membrane potential V_m (effectively the generator potential, though these authors did not call it so) using a conductance-based model of a neuron. It then converts this membrane potential into a firing rate but the spiking mechanism itself has no influence on the membrane potential.

[2]The case where the spike mechanism is electrotonically distant from the site of input will be dealt with later, in the chapters devoted to shunting inhibition (chapter 4) and time constants (chapter 5). The spiking mechanism can still influence the average voltage at electrotonically distant sites and still should not be neglected.

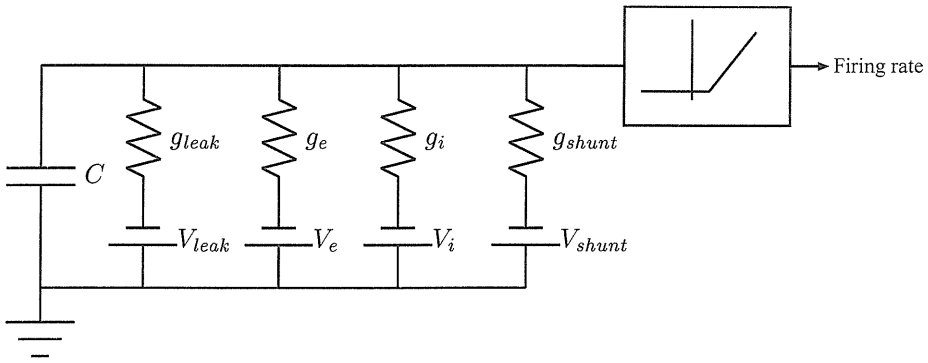

Figure 1.4: The model of Carandini and Heeger (1994) and Carandini *et al.* (1996b, 1997). The key feature of this model is that an above-threshold voltage is computed using the usual RC model of a neuron. This above-threshold voltage is turned into a firing rate, but the firing mechanism itself has no effect on the voltage.

This model is singled out only because it has been quite popular lately. Many other point-neuron models are based on the same idea (e.g., Sejnowski, 1977; Hopfield, 1984; Nelson, 1994) and the results from this thesis apply equally to them. The same is also true of some compartmental models which examine closely the magnitude of the somatic EPSP, and treated the time course and amplitude of this EPSP as indicative of how the cell's firing rate will be affected, without actually modeling the firing mechanism (e.g., Koch *et al.*, 1983; parts of Bernander *et al.*, 1991; Rapp *et al.*, 1992). But since there is no place in the spiking neuron where the membrane voltage is equal to the generator potential, different physics apply to the membrane voltage when the neuron is firing and when it is not. Models which use passive cable properties to compute a generator potential, and then convert the above-threshold potential into a firing rate, are not properly based on the underlying biophysics. One consequence of this mistake is that shunting inhibition was thought to have a divisive effect on firing rates (chapter 4). A second consequence is that the membrane time constant was thought to be critical in determining the temporal dynamics of firing rate (chapter 5).

When the generator potential is a long slow depolarization as shown in figure 1.3, it is often better to think of the current injected into the neuron as fundamental rather than the voltage. The generator potential amplitude is proportional to the injected current, so the same information is present in both numbers. But the current is a real physical current, and to a first approximation its time-average value is unaffected by the existence of spikes (chapter 4). For this reason, it is a better predictor of the firing rate than an above-threshold membrane potential.

When the generator potential is not above threshold most of the time, but instead spends most of the time below threshold and has only short excursions above, then it may more appropriate to think in terms of voltage rather than current to predict the spiking pattern. Since the voltage is only

occasionally above threshold, spiking will not have as drastic an influence. This is a fundamentally different mode of operation: the spiking output is not determined by the sum of large numbers of small, independent inputs, but by the timing of fluctuations (Shadlen and Newsome, 1994; Softky, 1995). If the fluctuations arise from simultaneous synaptic inputs, then the neuron can be thought of as a coincidence detector (Abeles, 1982).

Which mode do neurons actually operate in? The classical conception of a neuron is based primarily on motoneurons, and it seems clear that their primary function is to sum up inputs and reporting the result as an analog value. It is still a matter of debate to what extent other neurons operate in different modes. In some cases, neurons obviously act as coincidence detectors, such as in the sound localization pathway, and they have clear anatomical specializations to enable them to do so. In neocortex, it is not yet clear what the best way to think of a neuron is. Most experimentalists and modelers assume the summing mode. This is true of the normalization models such as the model of Carandini and Heeger (1994) discussed above. It is also true of the so-called "canonical microcircuit" or cortical amplifier models that inspired the network analysis in chapters 6 and 7 (Douglas and Martin, 1991; Maex and Orban, 1992, 1996; Douglas *et al.*, 1995; Somers *et al.*, 1995; Ben-Yishai *et al.*, 1995; Suarez *et al.*, 1995; Holt *et al.*, 1996); in fact, attempts to explain the behavior of these models led to the considerations discussed in this section. For this reason, most of this thesis pertains to the summing mode.

1.4 Small circuits of neurons

The classic Hubel–Wiesel model postulates that orientation selectivity in simple cells in cat visual cortex arises primarily from convergent input of thalamic cells chosen so that the response is orientation selective. In the thirty years since their pioneering work, the mechanism has been hotly debated, especially the importance of inhibition in sharpening the response. It appears that the thalamic input onto cortical simple cells is orientation tuned but only weakly so (Pei *et al.*, 1994; Vidyasagar *et al.*, 1996; but see Reid and Alonso, 1995), although it is clear that the total synaptic input onto cortical cells is sharply orientation tuned (Ferster, 1986, 1987). Experiments with iontophoresed bicuculline appear to indicate that inhibition is important in generating direction and orientation selectivity (Sillito, 1975, 1977); however, blocking inhibition intracellularly in a single cell has only a small effect on the sharpness of orientation tuning (Nelson *et al.*, 1994). IPSPs are strongest for stimuli of the preferred orientation rather than for other orientations, and in fact seem to have the same orientation tuning as EPSPs (Ferster, 1986). Searches for hidden IPSPs (shunting inhibition) have uncovered no significant conductance changes (Douglas *et al.*, 1991; Dehay *et al.*, 1991; Berman *et al.*, 1991, 1992; Douglas and Martin, 1991; Ferster and Jagadeesh, 1992; but see

Borg-Graham *et al.*, 1996).

Models from our lab and other labs (Douglas and Martin, 1991; Maex and Orban, 1992, 1996; Douglas *et al.*, 1995; Somers *et al.*, 1995; Ben-Yishai *et al.*, 1995; Suarez *et al.*, 1995; Holt *et al.*, 1996) have been developed to explain these puzzling observations. Previously, all models had assumed that only feed-forward connections were important in generating the response. Yet over 95% of the excitatory synapses onto a layer IV cortical cell come from other cortical cells (Peters and Payne, 1993; Peters *et al.*, 1994). It is clear from a number of anatomical studies that cortical cells usually make excitatory connections only to other cortical cells in the same orientation column, or with cells in other columns that have similar receptive fields (Kisvárday *et al.*, 1997).Thus most of the excitatory input a cell receives comes from other cells with almost the same receptive field. This observation suggests that the cortical circuitry could be described as an amplifier. A small amount of thalamic current causes cortical cells to spike. Activation of recurrent synapses causes the cells to spike more, and so on; the resulting firing rate is much larger than if there were only feedforward input. Inhibition may be necessary for sharpening the orientation tuning, but only a small amount of inhibition is necessary to counter the small amount of geniculate input which triggers the amplification cascade; it is not surprising that it might not have been seen in intracellular recordings. The inhibition needs to be only slightly more broadly tuned than excitation, as found recently in anatomical work (Dalva *et al.*, 1997; Kisvárday *et al.*, 1997), to have a significant sharpening effect (Douglas *et al.*, 1995; Somers *et al.*, 1995); it is not surprising that experiments find that inhibition has approximately the same tuning as excitation. Blocking inhibition in a single cell has only a small effect, because most of the excitatory input into that cell is already orientation-tuned since it comes from other cortical cells.

How long does the recurrent circuitry take to act? A thalamic input triggers a few spikes which cause more recurrent input, leading to more spikes, leading to more recurrent input; but the whole process takes a certain amount of time. In positive feedback loops in electrical engineering, the time constant of an amplifier system is usually approximately the gain of the amplifier times the time constant involved in the feedback. Our models have assumed a gain of around 5, and the feedback will have a time constant of on the order of 80 ms if NMDA receptors are involved. As a result, the network time constant ought to be around 400 ms. This is rediculously long. Celebrini *et al.* (1993) argued that since orientation tuning seems fully developed in the first spikes, a recurrent mechanism is ruled out. However, recurrent models of orientation tuning show the same property (Somers *et al.*, 1995), and in general cortical amplifier models do not have such a long time constant. However, no detailed analysis of the factors that influence the dynamics of the response has been performed. In chapter 6, I use the considerations and formalism developed in chapter 5 to provide a simple explanation for why network models do not show such long time constants.

A second issue with recurrent models is the sensitivity to nonlinearities in the feedback. One kind of nonlinearity which is known to be present in some synapses is depression: if the presynaptic cell fires a train of action potentials, later EPSPs in the postsynaptic cell are smaller than the first EPSP. Although this phenomenon is well known in other systems (see Zucker, 1989 for a review), the extent of synaptic depression in neocortex was not appreciated until recently (Thomson and West, 1993; Thomson *et al.*, 1993b; Thomson and Deuchars, 1994; Stratford *et al.*, 1996; Markram and Tsodyks, 1996; Tsodyks and Markram, 1997; Abbott *et al.*, 1997). Synaptic depression turns out to have a profound effect on properties of such circuits, so much so that there is practically no steady state amplification, unless it is countered by facilitation at other synapses (chapter 7).

Chapter 2 Ephaptic interactions

2.1 Introduction

Studies on squid giant axons (Arvanitaki, 1942), crab motoneurons (Katz and Schmitt, 1940, 1942), and even algal strands (Tabata, 1990) showed that when two axons were placed in a medium with reduced extracellular conductivity, activity in one axon could depolarize the other. Such interactions are called *ephaptic* (Greek "touching onto", rather than *synaptic*, "touching together"; Arvanitaki, 1942). The early studies were done before the chemical nature of synaptic transmission in the CNS was understood, and were thought to be evidence that transmission was purely electrical (see Eccles, 1964; Faber and Korn, 1989). In extreme cases an action potential can be induced in an inactive axon by a nearby one. In fact, ephaptic transmission may underly pathological activity in motor neurons some kinds of facial spasms, or in crushed nerves or in nerves damaged by multiple sclerosis (see Faber and Korn, 1989; Jefferys, 1995).

What determines the magnitude of the potential around a neuron? Suppose, for example, we have an isotropic spherical cell with no dendrite. Because of conservation of charge and electroneutrality of the cell, the net current into the extracellular space is 0, and the extracellular potential will always be 0 no matter what electrical activity happens at the cell's membrane.[1] The same holds for a space-clamped axon. In fact, the total current through the membrane of any neuron must always equal 0, no matter what the neuron does, because of conservation of charge. However, current may enter at one point and exit at another. In this case, the current loop must be completed through the extracellular space. Current flow in the extracellular space causes potential differences which can be measured.

Currents in the extracellular space come from two distinguishable sources: synaptic currents and action potential currents. Synaptic currents are small in comparison with the action potential currents, but they last for several ms and in laminar structures the synaptic currents from thousands of neurons can sum up to make field potentials on the order of several mV. On the other hand, currents from action potentials are quite large, but they are usually very brief and diphasic, unlike the synaptic currents. As a result, it is rare for action potentials from adjacent cells to be aligned precisely enough to sum up; if they are misaligned by a fraction of a ms, they will tend to cancel

[1] This can also be seen from circuits. The equivalent circuit is the same as in figure 1.1 on page 8 with the intracellular resistive grid removed; the intracellular node (V_i) is floating and not connected to anything. It is clear from the circuit that there can be no transmembrane current, because the capacitive current must always equal the ionic current.

out. It is fairly clear that most slow field potentials (with time courses longer than a ms) and also potentials recorded over large areas (e.g., the EEG) are due primarily to synaptic currents rather than action potential currents (Creutzfeld and Houchin, 1974). In fact, a number of models of extracellular field potentials do not even include action potentials in the calculation (Rall and Shepherd, 1968; Klee and Rall, 1977; Wilson and Bower, 1989). Current source-density (CSD) analysis has been used extensively in laminar structures like neocortex and olfactory cortex to understand the sequence of events in response to electrical shock stimulation (see Mitzdorf, 1985), so a great deal is known about the extracellular potentials from synaptic currents.

There is some evidence that the electrical fields due to summed synaptic input from thousands of neurons are strong enough to influence firing significantly. Even fields as small as 2.5 mV/mm can significantly modulate population responses, and such fields certainly occur during normal operation (see Jefferys, 1995). These fields could have a small general excitatory or inhibitory effect over a large area of cortex, but the interactions are unlikely to be specific. I have chosen to concentrate rather on interaction based on the fields from single action potentials because their fields are less well studied and could have more specific effects.

See Rosenfalck (1969) for a thorough review of the earlier literature pertaining to axons, and Faber and Korn (1989) for a thorough review of ephaptic interaction in general. Plonsey (1988) discusses solutions and approximations for unmyelinated axons. A relatively readable review on the general theory of volume conductors is Malmivuo and Plonsey (1995), ch. 8. A general but old review on potentials from cells is Hubbard *et al.* (1969), ch. 7.

2.2 Extracellular potential produced by spiking activity

2.2.1 Axon in a volume conductor

The fields around axons have been extensively studied, largely because the geometry is fairly regular and the pulse propagates down the axon without change of shape. Since there are no barriers to conduction over large volumes of the central nervous system (assuming the ventricles and pial surface and other boundaries are far away), the potential around axons in the brain can be modeled by Laplace's equation (equation 1.9 on page 7),

$$\nabla^2 \phi = 0 \tag{2.1}$$

with the boundary condition that $\phi = 0$ at the point at infinity and

$$\sigma_e \nabla \phi \cdot \mathbf{n} = J_m, \tag{2.2}$$

where J_m is the transmembrane current density and $\mathbf{n}$ is the normal to the membrane, at membranes which are active.

These equations are identical to the equation for potential due to charges located at the same position as the current sources; σ_e is dual to the permittivity ϵ, and J_m is dual to the charge density on the sheet. As a result, solutions from electrostatics can be immediately applied to the problem of potential in a volume conductor.

For example, if we approximate the axon as a line (neglecting its thickness), then we can use the solution for potential from a line of charge. The potential from a single point[2] a distance R away is $\phi = I/4\pi R\sigma_e$, so the potential from a whole line of sources a distance r away is

$$\phi(r,z) = -\int_{-\infty}^{\infty} \frac{i_m(z')\,dz'}{4\pi\sigma_e\sqrt{r^2+(z-z')^2}} \tag{2.3}$$

where $i_m(z) = 2\pi a J_m$ is the transmembrane current per length.

This approximation, first made by Lorente de Nó (1947a), leads to relatively understandable expressions for the potential and shows qualitatively what factors influence it[3]. Furthermore, in an unbounded volume conductor, this approximation is very good even at the axon membrane (see section C.2.3).

The transmembrane currents from a simulated axon are shown in figure 2.1, and the corresponding field in figure 2.2. For axons, the extracellular potential at the neuron membrane is roughly proportional to the transmembrane current there, because the action potential is spread out over a large spatial distance and only nearby points contribute to the sum in equation 2.3.

The transmembrane current in an action potential is roughly a dipole, or two back-to-back dipoles (an axial quadrupole, sometimes in this configuration called a tripole): current flows out of the axon ahead of the action potential and behind it, and into the axon during the action potential (figure 2.1). Analytic expressions can be written for the potential from dipoles in an infinite volume conductor (put delta functions into equation 2.3). These considerations suggest that far away from the neuron, potentials should decline as $1/r^2$ as they do for a dipole (Rosenfalck, 1969) or $1/r^3$ as for a quadrupole (Plonsey, 1977).

In mammals, unmyelinated axons with diameters much larger than 1 μm are rare; one would

[2]The finite volume of the axon has only a negligible effect on the potential from a point source, so it is sufficiently accurate to use the Green's function for a point source in free space.

[3]It is often inconvenient to specify the transmembrane current J_m, since it is difficult to measure. The extracellular potential ϕ_e can also be computed directly from the intracellular potential (Geselowitz, 1966), since J_m can be computed from the spatial variation of the intracellular potential V_i (equation 1.12 on page 8) rather than from the membrane conductance and capacitance (equation 1.14). The resulting expression is

$$\phi = \int_{-\infty}^{\infty} \frac{\sigma_i}{\sigma_e}\frac{\partial^2 V_i}{\partial z^2}\frac{dz}{4\pi^2 a^2 r}. \tag{2.4}$$

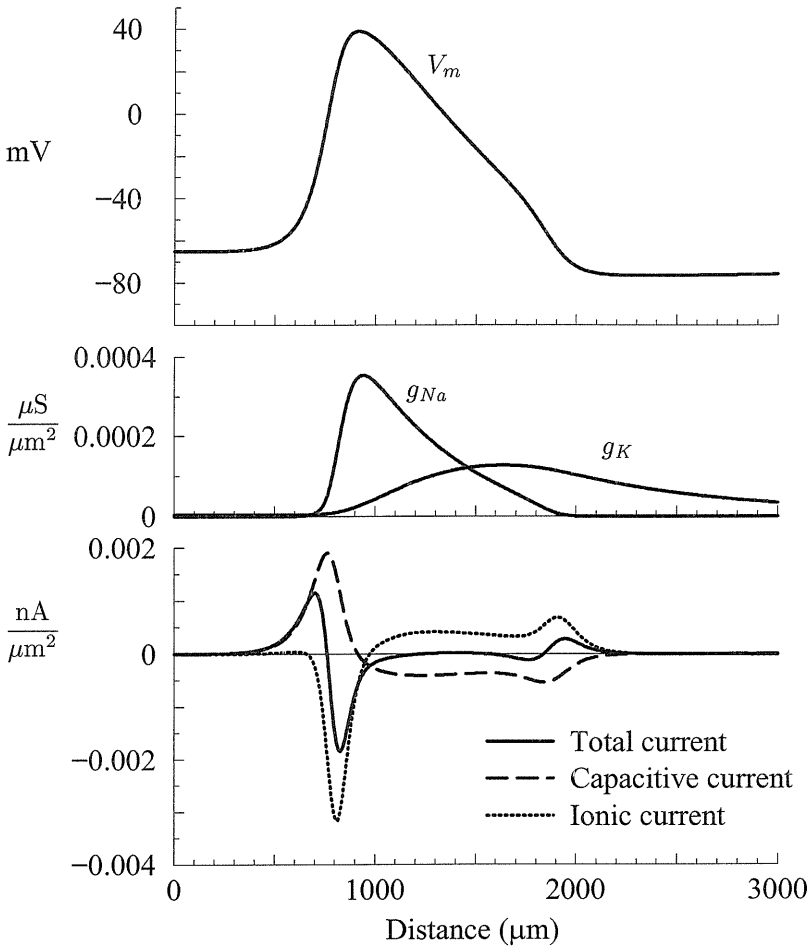

Figure 2.1: Current flow across the membrane in a propagating action potential propagating to the left at an instant in time. *Top*, transmembrane voltage; *Middle*, sodium and potassium conductances; *Bottom* current density as a function of position along the axon. The total current is first positive, then negative, and then there is a smaller positivity. Numbers are for an axon with a diameter of 1 μm and the conductance values from Hodgkin and Huxley (1952). The action potential propagates with a speed of 440 μm/ms. Only a short segment of the axon is shown. The capacitive (displacement) current is of course the derivative of V_m, The ionic current is close to $-dV_m/dt$ except that it is shifted. See Jack *et al.* (1983), ch. 9, for a discussion of the currents.

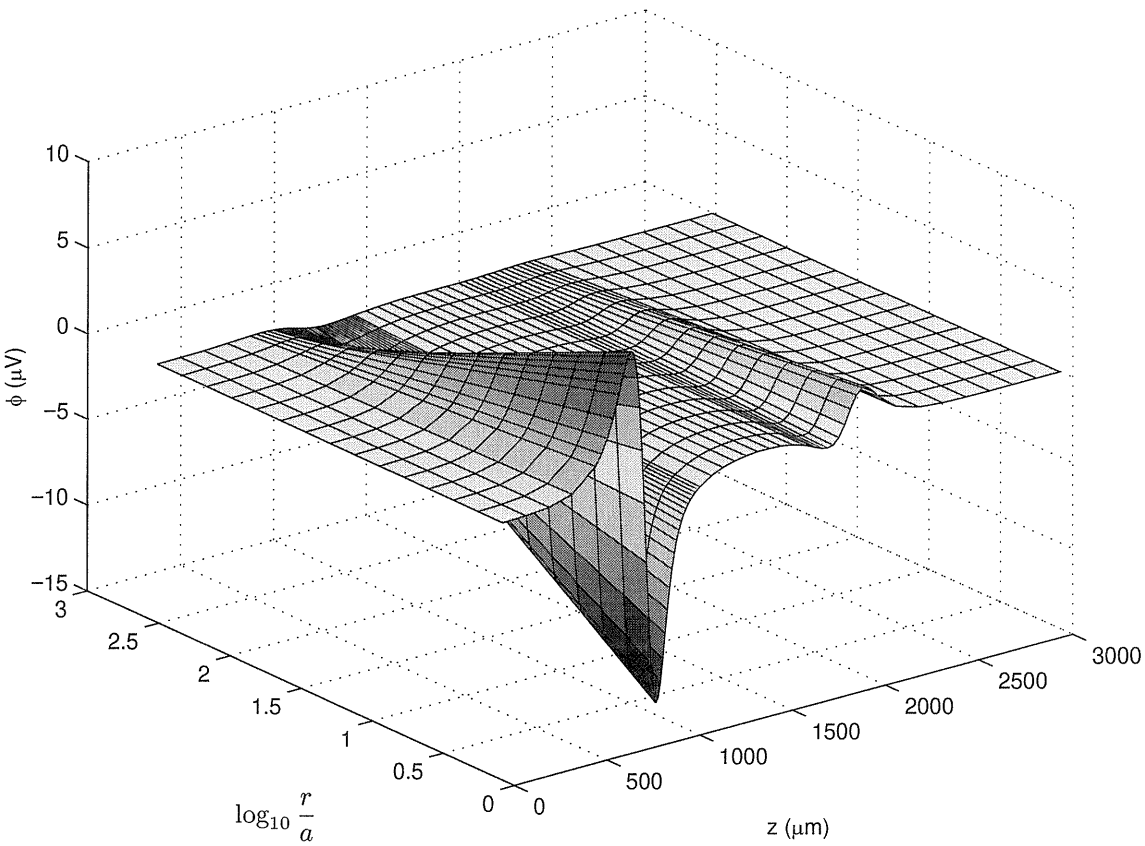

Figure 2.2: The extracellular potential around the axon of figure 2.1. See section C.2.2 for how the potential was computed.

not expect extracellular potentials to be orders of magnitude greater than shown in figure 2.2. Measured potentials from single axon activity are in general quite small, usually on the order of tens of microvolts. Potentials do not fall off drastically near the fiber, so there is no particular reason to think that the extracellular potentials are not accurately measured by the electrode because of tissue destruction or finite electrode size. It is unlikely that a unmyelinated mammalian axon in a volume conductor will have an extracellular potential larger than a few tens of microvolts. This is not enough for significant interaction (see below).

2.2.2 Axon in a sheath: the core conductor model

In the nerves of the peripheral nervous system, the extracellular space around axons is not well modeled as an infinite volume conductor. Peripheral nerves, even those which are unmyelinated, are surrounded by Schwann cells and a sheet of collagenous tissue (the *endoneurium*). Many axons join together into a fascicle which is surrounded by a second, thicker sheet of connective tissue, the *perineurium.* Fascicles are joined together to form the nerve, which is surrounded by a third, thick layer of connective tissue called the *epineurium.* One function of these sheaths, particularly the perineurium, appears to be analogous to the blood-brain barrier: to isolate the axons from changes in the extracellular environment (see Low, 1976; Peters *et al.*, 1991, ch. XII).

The perineurium is often modeled by a single cylindrical resistive or non-conducting sheath surrounding the axon at some distance from it. (The same model applies to experimental preparations where a nerve is lifted out of the tissue into air or oil; Stein and Pearson, 1971.) In this case, if the sheath is close enough to the axon, the current flow is essentially radial, and the core-conductor model holds.

If there is a sheath that surrounds the neuron and the diameter b of the sheath is small enough that the core-conductor approximation is valid, then the amplitude of the potential can be easily computed (Clark and Plonsey, 1968; Rosenfalck, 1969; Stein and Pearson, 1971; Plonsey, 1977):

$$\phi = -\frac{r_e}{r_i + r_e} V_m = -\frac{\sigma_i a^2}{\sigma_i a^2 + \sigma_e (b^2 - a^2)} V_m = -\frac{\sigma_i}{\sigma_e} \frac{a^2}{b^2} V_i \tag{2.5}$$

Note that the core conductor model predicts that the potential has the same shape as the intracellular action potential. This is different from the case of an unlimited volume conductor, where for a monophasic action potential there is a triphasic extracellular potential (Rosenfalck, 1969).

If there is no sheath or if the sheath is too far away to use the core-conductor approximation, then the solution is more complicated and there is no useful simple expression (see Plonsey, 1977 for a review). Obviously the solution must collapse to the core-conductor model when the sheath radius b is not too large compared to the radius of the fiber, but it has been difficult to find a simple

criterion for when this occurs. Rosenfalck (1969) argued that the core-conductor model breaks down for $b > 2a$. Trayanova *et al.* (1990) after a detailed analysis found empirically that it was valid up for $b < 5a$ but this will depend on the value of a (25 μm in their case) and shape of the action potential as well so this result is not generally useful. Stein and Pearson (1971) suggest without proof that the core-conductor model is valid as long as radial voltage variations are not significant, i.e., when the conductance between the neuron and the sheath is small compared to the conductance along the axon. This works out to $(b^2 - a^2)\log b/a \ll 2l^2$ where l is the length of the rising phase of the action potential.[4]

Another way of deriving limits on the validity of the core-conductor model is to compare it to another approximation which is known to be valid when b is large. The line-source model discussed above is known to be within 5% of the true solution when $b > 5a$ (Trayanova and Henriquez, 1991). Unfortunately, there is no simple expression for the potential from a line source when a sheath is present. Instead, it is necessary to resort to analysis in the spatial frequency domain. We first separate variables for a non-zero a, and later we take the limit as $a \to 0$ later; otherwise singularities appear in the solution too early.

We assume $\phi = R(r)Z(z)$. Laplace's equation then turns into:

$$Z'' + k^2 Z = 0 \tag{2.6}$$

$$rR'' + R' - k^2 rR = 0 \tag{2.7}$$

to which the solution is $Z = e^{ikz}$ and $R = AI_0(|k|r) + BK_0(|k|r)$ where A and B are constants determined by the boundary conditions. At the sheath boundary $r = b$, $dR/dr = 0$; also, R is normalized so that $R(a) = 1$. After some manipulation,

$$R = \frac{K_1(|k|b)I_0(|k|r) + I_1(|k|b)K_0(|k|r)}{K_1(|k|b)I_0(|k|a) + I_1(|k|b)K_0(|k|a)} \tag{2.8}$$

$$\phi(k,r) = \int_{-\infty}^{\infty} e^{ikz} R(k,r)\hat{\phi}(k,a)\,dk \tag{2.9}$$

where $\hat{\phi}(k,a)$ is the Fourier transform of the potential at $r = a$. [Since $R(k,a) = 1$, $\hat{\phi}(k,r) = \hat{\phi}(k,a)R(k,r)$.] We now apply the boundary condition at the membrane surface:

$$\begin{aligned} \frac{J}{\sigma_e} &= \frac{\partial \phi}{\partial r} \\ &= \int_{-\infty}^{\infty} e^{ikz} \frac{\partial R}{\partial r}\Big|_{r=a} \hat{\phi}(k,a)\,dk \end{aligned}$$

[4] Stein and Oğuztöreli (1978) also attempted to solve for extracellular potential, but they assumed a given surface potential instead of a transmembrane potential. Since the surface extracellular potential varies strongly with the radius of the sheath, this is not a useful way to understand what affects extracellular potentials.

implying that

$$\begin{aligned}\hat{\phi}(k,a) &= \frac{\hat{J}}{\sigma_e}\left[\frac{\partial R}{\partial r}\right]^{-1}_{r=a} \\ &= \frac{\hat{J}}{\sigma_e|k|}\frac{K_1(|k|b)I_1(|k|r) - I_1(|k|b)K_1(|k|r)}{K_1(|k|b)I_0(|k|a) + I_1(|k|b)K_0(|k|a)}\end{aligned}$$

To obtain a line-source model, we now let the axon radius $a \to 0$ while keeping the total current constant. Defining $\hat{J} = \hat{J}_0 a_0/a$, after some algebra

$$\lim_{a\to 0}\hat{\phi}(k,r) = \frac{\hat{J}_0 a_0}{\sigma_e}\left(\frac{K_1(|k|b)}{I_1(|k|b)}I_0(|k|r) + K_0(|k|r)\right). \tag{2.10}$$

This should be a good approximation as long as $ka_0 \ll 1$ and $a_0 \ll b$.

The core-conductor model is valid if the radial variation of potential is not significant, i.e., if the potential at $r = b$ is about the same as the potential at the surface of the axon. Using the identity $I_0(z)K_1(z) + I_1(z)K_0(z) = 1/z$, the potential at $r = b$ is

$$\hat{\phi}(k,b) = \frac{\hat{J}_0 a_0}{\sigma_e}\frac{1}{kbI_1(kb)} \tag{2.11}$$

By comparison, the extracellular potential from the core-conductor model is given by:

$$\frac{\partial^2\phi}{\partial z^2} = \frac{2\pi a J}{\pi(b^2-a^2)\sigma_e} \tag{2.12}$$

$$\hat{\phi}_{core}(k) = -\frac{2\hat{J}a}{\sigma_e(b^2-a^2)k^2} \approx \frac{2Ja_0}{\sigma_e k^2 b^2} \tag{2.13}$$

Therefore

$$\frac{\hat{\phi}(k,b)}{\hat{\phi}_{core}(k)} = \frac{kb}{2I_1(kb)}. \tag{2.14}$$

This is shown in figure 2.3. The core-conductor prediction is within 10% of the line-source prediction for $kb < 1$. This corresponds to $l > 2\pi b$, where l is the shortest significant spatial scale of the action potential.

If the action potential has a rise time of say 0.1 ms and a speed of 0.5 mm/ms, then the characteristic length l will be around 0.1 ms $\times$ 0.5 mm/ms = 50 μm. Hence the core-conductor model could be valid for sheath radii up to 300 μm.

In general, the actual potential will be larger than what is given by the core-conductor approximation[5]. Therefore the core-conductor approximation can be used to decide when extracellular

[5] $\hat{\phi}_{core} \approx \hat{\phi}$ for small b, and for large b, and $\hat{\phi}_{core} \to 0$, while $\hat{\phi}$ does not approach 0.

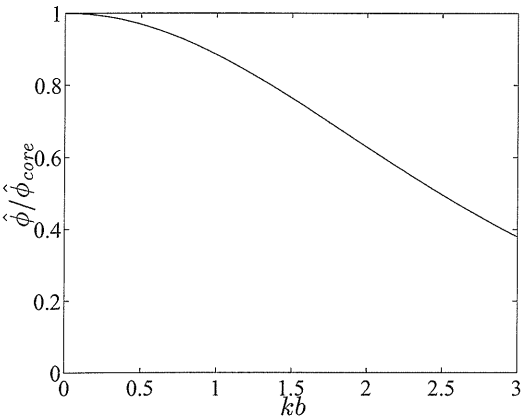

Figure 2.3: A comparison of the predictions of the core-conductor model with the line-source model as a function of spatial frequency normalized by sheath radius. The core-conductor prediction is quite good up until $kb = 1$, i.e., for spatial wavelengths in the action potential longer than 2π times the distance to the sheath.

potentials will be significant. It is reasonable to suppose that a 1 mV potential might have a significant effect (see section 2.3), while something smaller would probably be negligible. Equation 2.5 predicts that if $V_m = 100$ mV, then $\sigma_i a^2/\sigma_e b^2 > 0.01$ for a 1 mV potential. σ_i/σ_e is at most 5, so one would predict significant extracellular potentials only if $a/b > 0.04$. For an axon of radius $a = 1$ μm, this implies $b < 25$ μm. Mammalian perineurial sheaths usually have a radius greater than 50 μm (Low, 1976; Peters *et al.*, 1991), so interaction is unlikely.

There is a substantial body of work predicting the extracellular fields of myelinated axons (e.g., Marks and Loeb, 1976; Ganapathy and Clark, 1987; Stephanova *et al.*, 1989; Struijk, 1997). Since myelin decreases the capacitance of the membrane, much less current flows and the potentials are smaller. In keeping with this, it is much more difficult to record any neural activity in white matter (David Kewley, personal communication).

2.2.3 Cells with dendritic trees: theory and past work

Extracellular potentials from action potentials around cell bodies and dendritic arbors are different from the potentials around axons. Most obviously, they can be much larger, sometimes 5 mV or more[6] (Freygang, 1958; Freygang and Frank, 1959; Terzuolo and Araki, 1961; Rosenthal, 1972; Towe, 1973). A much larger area (the proximal dendritic tree) is simultaneously depolarized by currents at or near the soma, so the current that flows must be larger. Also, the shapes can be different because the action potential does not propagate in the same way. Analysis is complicated by the irregular geometry of dendrites and cell body, and in general the fields are not well understood.

One approximation which is sometimes made is based on the line source model, equation 2.3.

[6]So called "giant potentials" of 20 mV or more can be recorded when the electrode is pushed up against the membrane. These are caused by a resistive seal between the membrane and the electrode and are therefore an artifact of the electrode's presence. See Hubbard *et al.* (1969), pp. 282-283.

Since potential at any point is a sum of contributions of all points in the neuron weighted by $1/R$, where R is the distance to the point, only nearby points will have a large effect on potential unless there are very large current sources far away. Therefore, the potential at the membrane ought to be approximately proportional to the transmembrane current at that point. This is quite accurate for axons (compare figure 2.1 with figure 2.2). Although was once used to understand field potentials around cells, it does not accurate in this case (Rall, 1962) because the effect of sources and sinks near the soma or axon initial segment can be large compared to the effect of current through the dendrites at the point being considered. Nevertheless, determining where a particular peak in the extracellular field is largest can be a clue to its origin. This generalization also breaks down if a large population of spatially distributed neurons is active exactly simultaneously (Klee and Rall, 1977), such as in response to an electrical shock, or when the field is due primarily to slower events such as synaptic input.

A second tool for intuition is to formulate the problem in terms of volume sources. Because dendritic trees are complicated and irregular, the boundary conditions for solution of Laplace's equation (equation 1.9 on page 7) are prohibitively complicated. One can average the tissue over a small volume, changing current flux across membranes into current source density. From conservation of charge,

$$\nabla \cdot \mathbf{J} = I \tag{2.15}$$

where I (the current source density) is the sum of all the transmembrane currents in some small volume. Since $\mathbf{J} = -\sigma \nabla \phi$ (equation 1.5 on page 6),

$$\nabla \cdot \sigma \nabla \phi = -I. \tag{2.16}$$

If σ is a scalar (conductivity is roughly isotropic) then equation 2.16 has exactly the same form as Gauss's law in electrostatics (equation 1.4 on page 5). Current source density in volume conductors is dual to charge density in electrostatics. This means that the mathematical techniques which have been useful in electrostatics apply equally well to the fields around cells. This was used by Bishop and O'Leary (1942) and Lorente de Nó (1947b) for a population of neurons with a regular geometry to try to explain the different shapes of extracellular action potentials along the microelectrode track.

For example, suppose that the dendritic field of a given cell[7] is approximately spherically symmetric. Then the field from an action potential originating at or near the soma will also have spherical

[7]Or population of simultaneously activated cells in a nucleus, as Lorente de Nó (1947b) originally analyzed it. Approximations to this situation are not uncommon in the various nuclei in the brain.

symmetry. Taking integrals of both sides of equation 2.16 over a spherical volume of radius r and applying the divergence theorem,

$$\iint \sigma \mathbf{E} \cdot \mathbf{dS} = \iiint I(r)\, dV \tag{2.17}$$

where $\mathbf{E} = -\nabla\phi$ is the electric field and $I(r)$ is the total current inside a sphere of radius r. Using spherical symmetry,

$$4\pi r^2 E(r) = \int_0^r I(r')\, 4\pi r'^2\, dr' \tag{2.18}$$

For r larger than the radius of the dendritic field, the right hand side is 0 since all current that flows out through the soma must flow back in through the dendrites somewhere. Therefore no potential at all will be visible beyond a certain radius, no matter what activity there is in the dendrites; hence this is called a "closed field" (Lorente de Nó, 1947b).[8]

For r within the radius of the dendrites, there will be a measurable potential. When the action potential is in the rising phase at the soma, I at the soma will be negative, but in the dendrites I will be positive. When the action potential begins to repolarize, I will be positive at the soma and negative in the dendrites. The potential from this cell is therefore diphasic, in contrast to the triphasic potential from an axon. The shape of the potential will always be approximately the same (negative then positive) wherever it is recorded. This is different from the potential from an "open field" where the potential can be triphasic or be first positive then negative.

Rall (1962) used the closed field approximation to estimate the magnitude of the extracellular potential for stellate cells. Many kinds of cells do not have spherically symmetric dendrites, but part of their tree can be regarded as spherical. For example, in the case of a pyramidal cell the potential from the whole cell can be regarded as the sum of a closed field (the soma and basal dendrites) and a dipole source (the soma and apical dendrites). The extracellular potential is large and initially negative near the soma, and declines rapidly with distance. Probably most of the current from the somatic spike flows out through the basal dendrites, but a small fraction of it flows up into the apical dendrite. As a result, potentials around the apical dendrites are small and initially positive. Of course, this approximation breaks down since action potentials propagate actively up the dendrites, but it turns out that the potential due to dendritic spikes is much smaller than the potential due to the somatic spike.

It has been difficult to make general statements about extracellularly recorded action potentials beyond these qualitative considerations (Lorente de Nó, 1947b, 1953). The shapes and magnitudes

[8] A population with cell bodies at the periphery and dendrites in the center, such as in the superior olive, also is a closed field; its field potentials are opposite in sign from the closed field discussed above.

of the electric potentials depend sensitively on the membrane currents and when the action potential reaches different parts of the neuron. In early work the extracellular potentials at different positions were used to answer questions such as:

- Is synaptic transmission electrical or chemical? (For example, see the lively discussions by Eccles and others at a symposium on the spinal cord, Malcolm and Gray, 1953)

- Where does the spike initiate? The correct answer, in the axon, was determined by a number of extracellular studies (thalamic cells: Freygang, 1958; motoneurons: Freygang and Frank, 1959; Terzuolo and Araki, 1961) and incorrectly by others (Fatt, 1957).

- Do dendrites carry spikes? Extracellular recordings were interpreted to support dendritic spikes in some cell types for many years (cortical pyramids: Clare and Bishop, 1955; spinal motoneurons: Fatt, 1957; Terzuolo and Araki, 1961; hippocampal pyramids: Sperti *et al.*, 1967; Buzsáki *et al.*, 1996; Purkinje cells: Eccles *et al.*, 1966; Nicholson and Llinás, 1971), although there were some disagreements (Freygang, 1958; Freygang and Frank, 1959; Nelson and Frank, 1964; Rosenthal, 1972). Lorente de Nó (1947b) even showed that the action potential does not propagate as far into the dendrite of motoneurons in later spikes of a burst, evidently due to branch point failure. This result caused considerable excitement when it was rediscovered fifty years later with different techniques (Spruston *et al.*, 1995; Hoffman *et al.*, 1997).

Analysis of extracellular action potentials has been largely neglected in recent years (an exception is Buzsáki *et al.*, 1996), partly because extracellular potentials are difficult to interpret, and partly because dendrites were considered passive for theoretical convenience. More emphasis has been placed on the origin of field potentials due to synaptic input in a population of neurons (Mitzdorf, 1985; Bullock, 1997).

2.2.4 Cells with dendritic trees: model results

Since little is known about the fields around cells, I computed the extracellular potential directly from a compartmental model. The purpose of this thesis is not to develop an accurate detailed model of a cell, but instead to understand the electrical fields around it; so I used a previously published model of a neocortical cell (Mainen and Sejnowski, 1996) without modification. This model was chosen because its spikes initiate in the axon (Mainen *et al.*, 1995). Proper spike initiation is critical for computing the extracellular potential, because the potentials are much larger near the region of spike initiation than anywhere else (see below). In this model, the action potential initiates in the axon hillock and initial segment of the axon, where there is postulated to be a very large density of

sodium channels, as large as at a node of Ranvier.[9]

A second advantage of the model of Mainen and Sejnowski (1996) is that the dendrites are weakly active, and action potentials propagate actively up into the tree, so it can be used to study how active propagation in the dendrites affects the fields. The model uses measured sodium channel densities in the dendrites (for young rats; see Stuart and Sakmann, 1994). There is some controversy about these values, however, because they evidently change significantly with age. In the hippocampus in older rats, for example, the sodium channel density is much higher, but the sodium currents are balanced out by a high density of potassium A currents so the dendrites are still only weakly active (Hoffman *et al.*, 1997).

In the peripheral nervous system, cell bodies of neurons are usually surrounded by a sheath of Schwann cells. In the central nervous system, ensheathment of the cell body and axon initial segment is more variable. Müller cells in the retina ensheath ganglion cells (Stone *et al.*, 1995). Purkinje cells have a complete covering of astroglial processes around the cell body. Neocortical pyramidal cells appear not to have any covering at all. In neocortex, one finds dendrites and axons in abundance even directly apposed to the cell body and axon hillock (Peters *et al.*, 1991). Thus in neocortex we are justified in ignoring the complicating effects of a sheath.[10]

Calculation of the field potential was based on the line source model, with a homogeneous unbounded extracellular space with a conductivity of 0.3 μm/μS (330 Ω-cm; e.g., Ranck, 1963). The potential and field amplitudes are directly proportional to $1/\sigma_e$ so the effect of a change in σ_e is trivial to calculate. See section C.2.3 for details. Results are shown in figure 2.4 and figure 2.5. It is difficult to account for every detail of the field potential, but most of the obvious features can be understood. First consider the largest potentials, which occur near the axon hillock and initial segment. This area of the neuron has an extremely high density of sodium channels in the model (maximum conductance if all are open is 30,000 pS/μm ^{2}, in comparison with 20 pS/μm ^{2} in the soma and dendrites). The inward currents are large because current through the axon hillock is what depolarizes the soma and proximal dendrites.

The action potential initiates in the distal part of the initial segment (actually in the first node of Ranvier). It then propagates up the initial segment (not shown), slowing down considerably in the axon hillock because of the increasing diameter and the load of the soma and the dendrites. The initial negativity in the extracellular potential (the "A spike" in the nomenclature of Fuortes *et al.*,

[9]In EM views of axon initial segments, there is a dense undercoating below the plasma membrane similar to the dense undercoating at the nodes of Ranvier, and in fact fluorescent neurotoxin probes specific for the sodium channel stain the hillock of cultured motoneurons and cortical cells more brightly than the cell body (Angelides *et al.*, 1988). However, physiological measurements in hippocampal pyramidal cells by Colbert and Johnston (1996) indicated only a low density of sodium channels in the hillock/initial segment. It is still unclear exactly where in the axon the action potential begins.

[10]The sheath of satellite cells is probably more for maintaining a constant concentration of potassium and other ions; see chapter 3.

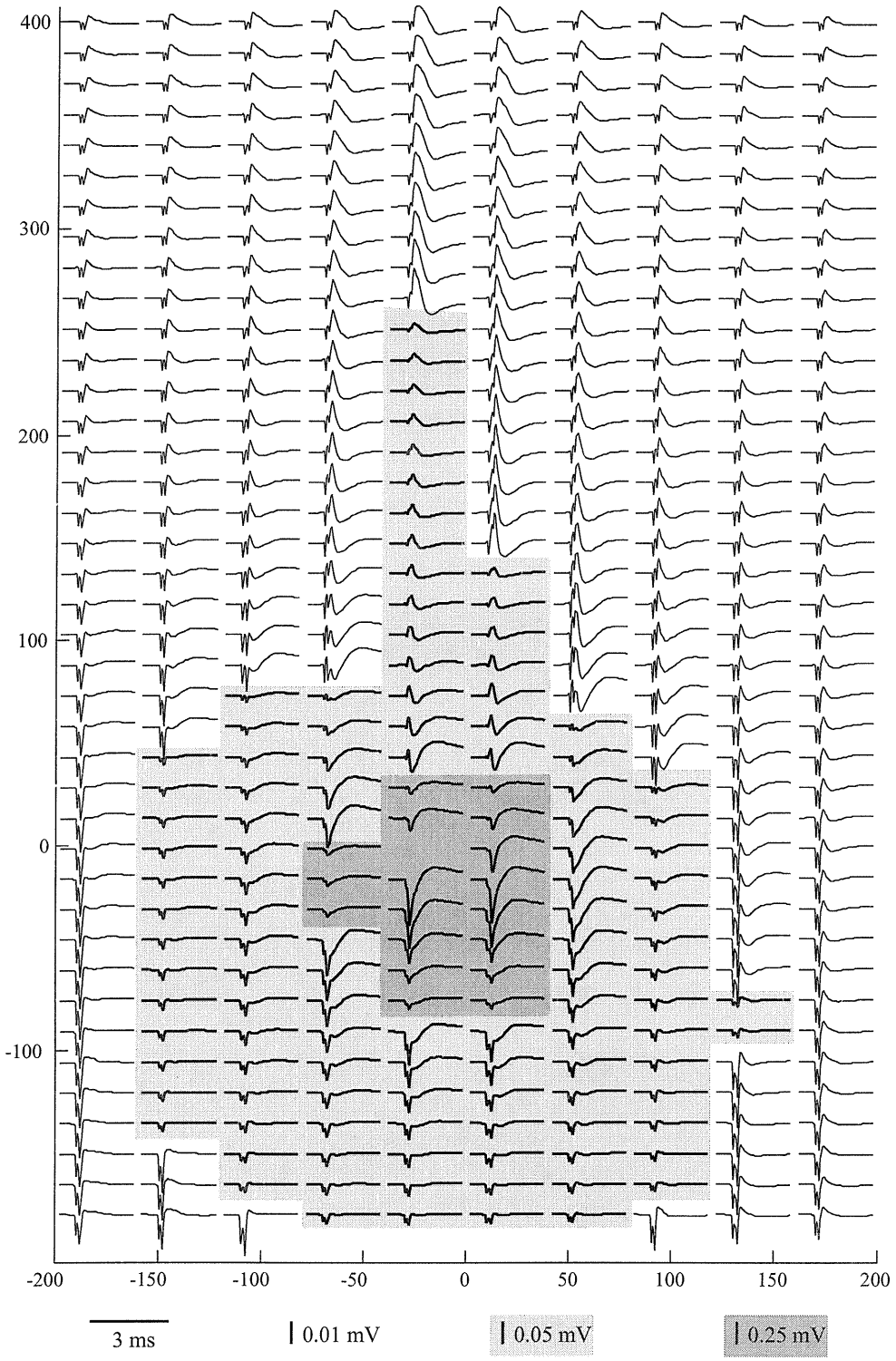

Figure 2.4: caption on page 32

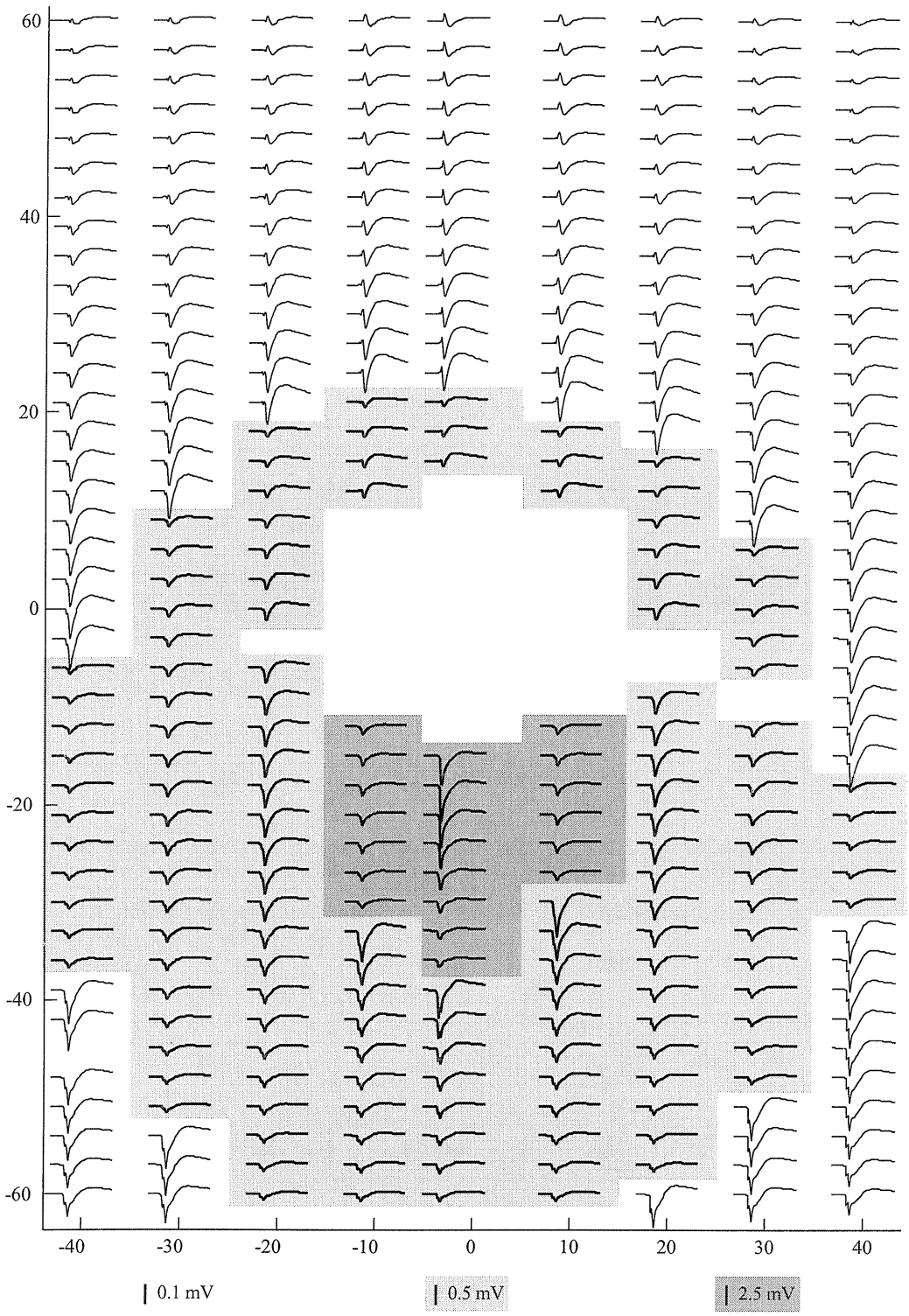

Figure 2.5: caption on page 32

Figure 2.4: Field potentials in a plane around the simulated layer V cortical pyramidal cell. x and y axes are in units of μm. Each trace was taken from a point at its center. Shaded areas indicate different voltage scales. Closer than 20 μm to the axon hillock, field potentials are much larger than shown here (see figure 2.5 for closeup). The soma is at $(0, 0)$, and the axon descends straight below it. The apical dendritic trunk is slightly to the left of $x = 0$ and goes up approximately straight, so the larger potentials at the top center are from the apical dendrite. The field potentials look roughly similar in other slices through the volume, so only this slice is shown.

Figure 2.5: Field potentials near the soma of the simulated layer V cortical pyramidal cell. The peak field potential is slightly over -5 mV and occurs next to the axon initial segment. Note that the peak amplitude on this graph is much higher than in figure 2.4 because the traces are closer to the axon initial segment.

1957 for motoneurons) is due to the action potential in the distal initial segment, since it occurs at the same time as the maximum current from the distal initial segment (see figure 2.6). Because of charge conservation, current flowing in through the initial segment must flow out somewhere in the cell; in fact, there is an initial positivity near the apical dendrite (figure 2.4) because the potential from the local outward current there was larger than the potential from the inward current at the initial segment. This sign reversal in the apical tree is commonly observed in physiology (e.g., Sperti *et al.*, 1967; Rosenthal, 1972).

A second negativity (the "B spike") in the field potential is due to the firing of the axon hillock, especially the proximal part (figure 2.6). This negativity is larger because the area of the hillock is larger than the initial segment, and also because the axon hillock is driving the depolarization of the soma and proximal dendrites. In fact, the field potential can be as large as -5 mV within a few microns of the hillock. Again, this reverses in sign far up the apical dendrite because of current outflow there.

Is this double-peaked structure observed, or is it an artifact of this model? The amplitude of the first peak is quite small in most places. With a noise level of 40 μV (primarily due to firing of other neurons; David Kewley, personal communication), it is unlikely that it could be resolved except by spike-triggered averaging. A peak with a shoulder might be observable very near the axon initial segment. Often a shoulder on the waveform is seen near the soma of a variety of neurons, including CA1 pyramidal cells (Sperti *et al.*, 1967; Buzsáki *et al.*, 1996), possibly pyramidal tract neurons (figure 1 of Rosenthal, 1972), and motoneurons (Fatt, 1957; Terzuolo and Araki, 1961; Nelson and Frank, 1964). In some of these examples, two separate peaks rather than just a shoulder can sometimes be discerned (e.g., Fatt, 1957). By direct comparison of intracellular with extracellular voltage, the extracellular A spike has classically been attributed to the axon hillock/initial segment, and the B spike to the soma and possibly proximal dendrites (Terzuolo and Araki, 1961). In the model here, however, the B spike is due not to currents from soma/dendrites but from the axon

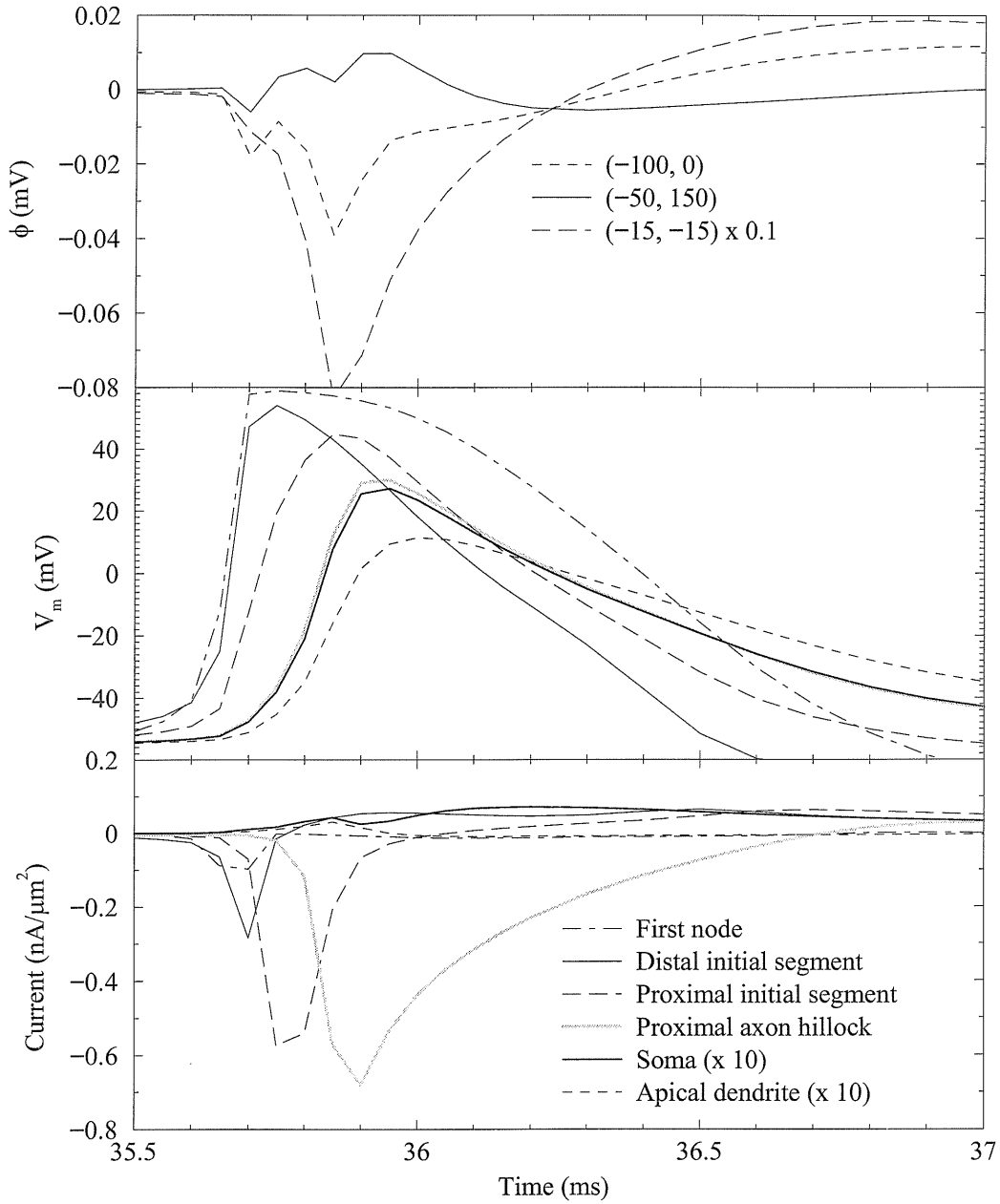

Figure 2.6: A comparison of the field potential and transmembrane currents. The first negativity in the field potential corresponds to the maximum current from the distal initial segment. The second negativity corresponds to the maximum current from the proximal axon hillock.

hillock; this probably could not be discerned experimentally because the potential in the soma very closely follows the potential in the axon hillock, and the transmembrane currents cannot be measured directly.

As illustrated by this model, extracellular field potentials can reveal a good deal about spike initiation and propagation within the cell. As mentioned above, there is still some controversy about exactly where in the cortical cell the action potential initiates, and whether the axon hillock/initial segment has sufficient numbers of sodium channels to be the site of initiation. Extracellular fields are a sensitive indicator of the location of currents. In the slice, where it is possible to visualize a single neuron within the tissue, it would be relatively easy to examine the extracellular fields around a cell which can be stimulated by an intracellular electrode. The location where where the earliest negativities are largest is an indicator of where the spike initiates. One could also determine whether the large negativity comes from the axon hillock as predicted from the model of Mainen and Sejnowski (1996), from the soma/proximal dendrites (from the classical motoneuron model), or from further out in the axon (Colbert and Johnston, 1996).

In the model, the action potential propagates up the apical tree[11], but dV_m/dt is very small because of the much lower sodium channel density. The field potentials are therefore extremely small (sometimes less than 10 μV) and are difficult to observe directly. However, Lorente de Nó (1947b) was able to examine the fields from thousands of simultaneously activated neurons to conclude that action potentials propagate into the dendrites, and that often propagation fails for successive spikes in a burst. Buzsáki *et al.* (1996) found the same result for a single hippocampal cell *in vivo* using spike triggered averaging to estimate the average extracellular waveform more accurately.

There are several important features of the extracellular action potential for ephaptic interaction. First, as noted above, it is very large, much larger than the extracellular fields around axons. Second, it is more confined in space than fields from axons. For an axon in a sheath, for example, $\phi \propto -V_m$ (equation 2.5 on page 22), so the field may be spread out over a mm or more depending on the speed of propagation (see figure 2.1 on page 20). In contrast, the extracellular field has a large amplitude over only a small region (50 μm for this particular model; sometimes over 100 μm measured experimentally). The field has a much larger gradient, and this turns out to be important for interaction.

2.3 Effect of extracellular potential on neural elements

Ephaptic interactions between axons have been observed in a variety of preparations where the extracellular resistance is artificially increased, including squid giant axon (Arvanitaki, 1942; Ramón

[11] A movie of this can be seen at `http://www.klab.caltech.edu/~holt/thesis/`.

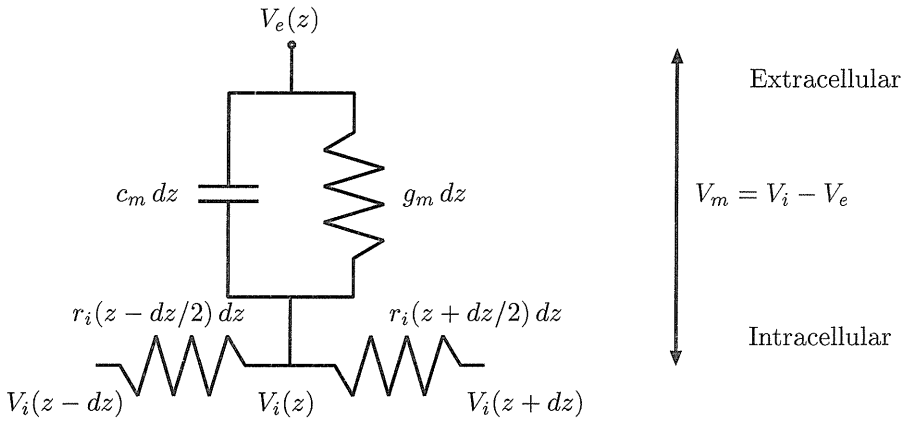

Figure 2.7: Circuit for computing the effect of extracellular potentials.

and Moore, 1978), crab motoneuron axons (Katz and Schmitt, 1940, 1942), frog sciatic nerve (Kocsis *et al.*, 1982), and even algal strands (Tabata, 1990). This situation has attracted a good deal of theoretical interest because of the simplicity of the geometry.

A number of studies have addressed the effects of electrical fields on axons, particularly myelinated axons, because of their importance in electrical stimulation experiments. Some modeling work in the hippocampus has shown the importance of coupling to the extracellular potential (Traub *et al.*, 1985a, 1985b) in epileptiform bursts. There has been almost no attempt to examine the effect of the field potential produced by a single spike on other cells. Rall (1962) guesses that coupling could have an effect based on preliminary calculations which he does not explain. I am unaware of any subsequent work on the problem of ephaptic interaction of cells rather than axons.

Obviously, if the potential of the whole brain is raised relative to a distant ground, there will be no effect at all on neural activity, since the intracellular potentials will rise by the same amount. It is the gradients of the extracellular potential, rather than the magnitude of the potential itself, determine the effect.

2.3.1 Infinite straight cables

Consider first the case of a passive unmyelinated cable with a varying extracellular electric potential V_e, as shown in figure 2.7[12]. Summing the currents into the junction gives (Clark and Plonsey, 1971;

[12]This figure assumes that V_e does not change significantly from one side of the cable to the other, i.e., that there is no θ dependence in V_e. If V_e does depend noticeably on θ, V_e and V_m can be replaced with their average over θ and exactly the same equation results.

Plonsey and Barr, 1995[13])

$$\begin{aligned} c_m \frac{\partial V_m}{\partial t} + g_m V_m &= \frac{1}{r_i} \frac{\partial^2 V_i}{\partial z^2} \\ &= \frac{1}{r_i} \left(\frac{\partial^2 V_m}{\partial z^2} + \frac{\partial^2 V_e}{\partial z^2} \right) \end{aligned} \tag{2.19}$$

since $V_m = V_i - V_e$. With the usual definitions $\tau = c_m/g_m$ and $\lambda^2 = 1/r_i g_m$, this becomes[14]

$$\tau \frac{\partial V_m}{\partial t} + V_m = \lambda^2 \left(\frac{\partial^2 V_m}{\partial z^2} + \frac{\partial^2 V_e}{\partial z^2} \right) \tag{2.20}$$

The extracellular potential acts like a distributed current (the *ephaptic current*) with a magnitude of $i_{eph} = (1/r_i)\partial^2 V_e/\partial z^2$ per unit length.

For an intuitive understanding of what this means, it is helpful to consider the Fourier transform of equation 2.20 in both space (k) and time (ω):

$$i\omega\tau \hat{V}_m + \hat{V}_m = -k^2\lambda^2 \hat{V}_m - k^2\lambda^2 \hat{V}_e \tag{2.21}$$

or

$$\hat{V}_m = \frac{-k^2\lambda^2}{1 + i\omega\tau + k^2\lambda^2} \hat{V}_e. \tag{2.22}$$

Clearly the biggest that $\hat{V}_m(k)$ can ever be is $-\hat{V}_e(k)$, and that occurs for large $k^2\lambda^2$. Therefore the largest $V_m(z)$ can be is $-V_e(z)$. This occurs when $V_i(z)$ is approximately constant, i.e., when the spatial scale of the changes of $V_e(z)$ is much less than the length constant of the fiber at the relevant frequencies.

Interaction between two axons

This upper bound is not reached in practice for axonal interaction. Instead, for the term $i\omega\tau$ in the denominator of equation 2.22 dominates, implying that most of the current is capacitive (Clark and Plonsey, 1971). For example, in the simulations of figure 2.1, if the axon is placed in a sheath, $V_e \propto -V_m$, so the dominant spatial frequency in V_e is about $k = \pi/1000/\mu$m (based on the half-width of the action potential), and the dominant temporal frequency will be $\omega = kv = 440\pi/1000/$ms. If

[13] An alternative formulation based only on V_i and V_e instead of V_m and V_e is possible but involves time derivatives of V_e (Rubinstein and Spelman, 1988). Electrodes sense V_i; however, membrane channels sense V_m, so V_m is more relevant for the biophysics.

[14] Note that this λ value is different from λ in the core-conductor model when the extracellular space was treated as one-dimensional (equation 1.17 on page 10). In that case we assumed that the only contribution to V_e was from the axon under study; here we assume that the contribution to V_e from the axon under study is negligible, and the only contributions come from other neurons.

there is another axon at rest with the same parameters nearby ($\lambda = 220$ μm and $\tau = 1.1$ ms), then $k^2\lambda^2 \approx 0.5$ and $\omega\tau \approx 1.5$; the difference between these is more extreme for the axon considered by Clark and Plonsey (1971). $k^2\lambda^2$ in the denominator can be neglected:

$$i\omega\tau\hat{V}_m \approx -k^2\lambda^2\hat{V}_e. \tag{2.23}$$

Taking the inverse transforms,

$$\tau\frac{\partial V_m}{\partial t} \approx \lambda^2\frac{\partial^2 V_e}{\partial z^2} \tag{2.24}$$

If the action potential is propagating with a velocity θ, then $z = \theta t$, and equation 2.24 becomes

$$\tau\theta V_m \approx \lambda^2\frac{\partial V_e}{\partial z}. \tag{2.25}$$

The membrane will therefore be excited with a spatial distribution given by $\partial V_e/\partial z$. Since in a nerve surrounded by a sheath V_e is proportional to the negative of the intracellular voltage of the active fiber (equation 2.5 on page 22), an inactive fiber's membrane will first be hyperpolarized, then depolarized.

This pattern of depolarization and hyperpolarization also explains the result when both axons conduct action potentials. If the action potentials are almost abreast, their current sources and sinks are lined up (figure 2.8 top). Each attempts to hyperpolarizes the other, and both will slow down. If one is slightly behind the other (figure 2.8 bottom), the leading axon will depolarize the lagging axon and speed its action potential up. Staggered action potentials are stable; the outward currents in one axon line up with the inward currents in another. As a result, even if the propagation velocities are different when each axon is alone, the two action potentials will still propagate in step. Both action potentials can propagate faster than either would alone (Katz and Schmitt, 1942; Maeda *et al.*, 1980; Tabata, 1990; Barr and Plonsey, 1992) because propagation of an action potential in the second fiber changes the effective extracellular resistance.

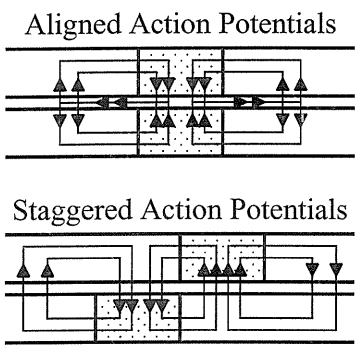

Figure 2.8: Patterns of current flow in two interacting axons. *Top*, action potentials exactly aligned. In this case, both axons try to hyperpolarize the other at the front of the action potential, so both slow down. *Bottom*, action potentials staggered, with sources and sinks lined up. The currents from the leading axon depolarize the lagging axon at the front of its action potential, speeding it up.

A battery of theoretical studies has addressed the phase-locking of action potentials in adjacent fibers mathematically and with simulations[15]. However, unless precise spike timing (less than 1 ms) is important for the information carried by small unmyelinated fibers, the synchronization and phase-locking effects will be unimportant even if the extracellular potentials were large enough to have a noticeable effect. For this reason, I will not consider ephaptic interaction between two axons further.

Myelinated axons are more sensitive to extracellular fields for several reasons. They have larger diameters and lower membrane conductances. Therefore λ is longer, and the $k^2\lambda^2$ terms in equation 2.22 are relatively larger. The capacitance is much lower, lowering the $i\omega\tau$ term. Therefore V_m will be closer to its limit of $-V_e$. The nodes of Ranvier have low thresholds, making it more likely that a transmembrane potential shift will initiate an action potential. Several studies have estimated the response of myelinated axons to various kinds of electrical stimulation by the experimenter (e.g., Ranck, 1975; MacNeal, 1976; Tranchina and Nicholson, 1986; Rattay, 1987; Altman and Plonsey, 1990; Rubinstein, 1991). Although myelinated axons are more sensitive to extracellular fields, they generate much smaller electrical fields, so interaction seems unlikely to be significant.

Interaction of cell bodies and infinite cables

Axons and dendrites in cortex also pass next to cell bodies, where the extracellular fields are much larger. The fields around cells are much more confined than around axons, and therefore $k\lambda$ is much bigger. From figure 2.6, the dominant spatial frequency in the action potential is around $k = \pi/50/\mu\text{m}$ and the dominant temporal frequency is $\omega = \pi/0.15/\text{ms}$. For the axon of figure 2.1 passing by this cell body, $k^2\lambda^2 \approx 190$ and $\omega\tau \approx 20$. Unlike axonal interaction, then, the capacitive current is much smaller than the axial currents. As a result, $V_m \approx -V_e$ and has the same time course as V_e.

Despite the crudity of this analysis, it is not a bad good predictor of the transmembrane potential. The actual transmembrane potential is shown in figure 2.9. In fact, V_m is almost equal to $-V_e$, especially near the cell body where V_e is changing rapidly with position.

Although ephapses can be characterized by localized current injection (section 2.3.1), just as synapses can, this example shows that they have somewhat different properties. Because the ephaptic current depends on the second derivative of the extracellular potential (equation 2.20), a peak in the extracellular potential produces an ephaptic current which is depolarizing at the peak and hyperpolarizing flanking the peak (see the currents in figure 2.9). In fact, the total ephaptic current

[15] Markin, 1970a, 1970b, 1973a, 1973b; Scott, 1977; Scott and Luzader, 1979; Maeda *et al.*, 1980; Eilbeck *et al.*, 1981; Keener, 1989; Barr and Plonsey, 1992; Bose and Jones, 1995

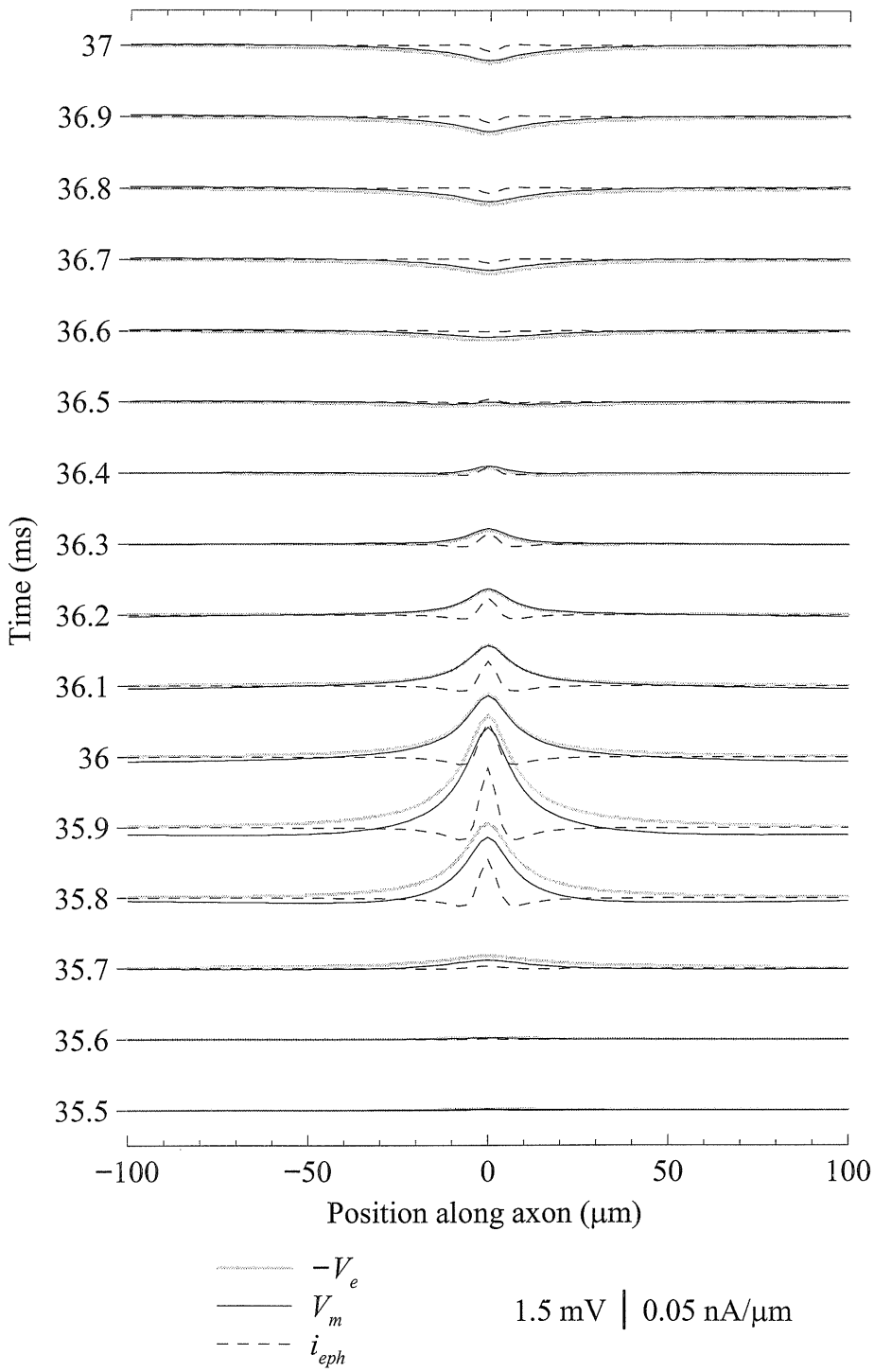

Figure 2.9: The membrane potential of a long straight passvive cable located near a cell body. Extracellular potential, induced transmembrane potential, and the ephaptic current are shown as a function of position for several different times during the action potential. This axon was perpendicular to the plane of figure 2.4 and intersected it at $(5, -20)$ (near the axon hillock).

into an cable is given by

$$\begin{aligned} I_{tot} &= \int_{-\infty}^{\infty} \frac{1}{r_i} \frac{\partial^2 V_e}{\partial z^2}\, dz \\ &= \frac{1}{r_i} \left(\lim_{z\to\infty} \frac{\partial V_e}{\partial z} - \lim_{z\to-\infty} \frac{\partial V_e}{\partial z} \right) \\ &= 0. \end{aligned}$$

As a result, the transmembrane potential is more localized and does not spread in the same way as a point current source injection would.

The Fourier analysis also predicts what the effect of parameter variations is on induced potential. Since $k^2\lambda^2 \gg \omega\tau$, changing $\tau = c_m/g_m$ by changing the capacitance within reasonable limits should have little effect on the result (figure 2.10A). Also changing $\lambda = \sqrt{\sigma_i a/2g_m}$ by changing the intracellular resistivity (figure 2.10B) or the cable diameter (figure 2.10C) within physiological limits has little effect because $k^2\lambda^2$ appears in both the numerator and the denominator. Changing the membrane conductance g_m has the same effect on both $k^2\lambda^2$ and $\omega\tau$ and has little effect on the result as long as $\omega\tau + k^2\lambda^2 \gg 1$ (figure 2.10D).

In general, for cables passing near cell bodies, parameter variations within reasonable physiological limits have only small effects on the peak amplitude or the time course of the induced transmembrane voltage. The only parameter that has a large effect on the magnitude of ephaptic voltage transients is the location of the cable. The magnitude of the extracellular electrical field decreases sharply with distance; more than 10 μm away from the axon hillock, the peak extracellular potential amplitude has dropped to less than 1 mV, and induced transmembrane voltages also drop by the same amount.

2.3.2 Finite or bent axons, cells, and dendrites

Neural elements are straight for long distances only in nerve tracts, and perturbations of action potential timing are unlikely to be of great significance in such cases. Potentially more interesting interactions occur in neuropil, where it is much more important to consider neural elements with sharp bends, terminations, and branches. The effect of the extracellular potential is mediated by the derivative of its gradient in the direction of the axon or dendrite, and the gradient changes abruptly when the direction of the axon or dendrite changes. Therefore the largest effects can be seen at bends in neural processes (Markin, 1973b; Tranchina and Nicholson, 1986).

In neuropil, the modified cable equation 2.19 on page 36 must be rewritten in terms of an arc length parameter s instead of distance z, where the cable is described parametrically by $x = x(s)$,

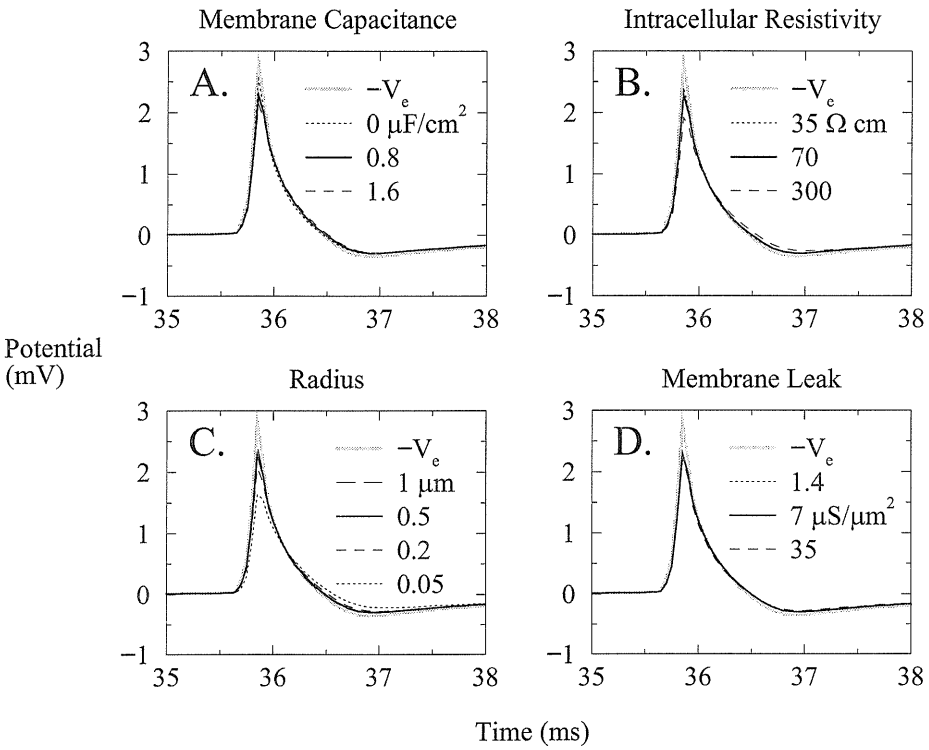

Figure 2.10: Effect of varying cable parameters on the transmembrane voltage induced by a spike in a nearby cell. Only the voltage at the center of the cable (the peak voltage) is shown. **A**: Variations in capacitance c_m, affecting only τ. **B**: Variations in intracellular resistivity, affecting only λ. **C**: Variations in the radius of the axon, which affects only λ. **D**: Variations in the membrane conductivity, which affects both λ^2 and τ proportionately. The parameter configuration used for figure 2.9 is shown with a solid black line in all four panels. In all cases, there is little effect within physiological parameter regimes.

$y = y(s)$, $z = z(s)$. With this modification, summing the currents into the node in figure 2.7 gives

$$\begin{aligned} c_m \frac{\partial V_m}{\partial t} + g_m V_m &= \frac{\partial}{\partial s}\left(\frac{1}{r_i}\frac{\partial V_i}{\partial s}\right) \\ &= \frac{\partial}{\partial s}\left(\frac{1}{r_i}\frac{\partial V_m}{\partial s}\right) + \frac{\partial}{\partial s}\left(\frac{1}{r_i}\frac{\partial V_e}{\partial s}\right) \end{aligned} \tag{2.26}$$

As discussed previously, this is exactly the standard cable equation except that V_m replaces V_i and there is a distributed current (the ephaptic current) injected into the cell of magnitude

$$i_{eph} = \frac{\partial}{\partial s}\left(\frac{1}{r_i}\frac{\partial V_e}{\partial s}\right) = \left(\frac{\partial}{\partial s}\frac{1}{r_i}\right)\frac{\partial V_e}{\partial s} + \frac{1}{r_i}\frac{\partial^2 V_e}{\partial s^2} \tag{2.27}$$

per unit length. The derivatives of the extracellular potential at the surface of the cable V_e depends on the extracellular potential ϕ in the tissue volume in a somewhat complicated way. We assume that ϕ on one side of the cable is approximately the same as ϕ on the other side of the cable, so we can treat the cable as one dimensional and use $V_e = \phi$ at a point instead of defining V_e as the average of ϕ over the cable's circumference.

$$\frac{\partial V_e}{\partial s} = \nabla\phi \cdot \mathbf{T} = -\mathbf{E} \cdot \mathbf{T} \tag{2.28}$$

where $\mathbf{E}$ is the electric field and $\mathbf{T}$ is the normalized tangent vector,

$$\mathbf{T} = \left(\frac{dx}{ds}, \frac{dy}{ds}, \frac{dz}{ds}\right). \tag{2.29}$$

The effective current is proportional to the second derivative,

$$\frac{\partial^2 V_e}{\partial s^2} = -\mathbf{T} \cdot \frac{\partial(E_x, E_y, E_z)}{\partial(x, y, z)}\mathbf{T} - \mathbf{E} \cdot \frac{d\mathbf{T}}{s} \tag{2.30}$$

where $\partial(E_x, E_y, E_z)/\partial(x, y, z)$ is the Jacobian of $\mathbf{E}$ (the Hessian of $-\phi$).

Axons and dendrites in neuropil tend to have kinks rather than smooth bends, so $\mathbf{T}$ is discontinuous and $d\mathbf{T}/ds$ is a sum of δ functions. As a result, the current source consists of a distributed current (the first term in equation 2.30) and a series of point current sources at each bend (the second term). The magnitude of each point current source is

$$I_{eph} = -\mathbf{E} \cdot \left(\frac{\mathbf{T}(s^+)}{r_i(s^+)} - \frac{\mathbf{T}(s^-)}{r_i(s^-)}\right) \tag{2.31}$$

where $\mathbf{T}(s^+)$ and $\mathbf{T}(s^-)$ are the tangent vectors on each side of the kink.

A similar situation occurs at a branch point. Summing the currents into the node in figure 2.11 gives

$$\frac{1}{r_{ia}}\frac{\partial V_{ia}}{\partial s_a} = \frac{1}{r_{ib}}\frac{\partial V_{ib}}{\partial s_b} + \frac{1}{r_{ic}}\frac{\partial V_{ic}}{\partial s_c}, \tag{2.32}$$

or

$$\frac{1}{r_{ia}}\left(\frac{\partial V_{ma}}{\partial s_a} + \frac{\partial V_{ea}}{\partial s_a}\right) = \frac{1}{r_{ib}}\left(\frac{\partial V_{mb}}{\partial s_b} + \frac{\partial V_{eb}}{\partial s_b}\right) + \frac{1}{r_{ic}}\left(\frac{\partial V_{mc}}{\partial s_c} + \frac{\partial V_{ec}}{\partial s_c}\right). \tag{2.33}$$

If we consider the transmembrane potential instead of intracellular potential, it looks like there is a current of magnitude

$$\begin{aligned} I_{eph} &= -\frac{1}{r_a}\frac{\partial V_{ea}}{\partial s_a} + \frac{1}{r_b}\frac{\partial V_{eb}}{\partial s_b} + \frac{1}{r_c}\frac{\partial V_{ec}}{\partial s_c} \\ &= \frac{1}{r_a}\mathbf{E}\cdot\mathbf{T}_a - \frac{1}{r_b}\mathbf{E}\cdot\mathbf{T}_b - \frac{1}{r_c}\mathbf{E}\cdot\mathbf{T}_c \end{aligned} \tag{2.34}$$

injected at the node.

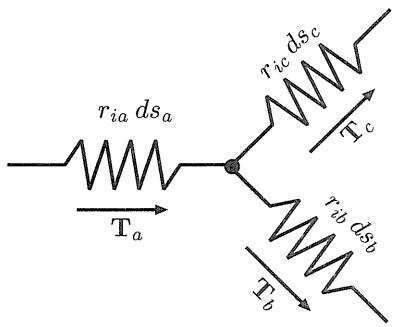

Figure 2.11: Calculation of ephaptic current at a branch point.

There is also an effective current injected at the ends of axons or dendrites. At the end of the cable, no intracellular axial current flows (sealed end condition):

$$\frac{1}{r_i}\frac{\partial V_i}{\partial s} = 0 = \frac{1}{r_i}\left(\frac{\partial V_m}{\partial s} - \frac{\partial V_e}{\partial s}\right). \tag{2.35}$$

Once again, in terms of V_m, it is as if there is a point current source of magnitude

$$I_{eph} = \frac{1}{r_i}\frac{\partial V_e}{\partial s} = -\frac{1}{r_i}\mathbf{E}\cdot\mathbf{T} \tag{2.36}$$

located at the end.

These special cases are all subsumed by a general rule: at any point along the cable, the ephaptic current is

$$I_{eph} = -\frac{1}{r_i}\mathbf{E}\cdot\mathbf{T} \tag{2.37}$$

summed over all of the cable segments that join at that point. This rule is also applicable for discontinuous changes in r_i.

How much influence do these ephaptic currents have? Extracellular potentials produced by cell spiking, at least from this particular pyramidal cell model, change very rapidly in space, and the induced transmembrane potential is already almost equal to the extracellular potential (section 2.3.1); V_m cannot grow any larger. For fields which do not change so rapidly in space, such discontinuities focus the effects of the electrical field and are likely to be important. For example, if electrical stimulation causes an action potential, it is much more likely to initiate at a discontinuity (Tranchina and Nicholson, 1986). With regard to interaction between cells, if the model for generation of extracellular potential is inaccurate and fields do not change as rapidly as it predicts, then kinks, terminals, and bifurcations will be the only places where $V_m \approx -V_e$.

2.4 Where does ephaptic interaction occur?

Ephaptic interaction has observed experimentally in a number of non-physiological situations, such as axons placed next to each other in a highly resistive medium (Katz and Schmitt, 1940, 1942; Arvanitaki, 1942; Ramón and Moore, 1978; Tabata, 1990) and in simultaneous electrical stimulation of many axons (Kocsis *et al.*, 1982) or cells (Nelson, 1966; Magherini *et al.*, 1976; Dalkara *et al.*, 1986; Turner and Richardson, 1991). It is clearly important in a number of pathological situations (reviewed in Faber and Korn, 1989; Jefferys, 1995). So far, there have been only two clear demonstrations of its effect in normal operations. In the case of the Mauthner cell (see Korn and Faber, 1980; Faber and Korn, 1989) the extracellular resistivity in the surrounding space is much larger than in most other systems by a factor of five or so, and as a result extracellular field potentials from firing of the Mauthner cell can be as large as 50 mV. In this case, inhibition has been observed bidirectionally, from the Mauthner cell to its inhibitory afferents and vice versa.

In the mammalian cerebellum, basket cells form a cap around Purkinje cell bodies. Because of glial cells and tight junctions, there is a strong barrier to current flow. The spike does not propagate actively into the synapses of the basket cell; as a result, there is a large current outflow from the synapse rather than an inflow, and the extracellular potential from the synapse is positive rather than negative. The Purkinje cell thus experiences a transient electrical hyperpolarization, followed by inhibition from the chemical transmitter (Korn and Axelrad, 1980).

The purpose for this electrical inhibition is unclear, since there is no obvious reason why a very fast inhibition is necessary. In fact, the purpose of the system may have nothing to do with ephaptic inhibition. For example, suppose that the tight junctions are present for some other reason (e.g., to prevent diffusion of neurotransmitter or some other chemical) and the ephaptic interaction is a side effect. There is also a reciprocal ephaptic interaction: when the Purkinje cell fires, the basket cell's synaptic terminals will be strongly depolarized. If active conductances were present in the

terminals, it might be possible for a spike to be initiated accidently ephaptically in the basket cell terminals. Perhaps for this reason the terminals are not active, and an unintended side-effect of inactive terminals is ephaptic inhibition.

So far there has been no clear evidence for ephaptic interactions in systems without such unusual geometries. For a long time there has been a suspicion that ephaptic effects could be important in the hippocampus, where the extracellular resistivity is somewhat higher than elsewhere in the brain. Several studies have shown significant effects of field potentials in response to electrical stimulation (Dalkara *et al.*, 1986; Turner and Richardson, 1991) but so far no interactions without electrical stimulation are known except in epilepsy (Snow and Dudek, 1984; Traub *et al.*, 1985a, 1985b).

Ephaptic effects are probably not interesting if all they do is accelerate or retard an action potential, as for a nerve bundle (section 2.3.1). Much more interesting are the cases where an action potential which would not otherwise be present occurs because of an action potential in a neighboring cell, or where an action potential that would have been present disappears. Ephaptic effects are not likely to be very large, since extracellular fields are almost never over a few mV, and probably never cause a spike on their own except in some pathological cases which are only of medical interest. They can affect action potential generation only in structures close to threshold: near the spike initiation zone of a neuron, or at points with low safety factor for propagation.

It is still unclear exactly where the spike initiates (Regehr and Armstrong, 1994). Early studies of motoneurons indicated clearly that the spike initiated somewhere in the axon, presumably the initial segment (Fuortes *et al.*, 1957; Coombs *et al.*, 1957a, 1957b; Dodge and Cooley, 1973). More recent studies reached the same conclusion for neocortical pyramidal cells (Stuart and Sakmann, 1994). In hippocampus, it was formerly thought that the fast prepotentials observed in somatic recordings were dendritic spikes, but now it seems more likely that these are impulses of adjacent neurons conducted through gap junctions (MacVicar and Dudek, 1981). In these cells too, action potentials appear to initiate in the axon, probably at the first node of Ranvier rather than the axon initial segment, and propagate into the dendrites (Colbert and Johnston, 1996). In all of these cases, the site of action potential initiation is somewhat removed electrotonically from the synaptic input and has a very high density of sodium channels in order for it to have a lower threshold than the soma. For several reasons one might expect ephaptic effects to be noticeable occasionally at the sight of initiation. First, it is close to several different geometrical inhomogeneities. There is a change in diameter from the soma and initial segment. Furthermore, bends and bifurcations near the soma are not uncommon. Second, cell bodies are lined up in layers in cortex and especially hippocampus; the sites of initiation are where the electrical fields are the largest are thus close to each other.

Once the action potential initiates, it propagates down the axon and up into the dendrites. For many years there has been speculation that under some circumstances propagation can fail at

branch points in the axonal arborization (Swadlow *et al.*, 1980). For example, action potentials from cerebellar granule cells might fail at the T-junctions with the parallel fibers (James Bower, personal communication). More recently, there is solid experimental evidence that failure occurs at dendritic branch points (Hoffman *et al.*, 1997) and also presumably at axonal branch points (Debanne *et al.*, 1997). In each of these cases, the place where the action potential is most likely to fail is also the place where ephaptic effects are largest: at a bifurcation. Interaction could occur if the action potential causing the large extracellular field is almost exactly coincident with the action potential in the dendrite or axon. Alternatively, if an A current is present (as suggested by recent results of Hoffman *et al.*, 1997 in dendrites and Debanne *et al.*, 1997 in axons), and it can be somewhat inactivated by ephaptic depolarization, ephaptic interaction might reduce branch point failure even if the spikes are not exactly coincident.

Dendritic bundles have been another candidate for ephaptic interaction (e.g., see Schmitt *et al.*, 1976; Roney *et al.*, 1979; Faber and Korn, 1989). Dendrites of many kinds of cells in many regions of the brain and spinal cord, including apical dendrites of neocortical pyramidal cells, come together in bundles (see Roney *et al.*, 1979 for a review) and the dendrites are often weakly active. Sometimes the dendrites are coupled through gap junctions[16]; sometimes gap junctions are absent and it is possible that ephaptic interactions mediate coupling (Matthews *et al.*, 1971; Zupanc, 1991). However, I find that potentials surrounding dendrites are likely to be very small, except possibly very near the soma, unless all the cells in the bundle fire together. If the purpose of dendritic bundling is to facilitate interaction, then the interaction is probably chemical rather than merely electrical.

Ephapses around cell bodies can be considerably stronger than typical excitatory chemical synapses between pyramidal cells. Unlike chemical synapses, however, they are difficult to modify once a neurite is grown because the magnitude of the depolarization is roughly independent of the cable properties of the post-ephaptic membrane (section 2.3.1). If ephaptic effects computationally useful, then it would be reasonable to expect that growth cones are directed by the electric fields set up by cell spiking activity.

Electric fields are known to have an influence on some growth cones. Depending on the type of cell and the experimenter, the magnitudes of the effect range from no effect even at fields as high as 200 mV/mm, to a noticeable effect at fields as weak as 2.5 mV/mm (see McCaig, 1988). Neurites are usually attracted to the cathode but in some cases they grow toward the anode. Axons and dendrites of the same cell may be affected differently; for example, dendritic growth cones on hippocampal cells in culture turned toward a cathodal microelectrode but axonal growth cones were unaffected (Davenport and McCaig, 1993). Substantial DC voltage gradients exist in the developing

[16]See Dermietzel and Spray (1993). In neocortex in development: Peinado *et al.* (1993); in adult hippocampus: MacVicar and Dudek (1981); in motoneurons: Magherini *et al.* (1976).

embryo, and electric fields may be one of the cues that growth cones use for guidance (McCaig and Zhao, 1997).

The vast majority of work on galvanotropism is concerned only with DC electrical fields; as far as I know, only one paper examines the effect of fields of the kind that might be produced by neural spiking activity (Patel and Poo, 1984). These experimenters found that *Xenopus* neural tube neurons grew asymmetrically when pulsed fields as low as 50 mV/mm (the lowest value tested) were applied; in general, the amount of asymmetry was the same as if the neurons were exposed to a DC field with the same time averaged value. Most neurites tended to grow toward the cathode, both in DC and pulsed fields. The same experimenters also performed time-lapse photography studies which showed that individual growth cones turned toward nearby microelectrodes when the field strength at the growth cone was as low as 6 mV/mm as long as the pulse frequency was sufficiently high. Fields of this magnitude certainly exist around spiking neurons, though they are very brief. If fields from action potentials do have an effect, it seems that they would guide the growing neurites nearer to cell bodies of neurons which are active in development.

Can the brain use short range ephaptic interaction to do anything useful, or is it just unwanted cross talk? Ephaptic interactions which affect branch point failure in axons could be used as a kind of switch: if cells in one region have just been active, then action potentials are more successfully propagated into that region. The purpose of action potential propagation in dendritic trees is not yet as clear; if it has to do with Hebb-based learning, ephaptic interactions could affect the signal that conveys the cell's own firing rate to its distal tips, so learning would occur only if the cell *and* neighbors located at strategic positions have both been active. In both of these cases, however, ephaptic interactions would be much smaller than the effect of repetitive activity in the axon or dendrite itself.

Ephaptic interaction is not trivial to observe experimentally using microelectrodes. Some investigators have used two electrodes, or a double-barelled pipette electrode and compared the extracellular and intracellular potentials directly. In hippocampal epileptic bursts, Snow and Dudek (1984) found that often the intracellular potential briefly decreased immediately before an action potential, raising the question of what triggered the spike. However, the transmembrane potential showed a clear depolarization leading up to the spike. This finding, that the actual change in V_m is opposite in sign to V_e, is typical of ephaptic interactions; V_e and V_i move in the same direction, but V_i moves less than V_e. A two-electrode experiment to test for ephaptic interaction on the distance scales examined here would be difficult because the two electrodes have to be so close together; one must be inside a small structure like an axon or dendrite, and the other must be within a few microns of the membrane.

Another way to look for specific ephaptic interaction would be to work in slices where synaptic

transmission has been pharmacologically disabled. Because of new microscopy techniques, it is now possible to record from the soma and the distal apical dendrites of the same pyramidal cell. Propagation of action potentials up the apical tree, and failure at branch points, have been observed in such preparations (Spruston *et al.*, 1995; Hoffman *et al.*, 1997). Action potentials could be evoked in the soma and recorded in the dendrites, while at the same time activating nearby cells either by glutamate iontophoresis, a minimal stimulation protocol, or even intracellular stimulation. Since normal chemical synaptic transmission is disabled, any effects on propagation failure must be electrical. Gap junctions can be ruled out by closing them pharmacologically, or possibly by examining the intracellular records for depolarization in one cell when the other spikes. Of course, propagation of action potentials up the apical tree of a neuron *in vivo* will be strongly influenced by the extensive ongoing synaptic activity, so this experiment can only indicate whether the effects are large enough to be significant. This technique is more difficult to apply to axonal branch point failure unless one can reliably trace an axon and measure intracellularly at different points in the arbor.

Ephaptic interactions with magnitudes of several mV are just on the border of being significant. The magnitude of these interactions is approximately proportional to the extracellular resistivity; if this were much higher, ephaptic effects would be much more widespread in the central nervous system. Some cross-talk may occasionally be useful for computation, but widespread crosstalk would probably be damaging. Extracellular resistivity is controlled primarily by the size and tortuosity of the extracellular medium. Since ephaptic effects are just on the border of being widespread, it is possible that the fundamental limits on average spacing between neural elements are set by the constraint to minimize ephaptic interactions.

Chapter 3 Extracellular potassium and other diffusible signals

3.1 Introduction

Besides the ephaptic effects considered in chapter 2, there are a number of other possible non-synaptic interactactions between neurons. Neurons clearly use some means of communicating without morphological specializations, e.g., gaseous messengers such as NO or CO. A number of other chemical interactions are possible, mostly based on byproducts of normal operation.

For example, there has been considerable interest in diffusion of neurotransmitter away from the synapse, possibly activating adjacent neural elements. Often glia are present around synapses to prevent such diffusion (see Peters *et al.*, 1991, pp. 288-290), but in some cases there is evidence of a significant effect (see Fuxe and Agnati, 1991).

Extracellular pH changes in neural activity because of neural metabolism, and extracellular pH has a profound influence on neuronal excitability. Rapid pH decreases of 0.1–0.2 pH units results in a net decrease in excitability (Syková, 1991). However, even during intense stimulation the pH rarely changes by more than 0.1 units except in pathological cases, so pH is unlikely to be a means of communication.

Other kinds of non-synaptic interaction have been suggested, mostly based on glia. For example, it is clear that NMDA receptors require glycine or D-serine in the extracellular medium to function at all. It is unclear where the required amounts come from. Interestingly, astrocytes do contain both glycine and D-serine, and they release it into the extracellular space non-synaptically via an antiporter mechanism in response to depolarization. Glial cells depolarized in response to ambient glutamate or other neurotransmitters or extracellular potassium increases (Attwell *et al.*, 1993; Shell *et al.*, 1995). Extracellular concentrations of other kinds of neurotransmitter are also controlled by glia (Cull-Candy, 1995; Pfrieger and Barres, 1996). It is possible, then, that glia modulate synapses in computationally interesting ways through controlling transmitter concentrations in the extracellular space. This area is not well enough explored experimentally to make any conclusions yet.

Probably the most important possible kind of chemical non-synaptic interaction is due to changes in extracellular ion concentrations. Concentration differences of ions across neural membranes give rise to most electrical activity in neurons, and therefore changes in these concentrations are po-

tentially of great significance for the computations neurons perform (see reviews in Somjen, 1979; Erulkar and Weight, 1979; Syková, 1983, 1991, 1997; Nicholson and Rice, 1991; Erecińska and Silver, 1994; Jefferys, 1995).

Outside the neuron, the concentration of potassium is low and the concentration of sodium is high. For this reason, the extracellular sodium concentration does not change significantly, while the extracellular potassium ion concentration can sometimes double or triple in periods of intense activity. Intracellularly, the situation is reversed, so potentially sodium accumulation could be important. However, the intracellular volume is usually much larger than the effective extracellular volume so concentration changes play little role (except in dendritic spines; Qian and Sejnowski, 1989, 1990).

In the peripheral nervous system, extracellular potassium seems to be cleared primarily through diffusion and reuptake by neurons. As a result, potassium transients can last up to 50–100 s (Hoppe *et al.*, 1991). In the central nervous system, potassium homeostasis seems to be one of the primary functions of astrocytes. At rest, their membrane has a large potassium permeability, enabling them to buffer it rapidly. They can also pump potassium faster than neurons. They are coupled through gap junctions, enabling potassium and other molecules to be moved more rapidly over long distances (Gardner-Medwin and Nicholson, 1983; Gardner-Medwin, 1983a, 1983b). There has been some speculation that the astrocytic network could regulate neuronal activity in computationally important ways by distributing extracellular potassium according to some blueprint, but at the present this seems unlikely (see Somjen, 1979).

Changes in extracellular potassium occur over large regions in epilepsy or when a nerve is repeatedly shocked electrically, because many cells are simultaneously active and the potassium homeostasis mechanisms are overloaded. In such cases, $[K^+]$ can rise from 3 mM to 10 mM or more (20–50 mM in the case of spreading depression). Extracellular potassium changes are therefore undoubtably important for various kinds of epilepsy (see Syková, 1983, 1997; Jefferys, 1995). It is less clear whether they are important in normal operation.

Small increases in extracellular potassium concentrations do occur in response to sensory stimuli. Large changes of up to 3 mM ($\Delta E_K \approx 20$ mV) can be measured in spinal cord 5–10 minutes after injecting formalin or turpentine into a rat's paw, apparently due to abnormal self-sustained neuronal firing in response to such painful stimuli (see Syková, 1991). More normal sensory stimuli cause less significant but still noticeable changes. For example, light touches or pinches cause a change of 0.1 to 0.5 mM ($\Delta E_K = 0.8$ to 4.2 mV) in spinal cord (Syková, 1991). When light is turned on a toad eyecup, there is a slow decrease in $[K^+]$ of up to 0.5 mM between the photoreceptors and the pigment epithelial cells, and an increase of 0.4 mM ($\Delta E_K = 3.4$ mV) primarily in the inner plexiform layer (Karwoski and Proenza, 1987). In visual cortex, passing a bar across a cell's receptive field caused

a change of 1–2 mV in E_K (Singer and Lux, 1975; Lux, 1976) or possibly higher ($\Delta E_K = 7$ mV, calculated from depolarization of glial cells). It is hard to see how such increases in extracellular potassium could be computationally useful, since they occur over a large area and they have a time course of hundreds of milliseconds; all neurons in the area would be affected, and the affect would last long after the stimulus is gone.

More interesting from a computational viewpoint is that extracellular potassium ions can act like a specific neurotransmitter over short distances. The action potential in the presynaptic neuron causes $[K^+]$ in the synaptic cleft to rise, depolarizing the postsynaptic cell. In some specialized systems, this effect is known to be important. For example, the calyx synapse from the type I hair cell completely surrounds the cell body of the hair cell. Goldberg (1996a, 1996b) has shown that because of this geometry, $[K^+]$ rises significantly in the cleft and augments the response to the traditional neurotransmitter (ACh). In some cases, K^+ is the only neurotransmitter. The giant interneurons of the cockroach come together in close apposition, and there is clearly an excitatory interaction between them, but there is no chemical synapse or gap junction. Instead, potassium released by an action potential in one is sufficient to depolarize the other (Yarom and Spira, 1982; Spira *et al.*, 1984).

There have only been a few attempts to record potassium concentration changes from single spikes. A change of 0.02 mM ($\Delta E_K = 0.2$ mV) was recorded for single spikes from mesencephalic reticular formation neurons. Bursts of activity caused larger responses (0.2 mM, $\Delta E_K = 1.7$ mV; Syková, 1991). For technical reasons, however, the actual change near the neuron is certainly much higher. First, ion-selective microelectrodes have a response time of at least several milliseconds due to the ion exchanger; simulations show that the largest local increases have a time course shorter than this (see below). Second, recording electrodes necessarily destroy the extracellular space. This is not a problem when recording field potentials because the voltage does not change much over distances comparable to the size of the electrode, but it is a serious problem when measuring concentrations, because the peak concentration change is expected to be localized to only the cleft immediately adjacent to the active neuron (see below). Hence the actual $[K^+]$ transients due to single action potentials cannot be measured experimentally with current technology except at considerable distances from the cell.

The transmembrane current caused by changes in extracellular potassium is proportional to the area of the membrane over which the change occurs (see section 3.7. As a result, the effect of changes in extracellular potassium will not be significant if it only occurs over a tiny area. Since I am not attempting to study increases in potassium over large volumes caused by the activity of many neurons, the only remaining kinds of possible interaction are cases where neural elements are apposed to each other for large areas, e.g., dendritic or axonal bundles. The changes in potassium

due to a spike at a cell body is likely to be larger because the potassium currents are larger, but it is also much more localized and so will have much less effect.

In this chapter, I have not attempted to compute the changes in extracellular potassium very precisely; instead, I have used simple approximations to estimate whether the effect is appreciable and worth modeling in some detail. These approximations indicate that potassium from single spikes is not likely to have a significant effect anywhere, so it is not worth simulating in detail on a fine spatial scale. A number of other theoretical studies have examined extracellular potassium on a much coarser spatial scale and longer time scale (Vern *et al.*, 1977; Cordingley and Somjen, 1978; Green and Triffet, 1985).

3.2 Nernst potential of Potassium

If the baseline extracellular potassium concentration is $n_{K,o\text{ before}} = 3$ mM (1.8×10^6 K^+ ions/μm^3; see Erecińska and Silver, 1994 for dozens of references) and it changes to $n_{K,o\text{ after}}$, the potassium reversal potential changes by

$$\begin{aligned}\Delta E_K &= \frac{kT}{e}\log\frac{n_{K,o\text{ after}}}{n_{K,i}} - \frac{kT}{e}\log\frac{n_{K,o\text{ before}}}{n_{K,i}} \\ &= \frac{kT}{e}\log\frac{n_{K,o\text{ after}}}{n_{K,o\text{ before}}}\end{aligned}$$

ΔE_K is approximately a linear function of Δn_K over the possible parameter range (figure 3.1) with a slope of $kt/en_{K,o} = 1.4 \times 10^{-5}$ mV-μm^3/ion.

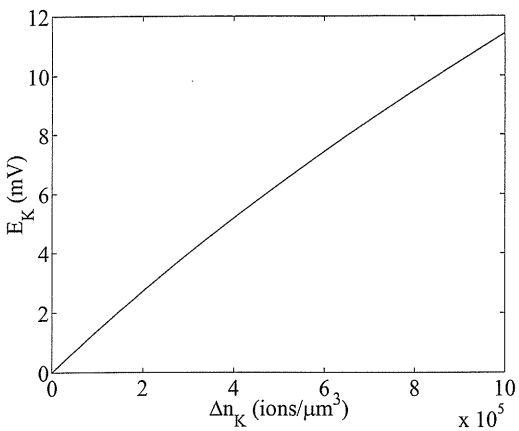

Figure 3.1: Potassium reversal potential as a function of the change in concentration of potassium. Over the possible relevant parameter regime, this is approximately linear.

3.3 Magnitude of potassium flux across membrane

If the membrane capacitance is 0.8 μF/cm^2, it is easy to show that about 5000 ions/μm^2 must flow across the membrane to change the voltage by 100 mV (approximately the height of an action potential). The number of potassium ions that actually flow across the membrane is considerably larger than this, however, because the sodium channel has not entirely shut off when the potassium channels open; there is overlap in the conductances. In measurements with radioactive tracers in a variety of unmyelinated invertebrate systems, the actual number of ions is usually about a factor of 3 larger than this minimum estimate (Cohen and De Weer, 1977). As a result, about 15,000 potassium ions/μm^2 cross the membrane. (I could calculate exactly how much K^+ crosses the membrane given a particular model of the action potential, but I do not have a model I am sufficiently confident in to make the prediction better than the empirical estimate.)

In the discussion that follows, I will assume that the flux of potassium, J_K, is constant for the time of repolarization and then suddenly drops to 0. It would be possible to calculate exactly the detailed time course of the extracellular potassium given a particular model, but since model parameters are not known, there is no advantage in using a smoothly varying time-dependence for J_K. Since the action potential repolarization phase lasts about 0.5 ms, this gives us $J_K \approx 30,000$ ions/μm^2/ms. This provides an upper limit on $[K^+]$ changes since it is likely that a significant fraction of the potassium crosses the membrane more than 0.5 ms later than the repolarization of the action potential.

3.4 Diffusion model

On the time scales we are interested in, potassium mobility is governed entirely by diffusion (the Nernst–Planck equation, equation 1.1 on page 5) and passive transport across membranes; active pumping is much too slow. The extracellular space is full of barriers to diffusion; there are membranes of axons, dendrites, and glia. To obtain an upper bound, I assume that these membranes are relatively impermeable to potassium on. Glial membranes are highly permeable to potassium, and this undoubtably a major means of potassium transport over long distances (Gardner-Medwin and Nicholson, 1983; Gardner-Medwin, 1983a, 1983b). However, it turns out that peaks in potassium concentration are localized to areas so small that there might not be any glia.

The Nernst–Planck equation can be used in a tortuous medium such as the extracellular space simply by modifying the diffusion constant:

$$D_K^* = \frac{D_K}{\lambda^2} \tag{3.1}$$

where λ is an empirical constant called the tortuosity of the medium (Nicholson, 1980; Nicholson and Phillips, 1981; see reviews in Nicholson and Rice, 1986, 1991; Nicholson, 1995). Tortuosities have been measured for a variety of tissues and are usually around 1.6 (Nicholson, 1995; Syková, 1997). If $D_K = 2.5\ \mu\text{m}^2/\text{ms}$ (Gardner-Medwin, 1983b; Qian and Sejnowski, 1989), then $D_K^* = 0.75\ \mu\text{m}^2$. This may be an overestimate; measurements suggest a value about 5–6 times lower than the coefficient in physiological saline ($0.39\ \mu\text{m}^2/\text{ms}$; see references in Vern *et al.*, 1977; Cordingley and Somjen, 1978).

The other necessary modification to the equation is that only a small fraction (usually about 20%, but about 30% in the molecular layer of the cerebellum; Nicholson, 1995; Syková, 1997) of the volume of the tissue is actually extracellular. This means that the concentrations of ions change by a factor of five more than they would in a liquid with the same D_K^*.

The Nernst-Planck equation describes electrodiffusion in three dimensions. However, for axons, we can take advantage of cylindrical symmetry and discard the angular dependence of ϕ and n_K. Furthermore, action potentials are spread out over a significant length of axon; if the propagation velocity is 0.1 mm/ms (for the slowest of the parallel fibers in the mammalian cerebellum), and the repolarization lasts 0.5 ms, potassium is being exuded over a length of 50 μm, which is much longer than the relevant diffusion lengths for short times (see below). In other axons, the action potential will be spread out over much larger distances so axial diffusion will be even less important. Therefore, to estimate the short time concentration changes, we also discard the dependence on location along the axon. The problem is reduced to finding the radial dependence of concentration changes around an infinite cylinder.

The most significant outflow of potassium ions occurs during the repolarization phase of the action potential, where the extracellular field is positive and the gradient is directed away from the axon. This electric field will encourage positive charges to migrate away from the axon, so the concentration changes near the axon will be smaller than they would be without the electric field. Mathematically, this can be seen from equation 1.1 on page 5 by noting that for fixed J_K, a larger $|\nabla\phi|$ means a smaller $|\nabla n_K|$. J_K will of course not be exactly fixed, but unless concentration changes or electric potentials are very large, it is approximately independent of Δn_K and ϕ.

Therefore if we want to estimate the largest possible magnitude of the concentration changes, it is a reasonable simplification to ignore the electric field. This is in fact not a bad approximation, since the extracellular potential is usually very small, on the order of microvolts except in situations where current flows through a restricted volume (section 2.2.2). Furthermore, the extracellular potentials decay less steeply than the concentration gradients[1]. So if extracellular potassium ion concentrations

[1]The same equation governs extracellular current flow as extracellular ionic diffusion, except that for practical purposes extracellular current flow is always in equilibrium whereas time is very important for diffusion. Therefore the the gradients will be the same as for diffusion which has reached steady state, and these gradients are smaller

change significantly, then $|\nabla n_K|/n_K$ will be significantly greater than $|\nabla\phi|/\alpha_K$.

After all these simplifications, the problem is reduced to a one-dimensional equation:

$$\frac{\partial n_K}{\partial t} = D_K^* \left(\frac{\partial^2 n_K}{\partial r^2} + \frac{1}{r}\frac{\partial n_K}{\partial r} \right) \tag{3.2}$$

with the boundary condition that $J_K = D_K^* \partial n_K/\partial r$ at the membrane ($r = r_0$) is a given value.

The Green's function solution to equation 3.2 can be obtained using an integral transform (Özişik, 1993, p. 111, or Carslaw and Jaeger, 1959, pp. 341-345). The full solution is

$$\Delta n_K = \int_0^t r_0 G(r, t|r_0, t') \frac{J_K}{\alpha} dt' \tag{3.3}$$

$$G(r, t|r', t') = \int_0^\infty \frac{\beta e^{-D^*\beta^2 t} R_\beta(r) R_\beta(r')}{N(\beta)} d\beta \tag{3.4}$$

$$R_\beta(r) = J_0(\beta r)Y_1(\beta r_0) - Y_0(\beta r)J_1(\beta r_0) \tag{3.5}$$

$$N(\beta) = J_1^2(\beta r_0) + Y_1^2(\beta r_0), \tag{3.6}$$

where Δn_K is the change in potassium concentration. (The absolute concentration n_K is unimportant if we neglect the electric fields.)

We are only interested in sources located at $r' = r_0$ (at the membrane). Using the identity that $J_1(z)Y_0(z) - J_0(z)Y_1(z) = 2/\pi z$, the Green's function $G(r, t|r_0, t')$ simplifies to

$$G(r, r_0, \Delta t) = \frac{2\pi}{r_0} \int_0^\infty e^{-D^*\beta^2 t} \frac{J_0(\beta r)Y_1(\beta r_0) - Y_0(\beta r)J_1(\beta r_0)}{J_1^2(\beta r_0) + Y_1^2(\beta r_0)} d\beta \tag{3.7}$$

I believe this integral cannot be solved in closed form in terms of common special functions (see, e.g., Jaeger, 1942, and the asymptotic expansions in Zonneveld and Berghuis, 1955)[2]. I approximated this under some limiting conditions and analyzed it numerically for the remainder.[3]

3.5 Analytic solution for large axons

It is possible to treat the axon as a thine line instead of a cylinder. The solution for this special case can be expressed in terms of exponential integrals, a well-understood special function. Unfortunately, although the line source approximation worked well for the fields around axons (section 2.2.1 on page 18), it does not work well for diffusion of potassium. Potassium falls off very steeply with

than for time-dependent diffusion.

[2]Some variations on this problem can be solved easily, such as a Gaussian cylinder (Vern *et al.*, 1977) or a point source (Nicholson and Phillips, 1981).

[3]A similar unpublished analysis (a Ph. D. thesis) is briefly described in Cordingley and Somjen (1978) but only for much longer time scales.

distance on short time scales (see below), and the falloff over the radius of the axon as predicted by the line source model is significant.

Instead of treating the radius of the axon as very small, as in the line source model, it is better to treat it as extremely large. Qualitatively, we expect larger changes in potassium ion concentration around large axons than small axons, simply because there is more space within a given distance around a small axon than a large axon.[4] Thus to estimate the maximum effects we should look at large axons. If we let $r_0 \to \infty$, the geometry changes from a cylinder to an infinite sheet. The Green's function for this geometry is well known to be[5]

$$G(r, r', t) = \frac{Q}{\alpha\sqrt{\pi D^* t}} e^{-(r-r')^2/4D^*t} \tag{3.8}$$

where r is the distance from the sheet. If the only source is at $r = 0$ and diffusion is only allowed in the positive r direction, then the concentration is:

$$\begin{aligned} \Delta n_K &= \int_0^t G(0, r, t') \frac{J_K}{\alpha}\, dt' \\ &= \frac{J_K}{\alpha\sqrt{\pi D^*}} \int_0^t \frac{e^{-r^2/4D^*t'}}{\sqrt{t'}}\, dt' \end{aligned}$$

This is still an intractable integral[6] but if we look at the place where the concentration is the highest ($r = 0$), it is easy:

$$\Delta n_{K,\max} = \frac{2J_K}{\alpha}\sqrt{\frac{t}{\pi D^*}} \tag{3.9}$$

Using the values discussed above, we find that after a 0.5 ms repolarization, $\Delta n_K = 1.4 \times 10^5$ ions/μm^3 and $\Delta E_K = 2$ mV. While this only gives the upper limit on a concentration change, it roughly shows how the change should depend on the various parameters. For example, if the same amount of potassium is exuded over a 1 ms time course instead of a 0.5 ms time course, then J_K is halved and t is doubled, decreasing Δn_K by a factor of $\sqrt{2}$.

[4] Crudely speaking, suppose ions can diffuse a distance Δr in the relevant time. Then the volume they occupy will be $\pi(r_0 + \Delta r)^2 - \pi r_0^2 = \pi(2r_0\Delta r + \Delta r^2)$. Into this volume, $2\pi r_0 \cdot J_K \Delta t$ ions/μm are discharged. The change in concentration will be $2\pi r_0 J_K \Delta t / \pi(2r_0\Delta r + \Delta r^2)$. This function initially increases linearly with r_0 but then saturates; the more exact solution has the same qualitative behavior.

[5] This can also be derived as a limiting case of equation 3.7.

[6] Actually, it can be written in closed form in terms of degenerate hypergeometric functions (Whittaker's functions). However, I didn't find this form enlightening.

3.6 Numerical solution

This upper limit is attained for realistic values of r_0. I evaluated equation 3.3 numerically[7] and found that Δn_K has basically reached its maximum value of about 2 mV for $r_0 = 2$ μm. Note that Δn_K is proportional to J_K, so if the ion flux is different, the y axis in figure 3.2 can be rescaled proportionately.

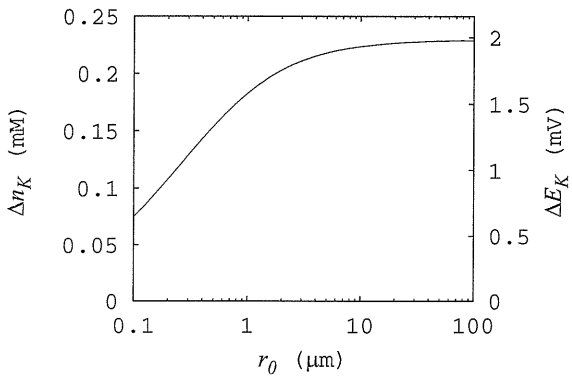

Figure 3.2: Change in concentration of potassium ions at the axon membrane as a function of axon radius at the end of 0.5 ms for $J_K = 30,000$ ions/μm ^{2}.

The potassium ion concentration changes fall off roughly exponentially with distance over the relevant range (figure 3.3). Given an exponential decay, unit analysis predicts that the form of the function must be $Ae^{-Br/\sqrt{D^*t}}$ where A and B are unitless constants, since $\sqrt{D^*t}$ is the only way to combine the relevant parameters to give units of length. I found that $B = \sqrt{2}$ provides close fits to the slope.

Figure 3.4 shows how the the potassium ion concentration changes vary with both distance and time for various values of r_0. It is clear that the spatial scale of potassium diffusion is very limited on these time scales; noticeable concentration changes will only be seen by the cell's immediate neighbor, and in fact only at the places where the membranes are apposed, not on the other side. In fact, the limited spatial scale suggests that a continuum diffusion model is not appropriate; it might be more useful to make a model with discrete elements. I do not expect changes of orders of magnitude in these numbers with such a model, however. In fact, a model by Lebovitz (1996) explicitly includes only the immediately adjacent 20 nm of extracellular space and models the rest of the tissue by a simple permeability to a constant reservoir.

[7]For $r = r_0$, we can use the identity $J_0(\beta r_0)Y_1(\beta r_0) - J_1(\beta r_0)Y_0(\beta r_0) = -2/\pi\beta r_0$ again to simplify the computation:

$$\Delta n_K = \frac{4J_K r_0}{\pi^2 D^* \alpha} \int_0^\infty \frac{1 - e^{-D^*\gamma^2 t/r_0^2}}{\gamma^3 [J_1^2(\gamma) + Y_1^2(\gamma)]}\, d\gamma \tag{3.10}$$

where $\gamma = \beta r_0$. For large γ, $J_1^2(\gamma) + Y_1^2(\gamma) \sim 2/\pi\gamma$, and $e^{-D^*\gamma^2/r_0^2} \approx 0$, so the integral from some point onward can be evaluated analytically. The remainder was evaluated numerically using Matlab's 4'th order adaptive Runge–Kutta–Fehlberg method.

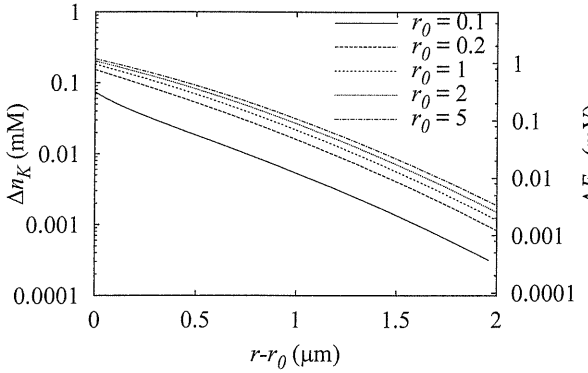

Figure 3.3: Change in potassium ion concentration as a function of distance from the axon after all the ions have been exuded ($t = 0.5$ ms). This is the maximum concentration at $r = r_0$; maximum concentration changes occur slightly later for $r > r_0$ (see figure 3.4). The concentration falls off roughly exponentially with distance.

The time scale for changes in extracellular potassium is very short. Concentration falls precipitously after J_K drops to 0. This can be seen more clearly in figure 3.5 for several different r_0 values. Modulations in extracellular potassium are important only during the time that the potassium is actually crossing the membrane; as soon as potassium ceases to cross the membrane, extracellular levels fall very rapidly. If there is short range interaction between neurons based on extracellular potassium, it has a very short time course.

3.7 Significance of changes in E_K

Are these changes in extracellular K^+ significant? No matter what happens, they cannot result in a larger membrane potential change than 2 mV, since E_K changes by at most 2 mV. However, an EPSP of 2 mV would be large in cortex and could have a significant effect.

A better way to estimate the significance is to calculate the extra current due to the increased extracellular potassium concentration:

$$\Delta I = g_K \Delta E_K \tag{3.11}$$

In dendrites, a typical time constant is $\tau = 20$ ms and the membrane capacitance is 8×10^{-6} nF/μm^2 (0.8 μF/cm^2), so the membrane conductance is 4×10^{-7} μS/μm^2, most of which is due to potassium channels. Roughly, then, if $\Delta E_K = 2$ mV, there is a peak current of 8×10^{-7} nA/μm^2. It seems unreasonable to suppose that membranes could be in apposition for more than 100 μm^2, so the maximum current into the cell would be 0.08 pA. By contrast, the peak current from a typical cortical synapse with a peak conductance of 0.5 nS and a 60 mV driving force is 30 pA, and this current may last several ms. In dendrites, one also finds that action potentials take much longer than 0.5 ms to repolarize, so the actual flux of potassium may be much lower. Brief potassium

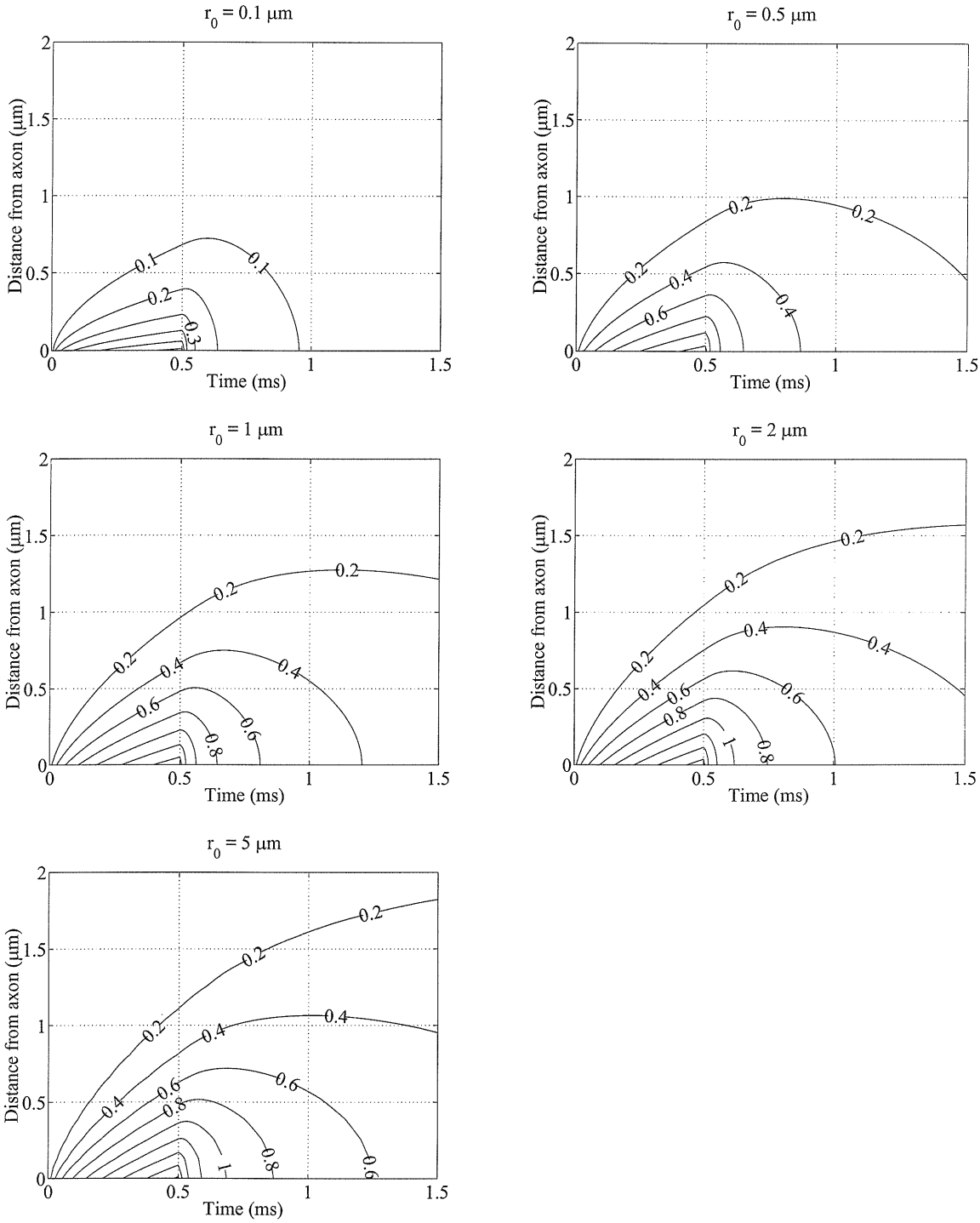

Figure 3.4: Contour plots of the changes in K^+ concentration around an axon for various sizes of axons. Numbers on the contours are changes in E_K (mV).

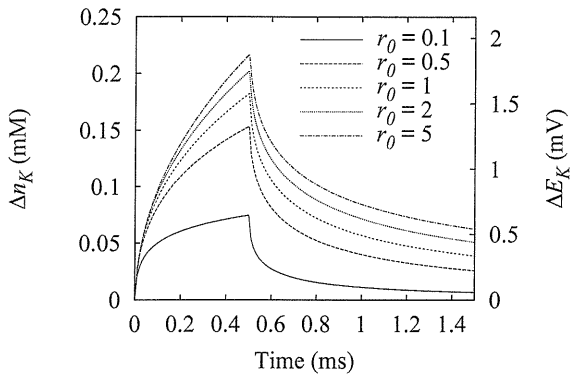

Figure 3.5: The time course of a change in extracellular K^+ at the membrane of the axon. Extracellular K^+ concentrations drop rapidly from their peaks as soon as the current is shut off (at $t = 0.5$ ms). The different curves correspond to axons of different sizes.

transients from single action potentials are therefore unlikely ever to be significant in interaction between dendrites in bundles.

Sustained potassium increases of this magnitude have been shown to cause small increases in conduction velocity of cerebellar parallel fibers, presumably because the axon is about 1 or 2 mV more depolarized everywhere (Kocsis *et al.*, 1983). Axons typically have shorter time constants (about 1 ms or less), implying that they could come close to their steady state value during the time course of an action potential. As a result, it is possible that in a bundle of unmyelinated axons, very transient extracellular potassium increases could speed up conduction slightly. However, as discussed in section 2.3.1 on page 36, a small change in latency is unlikely to be critical for most computations.

Lebovitz (1996) in his simulations found significant effects of extracellular K^+ changes only when he assumed a very narrow extracellular cleft and a large distance (20 μm) to the reservoir where $[K^+]$ was held constant. His model is difficult to compare directly because he modeled the extracellular space in terms of a monolayer of tiny rectangular cells surrounding one very large cell. It appears, however, that in the cases where he found significant interaction via K^+, his extracellular volume fraction was much too small (5% or even much less). He also adjusted his diffusion coefficient for tortuosity even though he explicitly models all of the membranes; however, this only changes the diffusion constant by a factor of 1.5, which does not explain the three orders of magnitude difference. There are some other details of his calculations which are unexplained in the paper. With the numbers he gives, the peak ΔE_K is about 7 mV, and yet for that case he calculates that the transmembrane voltage change is also about 7 mV. This is difficult to understand since the shift in E_K is very short-lived by my calculations. Lebovitz does not show the time course of Δn_K but he fits it to an exponential; in my calculations it seems to fall much faster than exponentially from its peak.

The effect of the slow evoked potassium transients that are measurable with ion-selective electrodes (e.g., Singer and Lux, 1975; Karwoski and Proenza, 1987) will be much larger than the transients from single spikes. First, the relevant area is larger, since $[K^+]$ is elevated over the entire surface of the neuron, which is from 10^4 μm^2 to 5×10^4 μm^2. This raises the above estimate of current by two or three orders of magnitude. Second, such large scale extracellular potassium transients are very slow, so the result will be a sustained current with an amplitude comparable to the peak of a synaptic current. It is not surprising, then, that such potassium transients cause a noticeable change in neural excitability.

Increases in extracellular potassium also affect synaptic transmission because they depolarize presynaptic terminals. Initially, this results in an increase in release probability. Beyond a certain point, however, it results in a *decrease* in transmitter release, evidently because the spike fails to propagate into the terminal because sodium conductances are inactivated (Somjen, 1979; Syková, 1983, 1987).

Part II

Implications of Cable Theory

In the space of one hundred and seventy-six years the Mississippi has shortened itself two hundred and forty-two miles. Therefore... in the Old Silurian Period the Mississippi River was upward of one million three hundred thousand miles long.... Seven hundred and forty-two years from now the Mississippi will be only a mile and three-quarters long.... There is something fascinating about science. One gets such wholesome returns of conjecture out of such a trifling investment of fact.

— Mark Twain

Chapter 4 Shunting Inhibition and Firing Rates

4.1 Introduction

Many neuronal models treat the output of a neuron as an analog value coded by the firing rate of a neuron. Often the analog value is thought of as what the somatic voltage would be if spikes are pharmacologically disabled (sometimes called a *generator potential*; see section 1.3). The neuron is modeled as if the spiking conductances were not present, as shown in black in figure 4.1.

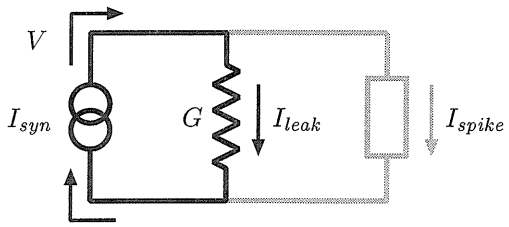

Figure 4.1: A simplified neuron at steady state. Synaptic current can be discharged either through the leak or the spiking mechanism. If the cell does not spike, then the current through the resistor will be equal to I_{syn}; changing G will change V proportionately. If the cell is spiking, then some of the synaptic current will be discharged through the spike mechanism (grey) so changing G will not have the same effect.

If there are no spikes, all the synaptic current I_{syn} must flow through the the leak (figure 4.1), so the voltage will be proportional to the synaptic current:

$$V = \frac{I_{syn}}{G}$$

where I_{syn} is the synaptic current and G is the input conductance. A firing rate is then computed directly from this above-threshold membrane potential:

$$f = g(V)$$

where g is some monotonic function. For example, $f_{out} \propto V^2$ in Carandini and Heeger (1994) or $f_{out} = \tanh(V)$ in Hopfield (1984).

Varying G, for instance via activation of inhibitory input with a reversal potential close or equal to the cell's resting potential (also known as "silent" or "shunting" inhibition), will directly affect the generator potential V in a divisive manner. A recent and quite popular model (Carandini and Heeger, 1994; Nelson, 1994) has suggested that changing G by shunting inhibition would be a useful way to control the gain of a cell: when the inhibitory input rate increases, the slope of the

Most of the contents of this chapter can be found in Holt and Koch (1997).

input–output relationship decreases (figure 4.2A) but the threshold does not change much.

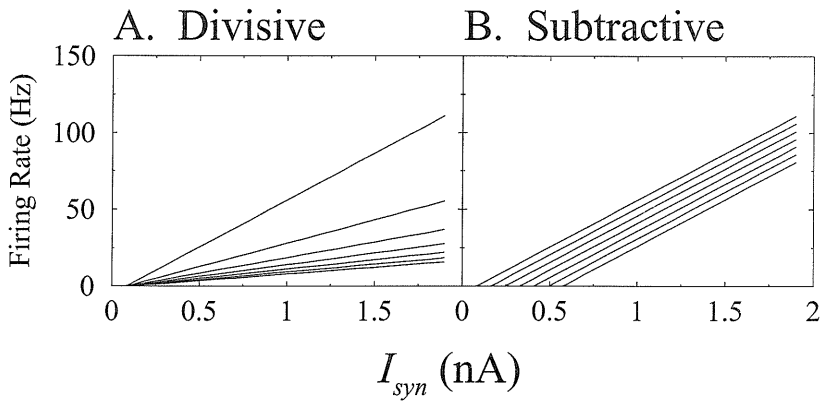

Figure 4.2: A comparison of divisive and subtractive inhibition. **A.** Divisive inhibition changes the slope of the input–output relationship. In this case, $f = g(V)$ was a linear function of V and G was varied from 10 to 70 nS in equal steps. **B.** Subtractive inhibition shifts the curves by subtracting a current. Here I_{inh} varies from 0.08 to 0.058 nA in equal steps.

On the other hand, inhibition which is not of the shunting variety should have a subtractive effect on the input–output relationship. If the reversal potential of the inhibition is far from the spiking threshold, then the inhibitory synapse will act more like a current source; the cell's conductance is not changed much, but a hyperpolarizing current is injected. This current simply shifts the input–output relationship by changing I_{syn} to $I_{syn} - I_{inh}$ (figure 4.2B) where I_{inh} is the inhibitory current.

Simplified models based on a generator potential ignore the effect of the spiking mechanism (figure 4.1 and assume that the behavior of the neuron above threshold is adequately described by the subthreshold equations. But when the cell is spiking, not all the current flows through the conductance G. The spiking mechanism itself removes charge, primarily through the potassium conductances that are responsible for repolarizing the spike (Koch *et al.*, 1995). Because of the spiking mechanism, we find that changing the membrane leak conductance by shunting inhibition does not have a divisive effect on firing rate, casting doubt on the hypothesis that such a mechanism serves to normalize a cell's response. A similar conclusion has been reached independently by Payne and Nelson for certain classes of neuron models (personal communication; Payne and Nelson, 1996).

4.2 Model description

Compartmental simulations were done using the model described by Bernander *et al.* (1991, 1994) and Bernander (1993) and Koch *et al.* (1995). The geometry for the compartmental models were derived from a large layer 5 pyramidal cell and a much smaller layer 4 spiny stellate cell stained

Type	Reversal potential	Number	g_{max}	τ	Area density	
					Near	Far
AMPA	0 mV	4000	1 nS	0.5 ms	$1+\tanh\left(\frac{x-40}{22.73}\right)$	$1+\tanh\left(\frac{x-100}{22.73}\right)$
$GABA_A$	−70 mV	500	1 nS	5 ms	$e^{-x/50}$	$1+\tanh\left(\frac{x-100}{22.73}\right)$
$GABA_B$	−95 mV	500	0.1 nS	40 ms	$xe^{-x/50}$	

Table 4.1: Parameters of synapses in the compartmental models. x is the length of dendrite in μm that separates this compartment from the soma. The "near" area density was used for figure 4.3; the "far" area density was used for figure 4.5 on page 70. The normalization for the area density is not included in the expression because it depends on the geometry; different neurons have different fractions of their membrane at a given distance from the soma.

during *in vivo* experiments in cat (Douglas *et al.*, 1991) and reconstructed. Geometries of both cells are shown as insets in figure 4.3B. Each model has the same eight active conductances at the soma, including an A current and adaptation currents (see Koch *et al.*, 1995 for details). The somatic conductance values were different for each cell, but the same conductance per unit area was used for each type of channel. Dendrites were passive. Simulations were performed with the program NEURON (Hines, 1989, 1993a).

To study the effect of $GABA_A$ synapses and shunting inhibition, we did not explicitly model each synapse; we set the membrane leak conductance and reversal potential at each location in the dendritic tree to be the time-averaged values expected from excitatory and inhibitory synaptic bombardment at presynaptic input firing rates f_E and f_I (as described in Bernander *et al.*, 1991). To compute the time averaged values, synapses were treated as alpha functions with a given time constant and maximum conductance ($g(t) = g_{max}te^{-t/\tau}e^{-1}/\tau$). The area density of synapses at a given location on a dendrite was a function of the length of dendrite that separated the area from the soma (see table 4.1). Two different sets of densities ("near" and "far") were used, depending on whether inhibitory synapses were near the soma or far from the soma. The "near" configuration is identical to the distribution used by Bernander *et al.* (1991) and reflects the anatomical observation that inhibitory synapses are mostly located near the soma in cortical pyramidal cells. The "far" configuration is not intended to be anatomically realistic. For simplicity, we used the same number of synapses for both the spiny stellate cell and the layer V pyramidal cell models.

Our integrate–and–fire model is described by

$$C\frac{dV}{dt} = -Vg_{leak} + I_{syn} \qquad \text{for } V < V_{th} \tag{4.1}$$

where g_{leak} is the input conductance and C is the capacitance and I_{syn} is the synaptic input. When the voltage V exceeds a threshold V_{th} the cell emits a spike and resets its voltage back to 0. We

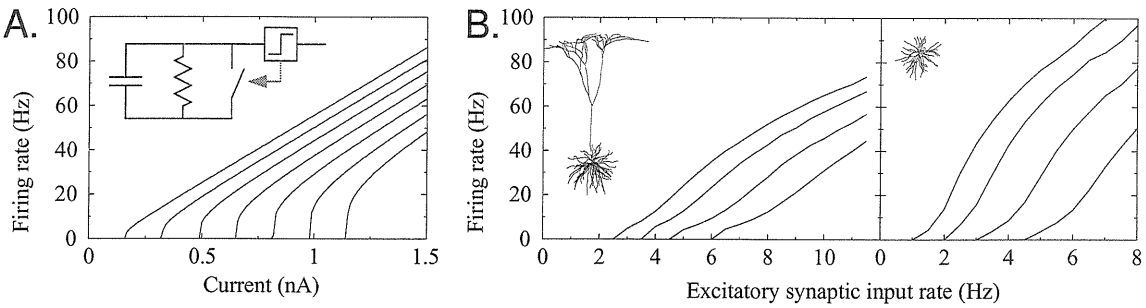

Figure 4.3: Changing g_{leak} has a subtractive rather than a divisive effect on firing rates. **A.** Current discharge curves for the integrate–and–fire model, with g_{leak} varying from 10 to 70 nS (from left to right) in steps of 10 nS. **B.** Fully adapted firing rates of the two cells as a function of excitatory input rate for different inhibitory input rates. From left to right, the curves correspond to a $GABA_A$ inhibitory rate of 0.5, 2, 4, and 6 Hz. Note that in all of these cases, the curve shifts rather than changes slope. In this case, inhibitory synapses were near the soma ("near" configuration in table 4.1 on the preceding page), as found in cortical cells.

used $C = 1$ nF, $g_{leak} = 16$ nS, $V_{th} = 16.4$ mV, which matches the adapted current–discharge curve of the layer 5 pyramidal cell model quite well (not shown). Results are not changed if a refractory period or an adaptation conductance is added to the integrate–and–fire model (also not shown).

4.3 Proximal inhibition

Changing g_{leak} does not change the slope of the current–discharge curve for integrate–and–fire cells (figure 4.3A); it primarily shifts the curves. It therefore has a subtractive rather than a divisive effect.

The compartmental models behave very similar to the integrate–and–fire unit. For two different geometries (a layer V pyramid and a layer IV spiny stellate cell), we computed the fully adapted firing rate as a function of the excitatory synaptic input rate for various different rates of inhibitory input to synapses with $GABA_A$ receptors (figure 4.3B). The slope of the input–output relationship does not change when the $GABA_A$ input amplitude is changed; the entire curve shifts. The same effect can be observed when considering the current–discharge curves (not shown).

This effect is most easily understood in the integrate–and–fire model. In the absence of any spiking threshold, V would rise until $V = I_{syn}/g_{leak}$ (figure 4.4 on page 68). Under these conditions, the steady state leak current is proportional to the input current. However, if there is a spiking threshold, V never rises above V_{th}. Therefore no matter how large the input current is, the leak current can never be larger than $V_{th}g_{leak}$. We can replace the leak conductance by a current whose value is equal to the time-average value of the current through the leak conductance ($\langle I_{leak} \rangle = g_{leak} \langle V \rangle$), and simplify the leaky integrate–and–fire unit to a perfect integrator. (Now, however,

$\langle I_{leak} \rangle$ will be a function of I_{syn}.) If the current is suprathreshold, the cell will still fire at exactly the same rate because the same charge $\int_0^T (I_{syn} - I_{leak})\, dt$ is deposited on the capacitor during one interspike interval T, although for the leaky integrator the deposition rate is not constant.

For constant just supra-threshold inputs, $\langle V \rangle$ will be close to V_{th} and $\langle I_{leak} \rangle$ will be large. For larger synaptic input currents, the time-averaged membrane potential becomes less and less (since V has to charge up from the reset point) and, therefore, the time-averaged leak current *decreases* for increasing inputs (compare figure 4.4A and B). It can be shown that

$$\langle I_{leak} \rangle = \begin{cases} I_{syn} & \text{if } I_{syn} < V_{th} g_{leak} \\ V_{th} g_{leak} \left(\dfrac{I_{syn}}{V_{th} g_{leak}} + \dfrac{1}{\log(1 - V_{th} g_{leak} / I_{syn})} \right) & \text{otherwise.} \end{cases} \tag{4.2}$$

For large I_{syn}, and even for quite moderate levels of I_{syn} just above $V_{th} g_{leak}$, the lower expression is approximately equal to $g_{leak} V_{th}/2$, independent of I_{syn} (figure 4.4C). Therefore it is a good approximation to replace the leak conductance by a constant offset current. The current–discharge curve for the resulting perfect integrate–and–fire neuron is simply[1]

$$f(I) = \frac{I_{syn} - \langle I_{leak} \rangle}{C V_{th}} = \frac{I_{syn}}{C V_{th}} - \frac{g_{leak}}{2C}. \tag{4.3}$$

Shunting inhibition (varying g_{leak}) above threshold acts like a constant, hyperpolarizing current source, quite distinct from its subthreshold behavior.

For currents just above the threshold, the initial slope is *larger*[2] for larger g_{leak} values (figure 4.3A), which is the opposite of divisive normalization. One way of understanding this is to observe that for larger g_{leak} there is a larger range of synaptic currents where I_{leak} is decreasing noticeably since g_{leak} is a scale parameter in equation 4.2. This effect is not visible in the compartmental models because they include adaptation currents which tend to linearize the current–discharge curve. The magnitude of this effect is also strongly reduced by noise (not shown).

A similar mechanism explains the result for the compartmental models (figure 4.3B). In these, the voltage does rise above the firing threshold. However, spiking conductances are so large that during a spike any proximal synaptic conductances will be ignored. Furthermore, the spiking mechanism acts as a kind of voltage clamp on a long time scale (Koch *et al.*, 1995) so that the time averaged voltage including the spike remains approximately constant (see appendix B and especially figure B.4 on page 132).

[1] This expression can also be derived from the Laurent expansion of the current–discharge curve for a leaky integrator, $f(I_{syn}) = -g_{leak}/C \log(1 - V_{th} g_{leak}/I_{syn})$, in terms of $1/I_{syn}$ around $I_{syn} = \infty$ (Stein, 1967).

[2] Actually, the slope is infinite for the leaky integrator at $I_{syn} = I_{th}$; however, for I_{syn} slightly greater than I_{th} it decreases more slowly to the constant value of $1/CV_{th}$ when g_{leak} is higher.

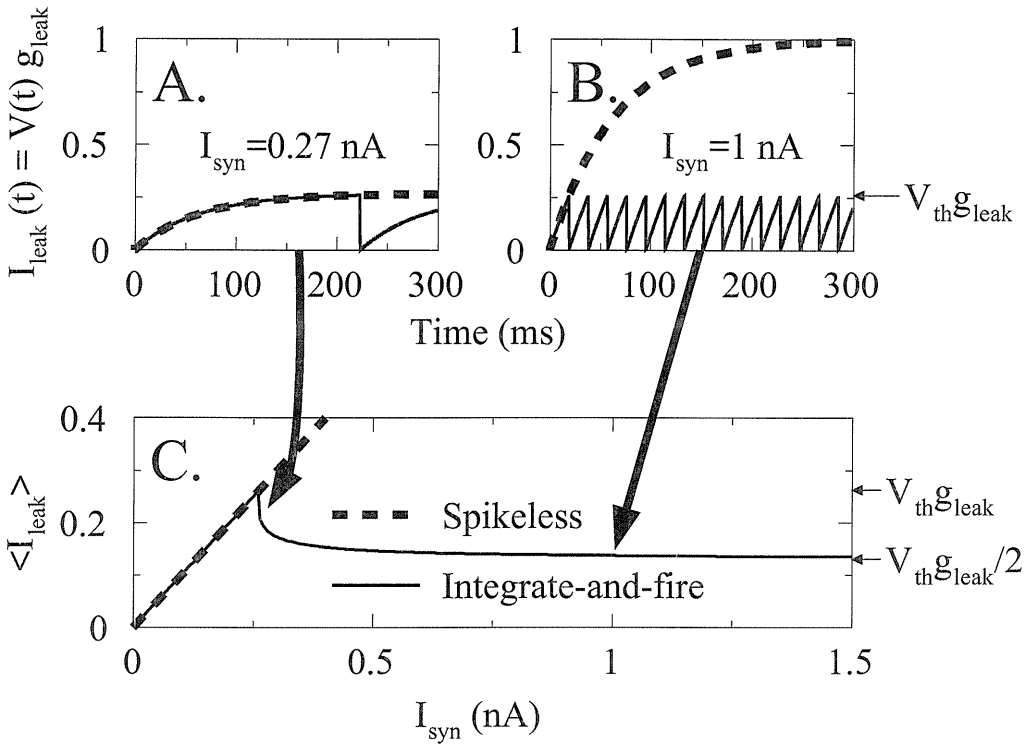

Figure 4.4: Why shunting inhibition has a subtractive rather than a divisive effect on an integrate–and–fire unit. **A.** The time-dependent current across the leak conductance I_{leak} (in nA) in response to a constant 0.5 nA current into a leaky integrate–and–fire unit with (solid line) and without (dashed line) a voltage threshold, V_{th}. The sharp drops in I_{leak} occur when the cell fires, since the voltage is reset. **B.** Same for a 1 nA current. Note that I_{leak} with a voltage threshold has a maximum value which is well below I_{leak} without a voltage threshold. **C.** Time-averaged leak current ($\langle I_{leak} \rangle$) in nA as a function of input current, computed from the analytic expression. Below threshold, the firing rate model and the integrate–and–fire models have the same I_{leak}, but above threshold $\langle I_{leak} \rangle$ drops for the integrate–and–fire model because of the voltage threshold. For I_{syn} just greater than threshold, the cell spends most of its time with $V \approx V_{th}$, so $\langle I_{leak} \rangle$ is high (panel A; at threshold, $I_{leak} = V_{th} g_{leak}$). For high I_{syn}, the voltage increases approximately linearly with time, so V has a sawtooth waveform as shown in panel B. This means that $\langle I_{leak} \rangle = (\max I_{leak})/2 = V_{th} g_{leak}/2$.

4.4 Distal inhibition

Shunting inhibition does not act divisively for an "anatomically correct" distribution of inhibition, where synapses are close to the cell body, because the spiking mechanism clamps the somatic voltage. However, distal synapses are not so tightly coupled electrically to the soma, so one might expect that distal $GABA_A$ inhibition might act divisively. Since the spiking mechanism can be thought of as a kind of voltage clamp (Koch *et al.*, 1995), one can study the neuron's response by examining the current into the soma when it is clamped at the time-averaged voltage V_s (Abbott, 1991). For analysis, we simplify the dendritic tree into a single finite cable which has an excitatory synapse (conductance g_E, reversal potential E_E) and an inhibitory synapse (g_I and E_I) located at the other end. The cable has length l, radius r, specific membrane conductance G_{leak}, intracellular resistivity R_i and a length constant $\lambda = \sqrt{r/(2R_iG_{leak})}$. Using the cable equation, one can show that at steady-state the current flowing into the soma from the cable is

$$I_{soma} = -g_\infty V_s + 2g_\infty e^{-L} \frac{g_E(E_E - V_s e^{-L}) + g_I(E_I - V_s e^{-L}) + g_\infty V_s e^{-L}}{(g_E + g_I)(1 - e^{-2L}) + g_\infty(1 + e^{-2L})} \tag{4.4}$$

where $L = l/\lambda$ is the electrotonic length of the cable and $g_\infty = \pi r^{3/2}\sqrt{2G_{leak}/R_i}$ is the input conductance of the cylinder but with infinite length. (In this equation, all voltages are relative to the leak reversal potential, not to ground.) Despite the simplification involved in equation 4.4, it it qualitatively describes the response of the compartmental model.

First, in the absence of any cable ($L = 0$), this equation becomes linear in both g_E and g_I and inhibition acts to subtract a constant amount from I_{soma}, as we have shown above.

When $L \neq 0$, some divisive effect is expected since g_I appears in the denominator. However, a subtractive effect will persist due to the term containing g_I in the numerator. The reversal potential of $GABA_A$ synapses (increasing a membrane conductance to chloride ions) is in the neighborhood of -70 mV relative to ground, while the time-averaged voltage when the model neuron is spiking is around -50 mV (Koch *et al.*, 1995). When a cell is spiking, therefore, a non-zero driving force exists for $GABA_A$ inhibition. In the pyramidal cell model, the subtractive effect turns out to be much more prominent than the divisive effect even for quite distant inhibition (figure 4.5 on the following pageA). Both the inhibitory and excitatory synapses have been moved to more than 100 μm (which is more than 1 λ) away from the soma. To a good approximation, inhibition still subtracts a constant from both the current delivered to the soma and the firing rate of the cell.

Equation 4.4 predicts that if the term containing g_I is removed from the numerator, then a divisive effect might be visible. When we changed the reversal potential E_I of the $GABA_A$ synapses as well as the leak reversal potential E_{leak} to $-50\ mV$, we found that there is indeed an observable

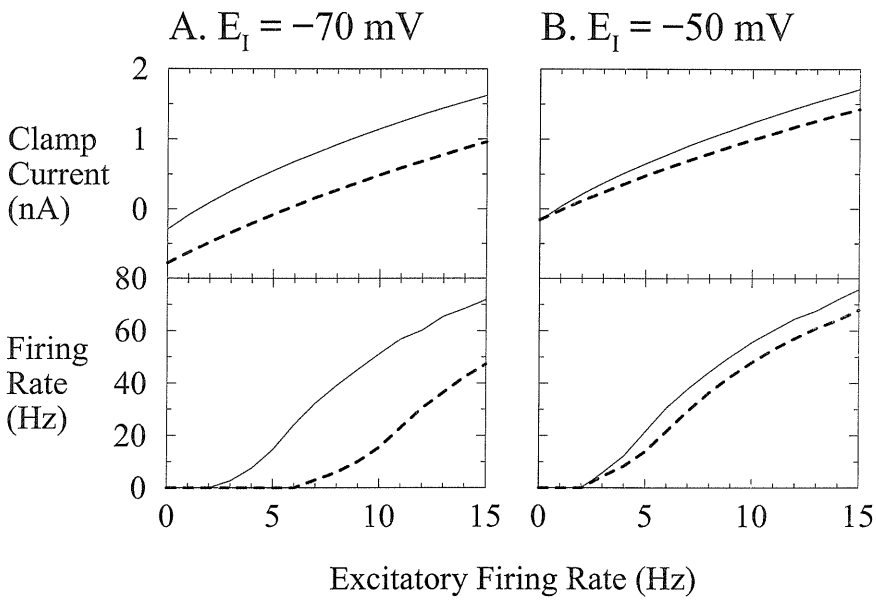

Figure 4.5: The effect of more distant inhibition on firing rates for the layer 5 pyramidal cell. **A**: The effect on the input–output relationship when inhibitory synapses are more distant from the soma ("far" configuration in table 4.1 on page 65). Inhibitory rates are 0.5 Hz (solid) and 8 Hz (dashed). In these simulations, E_I, the $GABA_A$ reversal potential, had its usual value of −70 mV. *Top*: The voltage clamp current when the soma is clamped to −50 mV, close to the spiking threshold of the cell. *Bottom*: The adapted firing rate when the soma is not clamped. Very little divisive effect is visible on the firing rate; there is a slope change for firing rates less than 20 Hz, but this is too small to have a significant effect. **B**: Same as A, except that E_I and the reversal potential of all leak conductances were changed to −50 mV so there is no driving force behind the $GABA_A$ synapses or the membrane passive conductance. A clear change in slope for low firing rates is evident. However, even for this rather unphysiological parameter manipulation, subtraction prevails at moderate and high input rates.

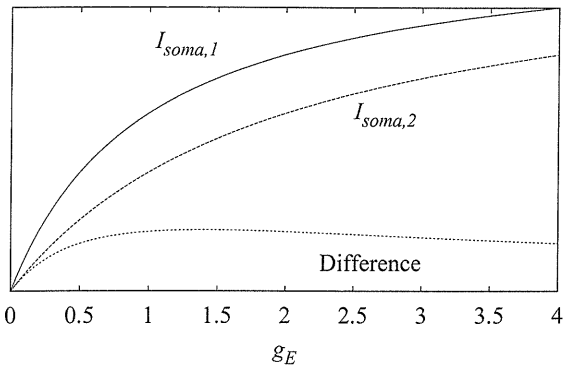

Figure 4.6: When g_E is not small compared to g_I, then inhibition acts more subtractively than divisively even when the IPSP reversal potential is equal to the somatic voltage. The two upper curves are I_{soma} as a function of g_E for two different values of g_I such that $g_I + B$ changes by a factor of two in equation 4.5. The lower curve is the difference between those two curves. For $g_E > g_I + B$, it is approximately constant over a large range. Units on g_E are chosen such that $g_E/(g_I + B) = 1$ for the smaller value of g_I.

change in slope at low firing rate (figure 4.5B). For higher firing rates, however, inhibition still acts approximately subtractively. We demonstrate this in the extreme case of moving both E_I as well as the reversal potential associated with the leak conductance to $-50\ mV$ (which is also the value to which the somatic terminal of the cable is clamped). Under these conditions, equation 4.4 simplifies to

$$I_{soma}(g_E, g_I) = \text{constant} + A\frac{g_E}{g_E + g_I + B} \tag{4.5}$$

where A and B are independent of g_E and g_I. Clearly if g_E is small, changing g_I simply changes the slope. When g_E is not small, then it turns out that changing g_I has an effect which is more subtractive than divisive (figure 4.6).

Another way of thinking about this is that $I_{soma}(g_E, g_I) \approx log(g_E/g_I)$ for $g_E > g_I$. Thus $I_{soma}(g_E, g_I) = log(g_E) - log(g_I)$ and inhibition is subtractive.

Since in the "far" model both kinds of synapses have the same distribution, their firing rates are proportional to the conductances. With the synaptic parameters we have used (table 4.1), $g_E/g_I = 0.8 f_E/f_I$; therefore, we expect to see a subtractive effect when $g_E > 6$ Hz, and this is approximately true (figure 4.5B).

4.5 Conclusions

Divisive normalization of firing rates has become a popular idea in visual cortex (Albrecht and Geisler, 1991; Heeger, 1992a; Heeger *et al.*, 1996). It has been suggested that this is accomplished through shunting inhibitory synapses activated by cortical feedback (Carandini and Heeger, 1994; Nelson, 1994). Most discussions of shunting inhibition have assumed that the voltage at the location of the shunt is not constrained and may rise as high as necessary (e.g., Blomfield, 1974; Torre and Poggio, 1978; Koch *et al.*, 1982, 1983). However, when the shunt is located close to the soma, the

voltage at the site of the shunt cannot rise above the spike threshold. Therefore the current that can flow into the cell through the shunting synapse is limited, and at moderate rates becomes a constant offset (figure 4.4C; appendix B). The current through the shunt is approximately independent of the firing rate. For this reason, shunting inhibition under these circumstances implements a linear subtractive operation.

Even if the conductance change is not located close to the soma, it may not have a divisive effect (figure 4.5A). First, when the cell is spiking, shunting inhibition is not "silent": there is a significant driving force behind $GABA_A$ inhibition, since the somatic voltage is clamped to approximately -50 mV by the spiking mechanism and the reversal potential for $GABA_A$ inhibition is in the neighborhood of -70 mV. Second, even if the reversal potential for $GABA_A$ and the leak reversal potential are set to -50 mV, inhibition acts divisively only if the excitatory synaptic conductance is small compared to the inhibitory conductance (figures 4.5B and 4.6). Large excitatory conductances are expected when the cell receives significant input (Bernander *et al.*, 1991; Rapp *et al.*, 1992) so the subtractive effect of large conductances is relevant physiologically.

Current–discharge curves are affected as predicted by the simple integrate–and–fire model in response to IPSPs and GABA iontophoresis in motoneurons *in vivo* (Granit *et al.*, 1966; Kernell, 1969) and cortical cells *in vitro* (Connors *et al.*, 1988; Berman *et al.*, 1992). The input–output curves for different amounts of inhibition do not diverge for larger inputs, as would be required for a divisive effect; in fact, they converge at high rates because of the refractory period (Douglas and Martin, 1990). In recordings from *Limulus* eccentric cells, current–discharge curves show both a slope change and a shift (Fuortes, 1959) because the site of current injection is distant from the site of spike generation.[3] Rose (1977) showed that iontophoresis of GABA onto an *in vivo* cortical network appeared to act divisively. Because shunting inhibition has a subtractive effect on single cells, this could possibly be caused by a network effect (Douglas *et al.*, 1995).

For synapses close to the spike generating mechanism, as well as for the integrate–and–fire unit, the subtractive effect of conductance changes does not depend on the reversal potential of the conductance. Changing the reversal potential is equivalent to adding a constant current source in parallel with the conductance, and in a single compartment model this will obviously merely shift the current–discharge curve. Therefore, like inhibitory input, proximal excitatory input does not change the gain of other superimposed excitatory input.

Similarly, our results are not affected by a "weak reset" (where the voltage is reset to a voltage closer to V_{th} instead of to 0; Tsodyks and Sejnowski, 1995; Troyer and Miller, 1996); such models are mathematically equivalent to an integrate–and–fire model of the kind we consider here with a

[3] In this case, only the current–discharge curve was measured; the considerations in Figs. 4.5 and 4.6 are not relevant. A slope change is expected for current injection but not synaptic input.

lower V_{th} and a leak conductance with a non-zero reversal potential.

Our analysis assumes that synaptic inputs change on a time scale slower than an interspike interval. High temporal frequencies may be present in synaptic input currents for irregularly spiking neurons. Furthermore, our analysis assumes passive dendrites; active dendritic conductances complicate the interaction of synaptic excitation and inhibition.

Although we cannot rule out that under some parameter combinations shunting inhibition could act divisively on the firing rates, we have not found such a range for physiological conditions. In combination with our integrate–and–fire and single cable models, we believe that a different mechanism is necessary to account for divisive normalization.

The compartmental models and associated programs are available from `ftp://ftp.klab.caltech.edu/pub/holt/holt_and_koch_1997_normalization.tar.gz`.

Chapter 5 The Membrane Time Constant and Firing Rate Dynamics

5.1 Firing rate dynamics in single compartment neurons

Action potentials report only intermittently the activation of their source neuron. Therefore, the post-synaptic cells must estimate the activation either by averaging single presynaptic action potentials over times longer than the average inter-event interval, or by taking the near instantaneous average over multiple sources of similar presynaptic input. Whatever combination of these strategies is used, the speed of response of the post-synaptic cell is interesting because it bears on the rapidity with which a signal can propagate through a network of neurons.

5.1.1 Response time of non-spiking or firing-rate neurons

The passive membrane time constant is often used to characterize the time scale of a neuron's response to changes in its input. Injecting a constant current into the soma of a cortical neuron causes the membrane potential to increase gradually with a time course governed by the membrane's passive properties, if active currents are disabled. In a simplified one-compartment model, such as the kind considered by Hopfield (1984) and Carandini and Heeger (1994), the passive response to somatic input can be approximated by a simple equivalent electronic circuit consisting of a capacitance and a conductance in parallel (black lines in figure 5.1). The voltage response at the output node of this circuit to a current input is given by

$$\frac{dV}{dt} = -\frac{V}{RC} + \frac{I}{C} \tag{5.1}$$

where V is the membrane potential, C is the membrane capacitance, R is the membrane resistance, and $\tau = RC$ is the membrane time constant. This model can be simply extended to account for the effects on the time constant of variable parallel synaptic conductances that could control the gain and temporal integration of neurons (Bernander *et al.*, 1991; Rapp *et al.*, 1992; Carandini and Heeger, 1994). A neuron with a complicated dendritic geometry behaves qualitatively similarly in response to somatic current injection: the rate of somatic voltage change is also governed by the

This work was done in collaboration with Rodney Douglas and Misha Mahowald, to whom I am indebted for some of the text as well.

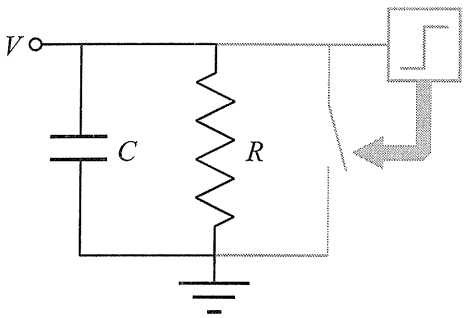

Figure 5.1: Simplified circuit models which ignore the spatial extent of the neuron and collapse it to a single point are usually based on this circuit. The time constant, $\tau = RC$, is the time it takes for the membrane voltage V to reach $1 - 1/e$ of its final value in response to a step change in current. Often in firing rate models (black), the voltage is computed using this circuit and then a firing rate is computed as a function of the voltage. The time constant then determines the dynamics of the firing rate because firing rate dynamics are essentially the same as the voltage dynamics. In models which represent spikes explicitly (grey), when the voltage reaches a threshold, it is reset to 0. The presence of the spiking mechanism completely changes the dynamics not only of the voltage but also of the firing rate; the voltage never reaches an equilibrium, so there is no time constant that governs the firing rate.

time constant τ (Rall, 1962, 1969). The differences between an extended and a point neuron will be considered in section 5.2.

The important issue is that the passive time constant is often seen to be crucial to the response, even if the response consists of action potentials. As discussed in section 1.3 on page 10, in some older literature and a number of newer models, voltage is viewed as the primary signal, and action potentials are thought of as merely minor perturbations. For this reason neuronal models that are concerned with average neuronal activation rather than individual spike timing commonly reduce the neuron to a single compartment whose dynamics are given by equation 5.1, and whose firing rate is some monotonic function of the somatic voltage:

$$f = g(V) \tag{5.2}$$

Usually, g is sigmoidal, that is, a monotonic increasing, positive and saturating function (as in the popular choice of $f = \tanh V$ in Hopfield (1984)). However, other functions have also been used (e,g, $f \propto V^2$ in Carandini and Heeger (1994)). Such *firing-rate models* incorporating a low-pass filter to capture the passive properties of the underlying membrane have been applied widely in abstract neural network analysis (e.g., Hopfield, 1984 and the innumerable papers spawned from it, such as Kleinfeld, 1986) and also in more biological models (e.g., Wilson and Bower, 1989; Wörgötter and Holt, 1991; Abbott, 1991; Carandini and Heeger, 1994; Carandini *et al.*, 1996a, 1996b, 1997). In this class of model the firing rate can only change gradually in response to a rapid change in I. For small steps in input current $g(V)$ is approximately linear. In the linear regime, the firing rate,

f, is simply I convolved with a first order low pass filter with time constant τ, and is therefore a smoothed version of the input.

The response to a step input current provides a useful case for comparisons. Suppose a firing-rate neuron has a constant input current $I_0 = 0$, and then at time $t = 0$ the current is suddenly changed to I_1. How long will it take the firing rate to reflect the new input value? The remarkable property of linear systems is that they take a single characteristic time to approach their equilibrium state, regardless of how far it is. Doubling the input current doubles the distance to the equilibrium state but the system still only takes a time τ to reach $1 - 1/e$ of equilibrium state. For this reason, the subthreshold time constant has been used as a measure of how long each stage in a feedforward neural network will take.[1]

It is possible to shorten the response time by introducing a nonlinearity. For example, if $g(V)$ is a saturating function (Hopfield, 1984) and the steady state firing rate of the neuron is close to its maximum rate, then the firing rate may reach $1 - 1/e$ of its final value much earlier than V reaches $1 - 1/e$ of its final value. Convergence time in a saturating neuron is the time that it takes V to rise high enough to saturate the firing rate, not the time for voltage to reach equilibrium. Increasing the current will allow V to reach that level faster.

However, in most parts of the brain, neurons are typically not either silent or firing at their maximum rates. Furthermore, this kind of a saturating nonlinearity has several disadvantages. First, the firing rate of this neuron responds more slowly to decreases in current than a linear neuron for precisely the same reason as it responds more rapidly to increases in current: the firing rate changes slowly as a function of voltage when the voltage is high. Second, the saturating neuron does not transmit analog information; it either discharges near its maximum rate, or does not.

5.1.2 Response time of spiking neurons

Another important kind of nonlinearity is the spiking mechanism itself. The integrate–and–fire model is the simplest spiking model, and has been used extensively ever since it was proposed by Lapicque (1907). This model neuron has a membrane voltage which also obeys equation 5.1. However, when the voltage reaches a threshold V_{th}, a spike is emitted and the membrane voltage is reset (figure 5.2A).

The dynamics of the firing rate of a leaky integrate and fire neuron differ fundamentally from the dynamics of the firing rate models governed by equation 5.2. In firing rate models or in a subthreshold integrate–and–fire neuron, τ measures the time to reach $1-1/e$ of a steady state membrane potential. However, if the neuron is firing the voltage never reaches equilibrium. Therefore τ is not a measure

[1]Note that the effective time constant can be increased in the presence of positive feedback; recurrent networks often have much longer time constants than their individual components (chapter 6).

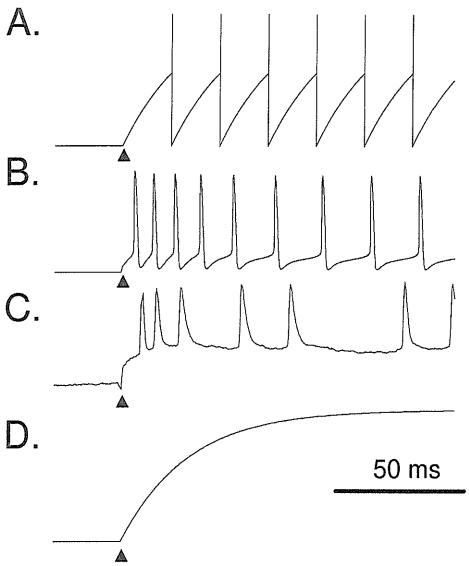

Figure 5.2: Sample spike rasters in response to a step current injection. Arrows mark onset of current. The firing rate in spiking cells does not gradually increase; the effect of the change in current is fully visible in the first interspike interval. **A.** An integrate–and–fire unit, $R = 20$ MΩ, $C = 1$ nF, $V_{th} = 16.4$ mV, $I = 1.6$ nA. **B.** A layer V compartmental model from Bernander *et al.* (1991), 1.5 nA. This model shows adaptation; the firing rate reaches its maximum after the first ISI and declines slowly after that. **C.** A cell *in vivo* from area 17 of the anesthetized cat responding to a 0.6 nA injection current. Taken from Ahmed *et al.* (1993). **D.** For comparison, the firing rate as a function of time from a non-spiking non-adapting model neuron with a time constant of 20 ms. Unlike the spiking neurons, this neuron's firing rate increases gradually.

of response time.

A spiking neuron's steady state is a limit cycle (an oscillation), not an equilibrium value. In its simplest form, the integrate–and–fire unit has only one state variable, its membrane voltage. When the neuron spikes, and the state variable is reset, it loses memory of the previous input current, and begins to respond to the new current by charging toward the threshold. If there is a step change in current, from these considerations it follows that the first complete interspike interval after the change reflects the new current; everything during the first interspike interval after the change is exactly the same as during the second interspike interval, so the second interval will not be different from the first.

Figure 5.2 shows the step response of an integrate–and–fire unit, a compartmental model of a cortical pyramidal neuron, and an experimental record derived from a neuron in cat visual cortex *in vivo*. The first interspike interval already reflects the new firing rate—the convergence occurs on as short a time interval as can be defined (i.e., the interspike interval).

More complicated spiking neurons behave similarly. Compartmental models (figure 5.2B) and cortical cells *in vitro* (figure 5.2C) also reach their maximum firing rate by the first interspike interval. Thereafter, the firing rate decreases slowly because of adaptation.

Unlike the firing rate neuron, the response time for a spiking neuron is not the time to reach an equilibrium voltage which is proportional to the input. In the case of the simplest possible spiking mechanism, the integrate-and-fire neuron, the neuron is on its new steady-state limit cycle immediately, as soon as the current changes, so in one sense it can be said that there is no delay at all. If one is looking at the spiking output of an ensemble of neurons, this means that the change

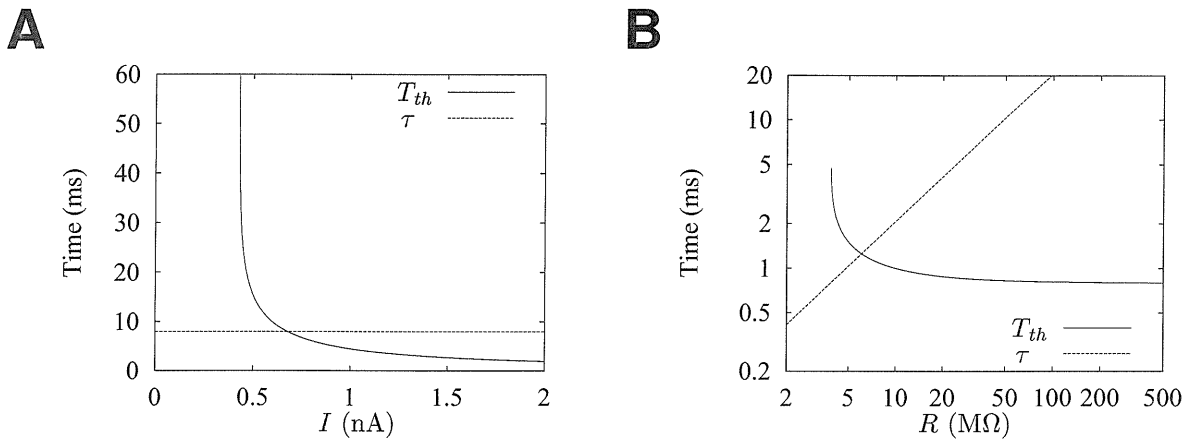

Figure 5.3: Measures of the response times of different kinds of neurons. T_{th} is the maximum time it takes for an integrate–and–fire cell to fire one spike; since the firing rate of such a neuron has reached its final value after the first interspike-interval after a change in input, this is a measure of the speed of response. τ is the subthreshold time constant, and is a measure of the response speed of the firing rate models. **A.** Effect of changing the current I on the response time. Using this measure, responses of a spiking neuron become faster with larger changes. **B.** Effect of changing the resistance R. Paradoxically, the spiking neuron becomes *faster* as τ increases. Parameters: $C = 0.207$ nF, $V_{th} = 16.4$ mV. In A, $R = 38.3$ MΩ, $\tau = RC = 8$ ms. In B, $I = V_{th}/R_{min} = 4.3$ nA.

can be detected instantly (see below); however, if one can only examine a single neuron's output, there will be no measurable effects until that neuron actually spikes.

For a single neuron, then, the relevant response time is the time required for V to reach a particular voltage: the threshold, V_{th}. In the case of the non-spiking neuron, the response time is the time to reach $(1 - 1/e)$ of its steady state value, which varies with the input; in this case, the response time is the time to reach a voltage which does not vary with the input. As a result, the response time will be shorter for stronger inputs.

Unless inhibition is strong, V will always be greater than the reset voltage. The maximum latency is therefore the time the membrane takes to charge up from reset with the current I_1:

$$T_{th} \leq -RC \log\left(1 - \frac{V_{th}}{I_1 R}\right) \tag{5.3}$$

When the final firing rate is higher, the latency is shorter. Although the time constant, $\tau = RC$, is independent of the input current, the latency, T_{th}, decreases with increasing current (figure 5.3A).

The situation is slightly different for step decreases in input current, because it takes more time to measure a low firing rate. In this sense, the response to a decrease in firing rate is slow because to measure the new firing rate a postsynaptic neuron will have to wait for one interspike interval

at the new low firing rate. However, after waiting for just one interspike interval at the old rate, a postsynaptic neuron can detect that the firing rate has decreased because the spike does not occur at the expected time. It may have to wait much longer to find out exactly how much the firing rate has decreased.

If τ is increased by increasing the neuron input resistance R, the rate of change of the subthreshold voltage is actually *higher* because increasing R reduces the leak current. Therefore the spiking neuron reaches threshold more quickly (figure 5.4). In contrast, although dV/dt is also higher in the firing rate model when R is increased, it takes longer to reach $1 - 1/e$ of the equilibrium voltage because the equilibrium voltage is also increased (figure 5.4A). In the extreme case, when $\tau \to \infty$, the firing rate model does not even asymptotically approach an equilibrium, but the integrate–and–fire emits spikes from its steady state limit cycle sooner than it does for a finite τ. Therefore decreasing τ will not make a spiking neuron respond faster, as is required by some models (Carandini and Heeger, 1994); if anything at all, it makes it respond slower.

The nonlinearity in the spiking model is in the membrane voltage, whereas in the saturating model the nonlinearity is in the translation between the membrane voltage and firing rate. Both kinds of nonlinearity can speed up the response because the voltage needs to rise to a given constant value rather than a value dependent on input. However, the spiking neuron communicates an analog value, whereas the saturating neuron communicates only a digital value (0 or maximum firing rate).

5.1.3 Response time of an ensemble of neurons

So far we have considered the temporal response of single neurons, in which the firing rate can be defined only for a whole interspike interval. In this case, it makes no sense to talk about response times on any time scale less than the interspike interval. However, postsynaptic neurons receive input from many different presynaptic neurons. The response times of an *ensemble* of spiking neurons may be a more relevant measure of response than the event times of only a single neuron. A PSTH of firing times can be constructed, not for the response of a single neuron to a repeated stimulus, but for the responses of many neurons to a stimulus presented once. As usual in neurophysiology, the PSTH can be used to define a firing rate during a short time interval dt: f = number of cells $\times$ P(one cell firing)$/dt$. There is no requirement that dt be longer than an interspike interval; the firing rate is well defined for much shorter time scales because we are examining the output from many neurons.

Suppose that many identical neurons which are independent of each other are all responding to the same input stimulus. (Knight, 1972 has analyzed this case in some detail for population encoding of a sensory stimulus.) For simplicity, suppose for the moment they are non-leaky integrate-and-fire

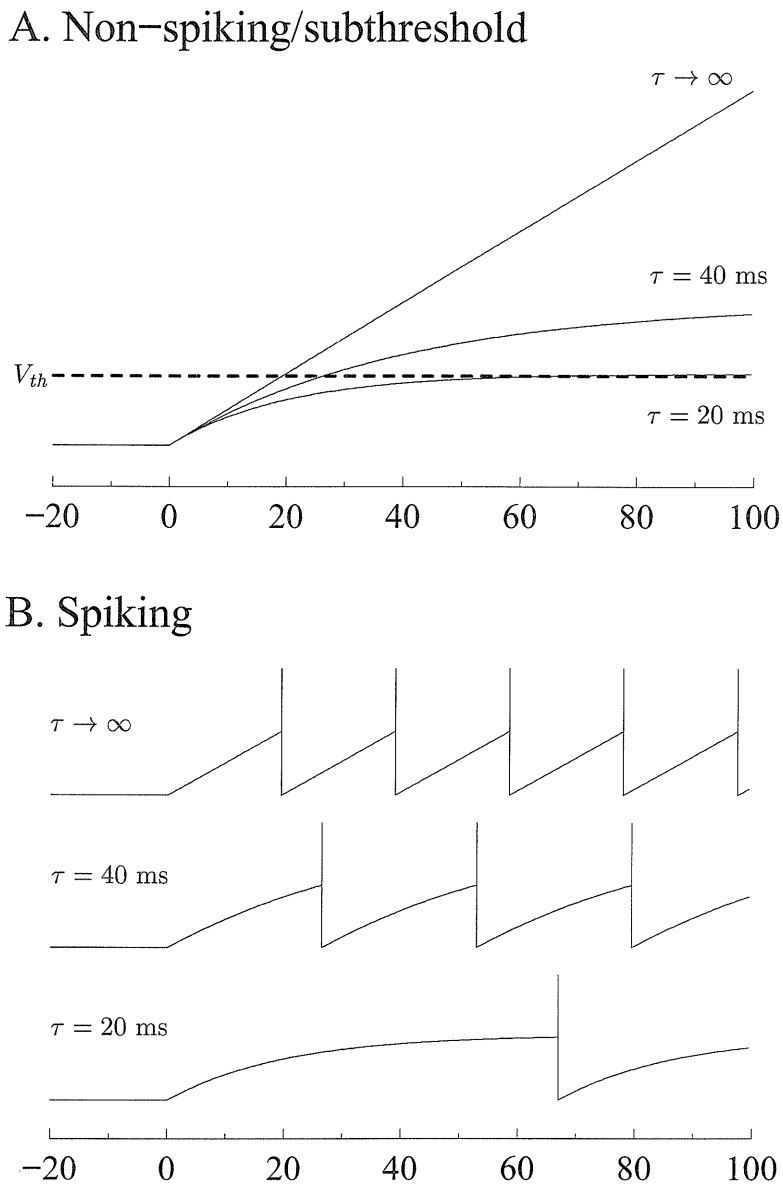

Figure 5.4: Increasing the membrane time constant makes firing rate models slower (**A**) and spiking models faster (**B**). The subthreshold voltage of the integrate and fire model (B) is exactly the same as the non-spiking model (A) until a threshold (dotted line in A) is crossed. Increasing R increases the rate of change of voltage for $V >$ the resting voltage, but it also changes the equilibrium voltage. Non-spiking neurons therefore converge more slowly as the time constant increases; as $\tau \to \infty$, the voltage continues rising until other nonlinear effects become important. In contrast, the integrate–and–fire model actually responds earlier for larger τ. In both A and B, parameters were the same. Current changed from 0 nA to 0.85 nA at time 0. $C = 1$ nF, and R was varied from 20 MΩ to ∞.

neurons. If the ensemble is completely desynchronized, then a histogram of voltages across the population will be flat, as shown in figure 5.5A. If the input stimulus is a steady current I_0, then the membrane potential of each neuron is steadily increasing according to $CdV/dt = I_0$; each neuron moves rightward along the voltage histogram at a rate proportional to the current. When a neuron reaches the voltage threshold V_{th}, it fires an action potential and resets its voltage. Hence, in this simplified system, the firing rate is described completely by the population's voltage histogram. The fraction of cells which fire in the small time interval dt is simply $p(V)\,dV = I\,dt/CV_{th}$, represented by the shaded area in the figure, and so the firing rate is $f = NI\,dt/C\,dt = NI/C$.

Note that f is directly proportional to the current and has no other time dependence, so if the current changes instantly, so does the ensemble's firing rate. If the voltage histogram starts out flat, it remains flat even if I changes, so the firing rate of the ensemble has exactly the same time course as the input current. Figure 5.5B shows a simulation of this for a step change in current. The change can be seen in the PSTH in the first bin; there is no need to wait a time T_{th}, as is necessary if there is only one presynaptic neuron. This is true for increases or decreases in input (simply reverse the time axis in figure 5.5). In theory, how fast a neuron postsynaptic to such a population could detect a change in its inputs is limited only by the number of statistically independent inputs (Panzeri *et al.*, 1996) and by the activation time of the sodium current (simulations not shown). This is unlike the response of a firing-rate neuron of the sort described by equations 5.1 and 5.2, or even an ensemble of such neurons. Because of the low-pass filtering stage (equation 5.1), the firing rate cannot change instantaneously in the firing-rate model.

This analysis depends critically on the assumption that different neurons of the ensemble are not synchronized to each other, i.e., that their phases are randomly distributed. Nothing can be said in general about what happens if the phases are nonuniformly distributed, because there are infinitely many kinds of nonuniform distributions. Also the mechanism by which the nonuniform distribution arises may influence the network response. Such situations must be analyzed on a case-by-case basis.

One case which has been analyzed in some detail is the effect of a leak on the response of otherwise independent integrate-and-fire neurons (Knight, 1972). A leak causes the ensemble to synchronize to transients. Suppose, for example, the input current is just about equal to the current threshold. Then, during one interspike interval, each leaky cell spends more time close to threshold than close to the reset potential (consider the bottom trace, $\tau = 20$ ms, in figure 5.4). Therefore most of the cells in the ensemble have their voltage close to the voltage threshold; the probability distribution in figure 5.5A will be sharply peaked near V_{th}. If the current is suddenly increased, most of them fire at about the same time. As a result, the system acts like a nonlinear high-pass filter—exactly opposite the low-pass filter behavior of firing-rate model cells.

This effect is less important if initially the cells were firing at moderate rates or if a moderate

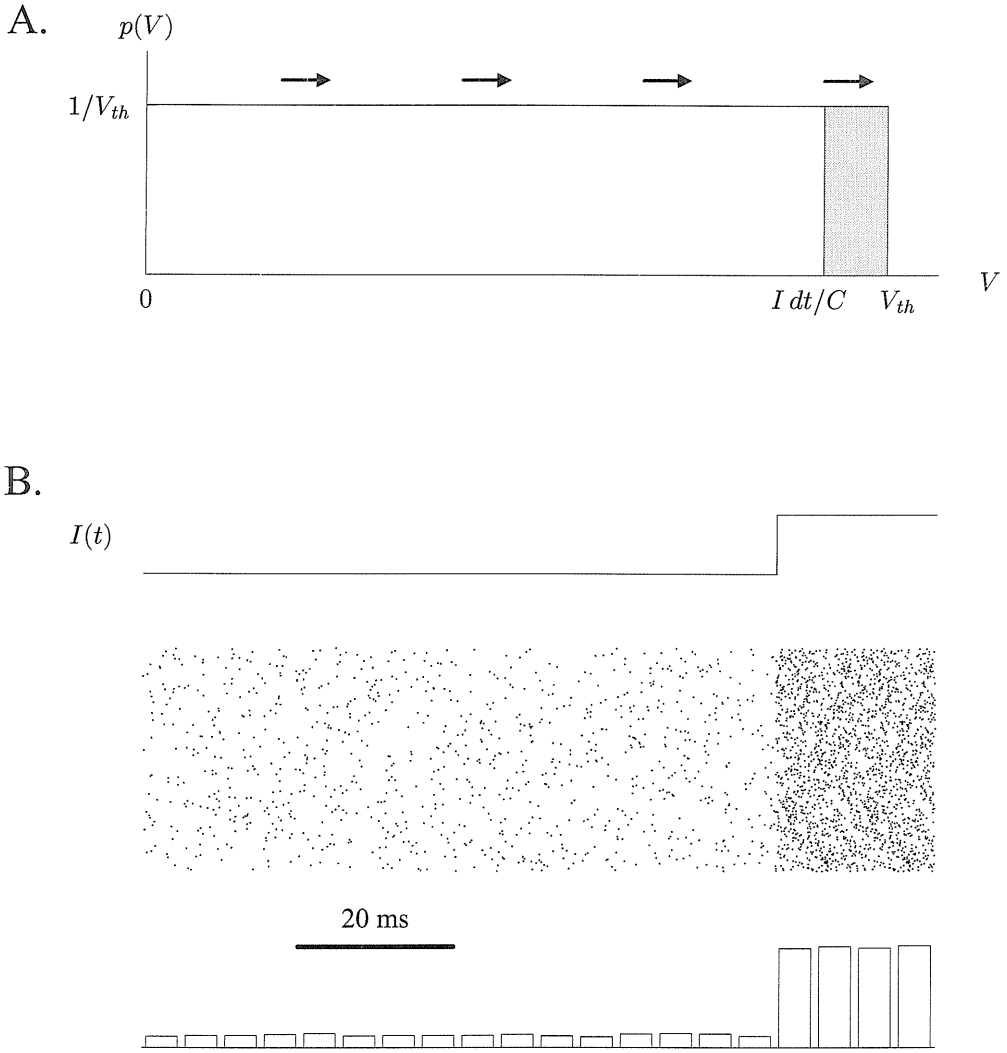

Figure 5.5: Response of a large number of identical non-leaky integrate–and–fire neurons to the same current. **A.** If the neurons are not synchronized to each other, the probability distribution of membrane potentials $p(V)\,dV$ will be uniform as shown. Each neuron's membrane potential is increasing at a constant rate (arrows) which is determined by the input current. The firing rate of the population is proportional to the fraction of cells that fire in a given time dt (the shaded area). dt can be as small as desired, so it is possible to define a firing rate for a population on a much smaller time scale than the interspike interval. **B.** A change is visible in the ensemble response immediately after the current step. *Top*, the current injected. *Middle*, spikes from the collection of neurons. *Bottom*, a histogram of the population response with a bin size of 5 ms. The fraction of cells which are firing increases discontinuously. This is unlike the behavior of firing rate models described by equations 5.1 and 5.2, which cannot change firing rate discontinuously. Parameters: $C = 1$ nF, $I_0 = 0.2$ nA, $I_1 = 1.6$ nA, $V_{th} = 16.4$ mV, 1000 neurons.

amount of noise[2] is present in the system (Knight, 1972). Since some level of noise seems reasonable, the analysis in chapter 6 assumes that firing rates of an ensemble are proportional to the input current with no additional time dependence.

5.2 Dynamics of passive spatially extended neurons

So far, we have only considered the response of a cell with no spatial extent. However, in a neuron with a dendritic tree, the voltage at the sites of synaptic input is not the same as the voltage at the locus of spike initiation. If the dendrites are largely passive, the current which reaches the soma has some high temporal frequencies removed and does not exactly represent the current at the synapses.

A great deal of work has gone into examining how EPSPs are affected by dendrites (e.g., Rall, 1977; Agmon-Snir and Segev, 1993; Zador *et al.*, 1995). Examining EPSP time courses and amplitudes at the soma assumes that the somatic voltage is free to rise, and that the somatic voltage determines firing rates. But when a spiking mechanism is present, this is not true; over long time scales, the soma's voltage is effectively clamped to a value approximately independent of the input (Koch *et al.*, 1995; chapter 4; appendix B).

Instead, it is better to look at the current which arrives at the soma. As discussed in section 5.1.3, the firing rate of an ensemble of point neurons follows the time course of the current to a high degree of precision. This is true also for neurons with passive dendritic trees (figure 5.6). The current from the dendrites was measured by voltage clamping the soma. Then the firing rates of an ensemble of neurons responding to the dendritic current was measured. The firing rate changes due to the dendritic current are virtually identical to the firing rate changes when the measured somatic current is injected at the soma rather than at the dendrites. Furthermore, the time course is almost exactly determined by the somatic current, rather than the somatic voltage.

5.3 Temporal dynamics are primarily dictated by the time course of synaptic currents

If the membrane time constant does not strongly affect the response of the neuron, what factors do? In real neurons, the lower bound on the response time to changes in injected current is determined by the activation time constant of the sodium current. This time constant is very short (in the neighborhood of 0.1 ms at physiological temperatures), and so other delays and time constants are likely to dominate circuit operation.

[2]Very large amounts of noise have a small nonlinear low-pass filtering effect dependent on the noise amplitude because of the way they disturb the voltage histogram (not shown).

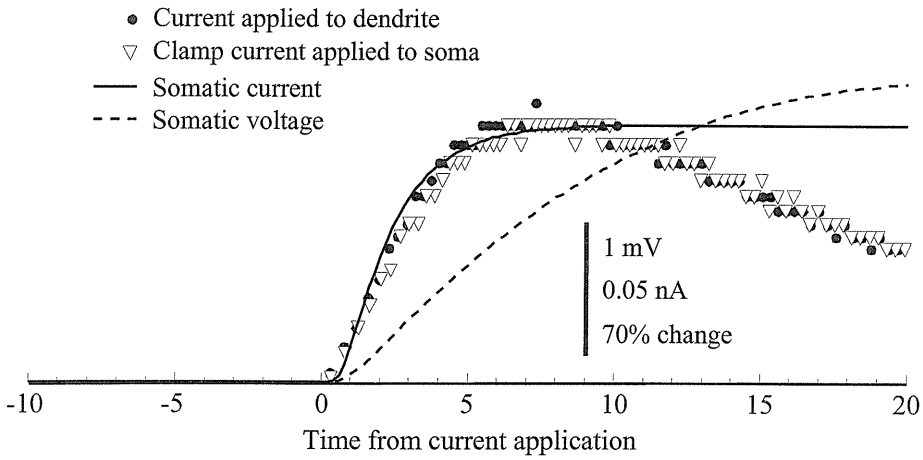

Figure 5.6: The time course of firing rate change in response to an electrotonically distant step current input of 0.1 nA. A current step at the tip one of the basal dendrites was applied to an ensemble of neurons firing with uniformly distributed phases, and the firing rate of the ensemble measured (curve with •). In a separate simulation, the voltage at the soma was clamped to -50 mV and the clamp current measured to determine the amount of current reaching the soma from the dendrite (solid line). This current was then applied to the soma of another ensemble of neurons (curve with $\bigtriangledown$). In a single neuron which was not firing, the time course of the voltage at the soma was measured (dotted line). Clearly the time course of the clamp current is a much better predictor of the ensemble firing rate than the somatic voltage. Adaptation currents were present in the soma, so the firing rate falls off although the clamp current does not.

First, currents from distal synaptic inputs are smoothed by passive membrane properties, as pointed out prominently by Rall (Rall, 1967, 1989) (for one way of quantifying this see Agmon-Snir and Segev (Agmon-Snir and Segev, 1993)). The contribution of voltage-dependent sodium and calcium current in the dendritic tree of neocortical and hippocampal neurons (Andersen *et al.*, 1980; Turner, 1988; Nicoll *et al.*, 1993; Stuart and Sakmann, 1994; Johnston *et al.*, 1996) in shaping the temporal dynamics of synaptic input under physiological conditions remains unclear at this moment.

Second, synaptic currents have a finite rise and decay time.[3] Excitatory transmission through AMPA synapses can be extremely fast (EPSCs have decay times less than 5 ms), but if current through NMDA receptors is important, then much longer time constants can be expected (up to 100 ms depending on the isoform of the NMDA receptor). The membrane time constant itself is largely irrelevant to synaptic integration (Koch *et al.*, 1996); instead it is the intrinsic time course of the synapses that dominate the process, particularly the EPSC decay time constant. Indeed, the temporal dynamics in our models of networks of spiking cells are governed primarily by the time course of synapses and adaptation currents (unpublished data; Suarez *et al.*, 1995). Synaptic low-pass filtering comes to replace the membrane low-pass filtering assumed in rate models, and

[3]Note that it is the time course of synaptic current rather than the EPSP time course which is important for firing rate dynamics.

so the removal of the membrane time constant makes little difference for many results that have been obtained from firing rate models that incorporate the membrane time constant. However, each neuron has multiple connection time constants, because there are different synaptic decay time constants depending on the kind of synapse (AMPA, NMDA, $GABA_A$, $GABA_B$, etc.), and some synapses have slow rise times as well, so the dynamics may be much richer (Buanomano and Merzenich, 1995). Furthermore, the passive membrane time constant decreases in the presence of synaptic input (because synaptic input increases the membrane conductance significantly; Bernander *et al.*, 1991; Rapp *et al.*, 1992), but the synaptic time constants will be unaffected by fast synaptic input. (Slow, neuromodulatory synaptic input can, of course, affect the channel opening or closing rates.)

Third, it takes a finite amount of time for impulses to propagate down an axon and activate the synaptic machinery. For local cortical circuitry, this delay is around 0.5 ms. However, for feedback connections to the thalamus, the delay can be as long as 10-20 ms (Tsumoto *et al.*, 1978; Tsumoto and Suda, 1980; Swadlow and Weyand, 1981; Swadlow, 1983) and sometimes even greater than 40 ms for the axons projecting from the visual claustrum to the cortex (Swadlow, 1983). Conduction time is important in the temporal dynamics of the response to lateral olfactory tract stimulation (Wilson and Bower, 1992); it is unclear how important it is in neocortical processing.

Network models based on explicitly spiking neurons have of course never fallen into the trap of assuming that the membrane time constant determines the dynamics of firing rate (e.g., Wilson and Cowan, 1972; Treves, 1992, 1993; Tsodyks and Sejnowski, 1995; Buanomano and Merzenich, 1995). Some network models based on firing rates, especially more recent ones, have properly replaced the subthreshold time constant by one or more synaptic time constants (Griffith, 1963; Amit and Tsodyks, 1991b; Amit and Brunel, 1993; Burkitt, 1994; Brunel, 1996) and written the firing rate as an instantaneous function of the input current. In symbols, equations 5.1 and 5.2 are replaced by (Frolov and Medvedev, 1986)

$$f = h(I) \tag{5.4}$$

where $h(I)$ is the current–discharge curve[4]. Because current–discharge curves are often quite linear over the relevant range of operations (Granit *et al.*, 1963; Ahmed *et al.*, 1993), a linear threshold unit with no intrinsic dynamics may be a satisfactory simplification of a real neuron. It obviously lacks some important features known to be present in real neurons (e.g., burst generation), but it may be useful whenever a neuron's firing rate rather than the timing of its spikes is important.

[4]Note that the response to synaptic current may be different from the response to a constant current if the current is just above threshold (Frolov and Medvedev, 1986; Amit and Tsodyks, 1992), because the leak makes the neuron sensitive to fluctuations if the interspike interval is long compared to the time constant. The function $h(I)$ could be adjusted accordingly.

Neglecting nonlinear synaptic interactions (Mel, 1994) and synaptic depression and facilitation (Markram and Tsodyks, 1996; Abbott *et al.*, 1997), we can write for the total postsynaptic current from one kind of synapse

$$I_{syn} = \sum_i w_i f_i * i_{rec} \tag{5.5}$$

where w is the weight, $i_{rec}(t)$ is the time course of the EPSC from a single spike, and $*$ denotes convolution. This applies to both excitatory and inhibitory currents, even for shunting inhibition, since shunting inhibition does not act qualitatively different from non-shunting inhibition (chapter 4).

If we assume that the postsynaptic current decays exponentially, i.e. if $i_{rec}(t) = i_0 e^{-t/\tau_{syn}}$, this equation becomes (Frolov and Medvedev, 1986):

$$\frac{dI_{syn}}{dt} = -\frac{I_{syn}}{\tau_{syn}} + i_0 \sum_i w_i f_i(t). \tag{5.6}$$

This is of the same form as equation 5.1, and indeed many modern attractor models have simply substituted I for V and τ_{syn} for τ.[5] Such a simple substitution is not possible, however, if there are two different kinds of synapses (e.g., excitatory and inhibitory) with different time courses.

Similarly, adaptation may be modeled by

$$I_{adapt} = f * i_{adapt} \tag{5.8}$$

where $i_{adapt}(t)$ is the time course of the current that comes into a cell after a single spike through the calcium dependent potassium current I_{AHP} and other adaptation conductances.

5.4 Conclusion

Firing rate point models of nerve cells which assume that the membrane time constant is relevant above threshold are widespread and continue to be used. We suggest that such models would be more accurate if the time constant were simply discarded. The idea of an above threshold voltage should also be abandoned and replaced by an input current (Amit and Tsodyks, 1991a, 1992). Reasoning about voltages above the spiking threshold as if they were equilibrium states leads not

[5] Another class of models attempts to compute not the instantaneous firing rate but the time averaged firing rate:

$$\langle f \rangle = f * e^{-t/\tau} \tag{5.7}$$

where τ is the temporal coarse-graining time constant (Wilson and Cowan, 1972, 1973), i.e., the time scale over which averaging is performed. Such a formulation also leads to equation 5.6. In this case, however, τ has no biophysical significance; it is an artifact of the conversion between a discrete spike train and a continuous firing rate (see Abbott, 1994). With an ensemble of neurons, however, there is no difficulty in converting a discrete spike train into a firing rate, so no arbitrary τ needs to be defined.

only to an erroneous view of the importance of the membrane time constant, but also to a mistaken understanding of synaptic effects such as shunting inhibition (chapter 4; Holt and Koch, 1997). It is more useful to think of the soma as receiving a current from the dendrite which it converts directly into a firing rate (Abbott, 1991; Amit and Tsodyks, 1991a, 1992; Bernander *et al.*, 1994; Carandini *et al.*, 1996b; equation 5.4).

The spiking mechanism is usually thought of as a means of transmitting an analog value over a long distance without distortion. However, a further important property of the mechanism is that it can speed up the response of individual neural elements. Without the spiking mechanism, each stage of a feedforward neural network would take at least as long as the membrane time constant to come close to its equilibrium value. With spiking neurons, however, each stage needs to take only as long as the synaptic delay plus the synaptic time constant. If only current through AMPA receptors is important, this time can be just a few milliseconds.

Part III

Applications to Networks

Chapter 6 Adaptation and recurrent circuits

6.1 Introduction

It is a well-known engineering principle that feedback slows down a system's response. Consider, for example, a simple discrete-time version of the cortical amplifier network in figure 6.1. The population of cells feeds its own output back as input with a synaptic weight w. If the synaptic delay time is τ, then this system can be crudely modeled by

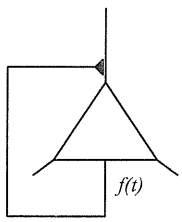

Figure 6.1: Simplified cortical amplifier circuit. Neurons in the population are connected to each other with excitatory connections.

$$f(t) = \alpha(wf(t-\tau) + I_{ff}) \tag{6.1}$$

where α is the slope of the current–discharge curve.

The impulse response of this system is obtained by setting $I_{ff} = 1/\alpha$ for $t = 0$ and $I_{ff} = 0$ for subsequent times:

$$f(t) = (\alpha w)^{t/\tau} = e^{t(\log \alpha w)/\tau}. \tag{6.2}$$

The response for various values of w are shown in figure 6.2. The system becomes very slow as the amount of recurrent input αw increases.

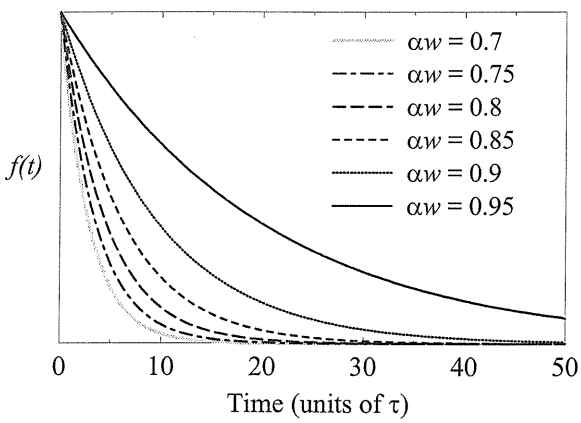

Figure 6.2: The impulse response of the discretized system of equation 6.1. Note that the system slows down dramatically as $\alpha w \to 1$.

From equation 6.2, the time constant of this network is given by

$$\begin{aligned}\tau_{net} &= -\tau / \log \alpha w \\ &= -\frac{\tau}{\log[1 + (\alpha w - 1)]} \\ &\approx \frac{\tau}{1 - \alpha w} \\ &= G\tau\end{aligned}$$

where G is the gain of the network, i.e., the ratio of the total current into the cell to the feedforward current. This is a general rule of these kinds of feedback systems: the network time constant is approximately equal to the gain of the system times the time constant associated with the feedback.

Maex and Orban (1992) suggest that the long time constants associated with recurrence might explain how the cortex does temporal low pass filtering. The network time constant will depend strongly on whether NMDA receptors are important for the response, since NMDA receptors have a long time constant (around 80 ms). NMDA receptors are less dense in layer 4 but still may play an important role in the response, especially the recurrent excitation (Miller *et al.*, 1989; Fox *et al.*, 1989; Armstrong-James *et al.*, 1993). The longest time constant in the system is the decay time of the NMDA receptor (80 ms); if the system's gain is moderately high, say 5, the network time constant will be hundreds of milliseconds. This is much too large. This chapter discusses one biophysically realistic way in which the time constant can be reduced.

6.2 Continuous time systems

The same general principles are true of continuous time systems, although the math is somewhat harder to analyze. The remainder of this chapter analyzes continuous time systems with excitatory feedback and inhibitory feedback.

Neural firing rates cannot become negative; the system becomes nonlinear when the current drops below threshold. However, if there is inhibition and adaptation, total current to a cell can drop below threshold. This makes the powerful mathematical tools which have been developed for linear systems analysis inapplicable to the system. For this reason, in the remainder of this chapter we analyze step responses instead of impulse responses.

Based on the formalism of equations 5.4 and 5.5 on page 86, a continuous time description of the network in figure 6.1 is

$$f(t) = \alpha(f(t) * i_{rec}) + I_{ff}(t), \tag{6.3}$$

where $f(t)$ is the firing rate of all the neurons, and $I_{ff}(t)$ is the LGN input, which we will take to be a step:

$$I_{ff} = \begin{cases} 0 & \text{if } t < 0, \\ 1 & \text{if } t > 0. \end{cases} \tag{6.4}$$

i_{rec} is the time course of feedback synaptic input; it is the current due to one input spike as a function of time after that spike.

This system can be solved explicitly by a Laplace transform:

$$\hat{f}(s) = \frac{\hat{I}_{ff}(s)}{1 - \hat{I}_{rec}(s)}. \tag{6.5}$$

For example, suppose we model the synaptic time course to be as simple as possible:

$$i_{rec}(t) = we^{-t/\tau}.$$

In this case, we can write the solution in closed form:

$$\begin{aligned} I_{syn} &= \frac{w}{\frac{1}{\tau} + s}, \qquad \hat{I}_{ff} = \frac{1}{s} \\ \hat{f} &= \frac{\hat{I}_{ff}}{1 - \hat{I}_{rec}} \\ &= \frac{(\frac{1}{\tau} + s)}{s(\frac{1}{\tau} - w + s)}. \end{aligned}$$

We invert the transform by evaluating the residues at $s = 0$ and $s = w - \frac{1}{\tau}$:

$$\begin{aligned} f(t) &= \int_{-\infty+i\infty}^{\infty+i\infty} \frac{-\frac{1}{s}(\frac{1}{\tau} + s)e^{st}}{\frac{1}{\tau} - w + s}\, ds \\ &= \begin{cases} 0 & \text{if } t < 0, \\ \dfrac{1 - w\tau e^{-t(1-w\tau)/\tau}}{1 - w\tau} & \text{if } t \geq 0. \end{cases} \end{aligned} \tag{6.6}$$

$f(t)$ has a discontinuity at 0 when the LGN input suddenly turns on, and then it approaches its asymptotic limit, determined by closed-loop gain $G = 1/(1 - \tau w)$. The time constant of the system is $\tau_{net} = \tau/(1 - \tau w) = G\tau$. As noted above, this is a general property: the longest time constant of the network (which is the only important time constant for approach to equilibrium) is the same order of magnitude as the product of the longest time constant of the feedback and the gain of the system.

As noted, if NMDA currents are important, then $\tau = 80$ ms and $\tau_{net} = 400$ ms. This is much too large. Suarez (1994) found that an adaptation conductance was critical for accelerating convergence to the steady state. According to his analysis, initially the system in its unadapted state has an open loop gain which is greater than 1, so the system rapidly increases its firing rate in response to a step input. As the adaptation current becomes stronger, the open loop gain drops to less than 1 but the system has already moved close to its steady state.

This analysis, while correct, is not entirely satisfactory in that 1) it does not help us understand how to set the time course or strength of adaptation; 2) it does not explain why simulated networks respond very rapidly to current offset as well as current onset.

6.3 How adaptation helps—heuristic arguments

A network of identical linear units with adaptation can be modeled as

$$f(t) = \alpha(f(t) * i_{rec} - f(t) * i_{adapt} + I_{ff}(t)) \tag{6.7}$$

where α is the slope of the current–discharge curve. The key to this analysis is that all the units have the same output firing rate, so adaptation and feedback synaptic input have the same form as shown above. In fact, the adaptation current in this model can be viewed as a kind of inhibitory synapse from the cell to itself.

Since feedback and adaptation have the same mathematical form, we can combine them into a single effective current $i_{eff} = i_{rec} - i_{adapt}$:

$$f(t) = \alpha[f(t) * i_{eff} + I_{ff}(t)]. \tag{6.8}$$

All of the dynamics of the system are contained in the form of i_{eff}, so by analyzing the shape of i_{eff} alone we can understand the time-dependent behavior of the system.

This is the same form as equation 6.3, and the general observation that the largest network time constant $\tau_{net} \approx G\tau$ (where τ is the longest time constant in i_{eff}) still holds. How then can adaptation possibly help? Adaptation must change the shape of i_{eff} so that its time constant is shortened. For example, suppose all of the feedback comes through synapses with the NMDA[1] time course:

$$i_{rec} = w(e^{-t/\tau_{N2}} - e^{-t/\tau_{N1}}) \tag{6.9}$$

[1]We are not concerned here with the voltage dependence of NMDA, though it could be a problem in an actual implementation.

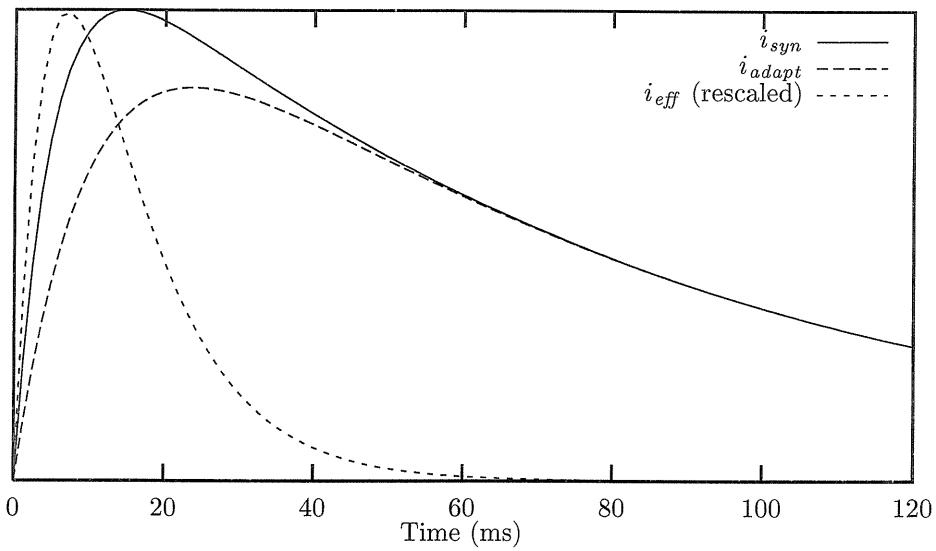

Figure 6.3: How adaptation speeds up the response time of the system. Recurrent synaptic input has a very slow time course (i_{rec}) but so does the adaptation current (i_{adapt}). However, if the time constant and amplitude of the adaptation current are set correctly, the slow components will cancel leaving only faster components.

where $\tau_{N1} = 5$ ms and $\tau_{N2} = 80$ ms. Without adaptation, then, if the gain $G = 10$, then the network time constant will be roughly 500 ms. Suppose we model our adaptation by

$$i_{adapt} = a(e^{-t/\tau_{A2}} - e^{-t/\tau_{A1}}). \tag{6.10}$$

Since $i_{eff} = i_{rec} - i_{adapt}$, we can choose $a = w$ and $\tau_{A2} = \tau_{N2}$:

$$i_{eff} = w(e^{-t/\tau_{A1}} - e^{-t/\tau_{N1}}). \tag{6.11}$$

Now the long time constant τ_{N2} has been eliminated from the system; i_{eff} has a much faster time course (see figure 6.3). Even if we increase w so that G is the same, the system will converge to its equilibrium point much faster.

This system can be solved again by a Laplace transform; after some algebra, the root of the denominator which is closest to zero is found to be

$$s = -\frac{\tau_{N1} + \tau_{A1}}{2\tau_{N1}\tau_{A1}} \left(1 - \sqrt{1 - \frac{4\tau_{N1}\tau_{A1}}{G(\tau_{A1} + \tau_{N1})^2}}\right). \tag{6.12}$$

For large gains, we can expand this in a Taylor series to give an approximate solution

$$s \approx \frac{-2}{G(\tau_{N1} + \tau_{A1})}. \tag{6.13}$$

The time constant is therefore $\tau_{net} \approx G(\tau_{A1} + \tau_{N1})/2$.

Actually, it turns out that unless τ_{N2} is extremely large, it is slightly better to make a (the adaptation strength) just larger than w (the recurrent weight) so that $i_{eff}(t)$ is negative for large t. But if a is too much larger, then the system oscillates and convergence is slowed down. See below for details.

6.4 Simplified linear model

The preceding argument suggests that adaptation might have a rise time which is slower than the rise time of recurrent excitation for it to speed up the network. This is actually not true; adaptation can speed up the system significantly even if it has the same rise time, as long as it has a slower decay time.

The simplest possible system which shows an effect of adaptation is given by:

$$f = \alpha(I_{rec} + I_{adapt} + I_{ff}) \tag{6.14}$$

$$\begin{aligned} I_{rec}(t) &= f(t) * i_{rec}(t) & i_{rec}(t) &= we^{-t/\tau_e} \\ I_{adapt} &= f(t) * i_{adapt}(t) & i_{adapt}(t) &= ae^{-t/\tau_a} \end{aligned}$$

where $\tau_a > \tau_e$, i.e., adaptation is slower than recurrent excitation.

Combining these equations, the firing rate of each excitatory neuron in the network should be given by

$$f(t) = \alpha(f(t) * i_{rec}(t) + f(t) * i_{adapt}(t) + I_{ff}) \tag{6.15}$$

where I_{ff} is the feedforward current from the LGN.

For convenience, through the rest of this analysis we normalize equation 6.15 by putting all times

in units of the excitatory time constant τ_e:

$$\begin{aligned} T &= t/\tau_e & \tau &= \tau_a/\tau_e \\ W &= \alpha w \tau_e & A &= \alpha a \tau_a \\ I_{ff} &= \alpha I_{ff}. \end{aligned} \tag{6.16}$$

Note that $W = \alpha \int_0^\infty w e^{-t/\tau_e}\, dt$ and $A = \alpha \int_0^\infty a e^{-t/\tau_a}$; this normalization expresses the synaptic weight in terms of the total charge deposited by a single spike.

With this normalization, equation 6.15 becomes

$$\begin{aligned} f(T) &= f(T) * W e^{-T} + f(T) * \frac{A}{\tau} e^{-T/\tau} + I_{ff} \\ &= f(T) * \left(W e^{-T} - \frac{A}{\tau} e^{-T/\tau} \right) + I_{ff}. \end{aligned} \tag{6.17}$$

Including adaptation is mathematically equivalent to changing the dynamics of the excitatory synapses: We^{-T} is replaced by $We^{-T} - Ae^{-t/\tau}/\tau$. The dynamics with adaptation are generally faster because $Ae^{-t/\tau}/\tau$ cancels out part of the long tail of We^{-T}. The net current actually becomes negative for large times; if parameters are adjusted properly, this does not necessarily cause oscillations.

At steady state, equation 6.17 has the simple solution

$$f = (W - A)f + I_{ff} = \frac{I_{ff}}{1 - W + A}.$$

For convenience, we define the gain

$$G = \frac{1}{1 - W + A}. \tag{6.18}$$

To examine the effects of adaptation, we hold G fixed and increase W and A together. The network therefore has the same steady state but the dynamics of the approach to steady state vary. In our analysis here, we express the results in terms of varying A; A ranges from 0 to arbitrarily high values.

6.4.1 Dynamics: analysis by Laplace transform

Since equation 6.17 is a linear integral equation, we can solve it using a Laplace transform. First, without adaptation ($A = 0$), the solution turns out to be

$$f(T) = I_{ff}(G - (G - 1)e^{-T/G}). \tag{6.19}$$

As in equation 6.6, the time constant of this system is very long (G) compared to the synaptic time constant (which is 1 in these units). For example, if most cortico-cortical current comes through the NMDA receptor, $\tau_e \approx 80$ ms. We usually think of G of 5–10, which implies that the network time constant will be 400–800 ms.

With adaptation, things are a little more complicated. The solution in the Laplace domain is

$$\hat{f}(s) = \frac{\hat{I}_{ff}(s)(1+s)(1+\tau s)}{\tau s^2 + \left(1 + \frac{\tau}{G} - A(\tau - 1)\right) s + \frac{1}{G}}. \tag{6.20}$$

We only analyze here the response to step changes in the LGN input, so $\hat{I}_{ff}(s) = I_{ff}/s$. As usual, once we have found the roots s_1 and s_2 of the denominator of equation 6.20, we can write down the result in the time domain:

$$f(T) = I_{ff}(G + C_1 e^{s_1 T} + C_2 e^{s_2 T}) \tag{6.21}$$

where C_1 and C_2 are constants given by

$$\begin{aligned} C_1 &= \frac{(1+s_1)(1+\tau s_1)}{s_1(s_1 - s_2)} \\ C_2 &= \frac{(1+s_2)(1+\tau s_2)}{s_2(s_2 - s_1)}. \end{aligned} \tag{6.22}$$

The basic form of the solution is therefore the sum of two terms which are exponentially decaying. If $\operatorname{Im} s \neq 0$, then the result will be a damped oscillation.

If we substitute the explicit values for s_1 and s_2 into equation 6.21, the resulting expression is nasty and unintuitive. To understand the possible behaviors of the system a more qualitative analysis is necessary (see section 6.7).

6.4.2 Network time constant

The time constants in equation 6.21 are determined by the roots s_1 and s_2 of the denominator of equation 6.20. The location of these roots for various values of A is shown in figure 6.4. As A increases, the root closest to zero moves leftward, shortening the network time constant. The other root moves in the opposite direction. When the two roots collide, they move off the real line; this means the system shows ringing. Their real part moves toward 0 again, which means that the longest network time constant grows. Eventually, the system becomes unstable when their real part becomes positive. Therefore the minimum network time constant is at the point when they collide.

All of the results described in the above paragraph can be shown analytically to hold for all values of τ

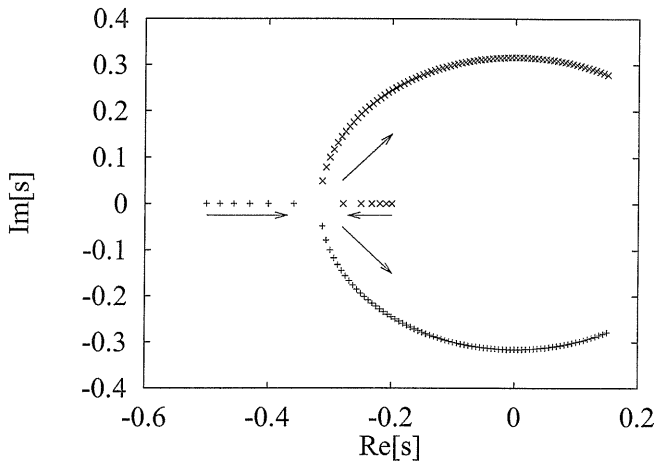

Figure 6.4: The location of the poles of $\hat{f}(s)$ for different values of A. Arrows show the direction the roots move as A increases. The roots begin at $s = -1/G$ and $s = -1/\tau$. As A increases, they move together, and then collide and move off the real line. The longest time constant of the system is determined by the root closest to the origin, so the minimum network time constant occurs when the roots collide, just before the onset of oscillations. In this example, $G = 5$ and $\tau = 2$. A was varied from 0 to 2 in steps of 0.025.

and G. Roots are located at

$$s = \frac{-(1 + \frac{\tau}{G} - A(\tau - 1)) \pm \sqrt{(1 + \frac{\tau}{G} - A(\tau - 1))^2 - 4\frac{\tau}{G}}}{2\tau} \tag{6.23}$$

where the minus sign corresponds to the root farthest from 0 and the plus sign corresponds to the root closest to 0. For $A = 0$, this works out to $s_1 = -1/\tau$, $s_2 = -1/G$. After some simplification, we can show that

$$\frac{ds}{dA} = \frac{\tau - 1}{2\tau}\left(1 \mp \frac{1 + \frac{\tau}{G} - A(\tau - 1)}{\sqrt{(1 + \frac{\tau}{G} - A(\tau - 1))^2 - 4\frac{\tau}{G}}}\right) \tag{6.24}$$

where the minus sign is for s_2 and the plus sign is for s_1. Note that the term in the radical in equation 6.24 is the same as in equation 6.23. Therefore ds/dA is real if s is real, and imaginary if not. If s is real, then

$$\sqrt{(1 + \frac{\tau}{G} - A(\tau - 1))^2 - 4\frac{\tau}{G}} < 1 + \frac{\tau}{G} - A(\tau - 1)$$

so ds/dA is negative for s_1 and positive for s_2. Therefore the two roots move together, as shown in figure 6.4. If $\mathrm{Im}\, s \neq= 0$, then $\mathrm{Re}\, ds/dA > 0$ and the real part of both roots moves toward 0.

At the collision point, then, the network time constant is a minimum. We know that $s_1 s_2 = 1/\tau G$ since the product of a polynomial's roots is its constant coefficient. Therefore $s_1 = s_2 = 1/\sqrt{\tau G}$, and $\sqrt{\tau G}$ is the minimum network time constant achievable. It can be shown that at the collision point, $A = 1 + \tau/G - 2\sqrt{\tau/G}$.

None of these results depend on the values of τ and G; there are no parameter regimes where the system behaves differently.

6.5 Detailed linear model—analysis of poles

The same results hold for a more complicated system where there is a finite rise time for both adaptation and recurrent excitation.

Consider again a system with the same synaptic and adaptation time courses as in equations 6.9 and 6.10. It is relatively straightforward to calculate the Laplace transform of the solution:

$$\hat{f}(s) = \frac{\hat{I}_{ff}(s)}{1 - \hat{I}_{eff}(s)} \tag{6.25}$$

To get the poles of the system we solve for the roots of the denominator of $\hat{f}(s)$:

$$\begin{aligned}(1+\tau_{N1}s)(1+\tau_{N2}s)(1+\tau_{A1}s)(1+\tau_{A2}s) - \\ w(1+\tau_{A1}s)(1+\tau_{A2}s)[\tau_{N2}(1+\tau_{N1}s) - \tau_{N1}(1+\tau_{N2}s)] + \\ a(1+\tau_{N1}s)(1+\tau_{N2}s)[\tau_{A2}(1+\tau_{A1}s) - \tau_{A1}(1+\tau_{A2}s)] = 0.\end{aligned} \tag{6.26}$$

Since both the synapses and the adaptation currents have their own time courses, equation 6.26 is a fourth[2] degree polynomial whose exact solution gives no intuitive understanding. Instead, the locations of the poles of $\hat{f}(s)$ were analyzed numerically. If the system does converge to a stable solution in response to a current step, then all poles must be in the left half-plane (i.e., they must have a negative real part). The inverse of the real part is the time constant, so the pole whose real part is closest to zero corresponds to the longest time constant in the system.

Note that if $w = a$, one of the roots of the denominator is equal to one of the roots of the numerator, and for large τ_{N2} or τ_{A2} this root may be the one which is closest to zero. The smallest achievable time constant is minimum of the time constant calculated from pole analysis and the time constant in equation 6.12. For many parameter values, it is possible to do somewhat better than the solution presented in section 6.3.

As a is increased[3] from 0, the two poles closest to the origin[4] move towards each other (figure 6.5). When they collide, the system's largest time constant is minimized because the magnitude of the real part of the closest pole to the origin is maximized. As a is increased further, the poles have non-zero imaginary components and the system begins to ring. For large enough a it oscillates uncontrollably.

[2] Or third—if $\tau_{A2} = \tau_{N2} = \tau_2$ then the term $(1 + \tau_2 s)$ may be factored out of both the numerator and the denominator.

[3] w is increased to keep G the same:

$$G = \frac{1}{1 - w(\tau_{N2} - \tau_{N1}) + a(\tau_{A2} - \tau_{A1})}$$

[4] Actually, since $\tau_{N2} = \tau_{A2} = 80$ ms, the denominator has a zero at $s = -1/80 = -0.0125$. But the numerator of $\hat{f}(s)$ also has a zero at this location, so I have ignored it.

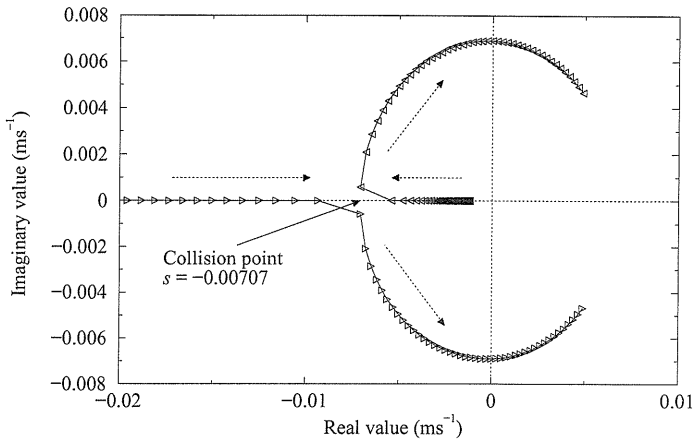

Figure 6.5: Locations of the two poles which closest to zero for large w and a values in the more complicated model. As in figure 6.4, as a increases, the two poles move toward each other (indicated by the arrows) until they collide, at which point they leave the real axis. At the collision point, the system has the shortest time constant because the pole closest to the origin is as far away as possible; increasing a further causes the real part of both poles to move closer to zero. a was increased from zero in steps of 0.00125. w was set for each a to give a gain $G = 10$. $\tau_{A1} = 20$ ms, $\tau_{N1} = 5$ ms, and $\tau_{A2} = \tau_{N2} = 80$ ms. When $a = 0$, the system has a time constant of 845 ms; this decreases to 141 ms at the collision point.

Therefore the solution with shortest network time constant has a as large as possible without ringing.

The minimum network time constant achievable depends on the specific time course of the adaptation (i.e., the values of τ_{A1} and τ_{A2}). From the intuitive model presented in section 6.3, one would predict that the best value of τ_{A2} (the decay time of adaptation) would be the same as τ_{N2}, the EPSP decay time, because the adaptation should cancel the slow part of the synaptic current. This is in fact the case (figure 6.6).

One would also predict that the rise time of the adaptation (τ_{A1}) should be close to the rise time of the feedback (τ_{N1}, set to 5 ms). This is born out by simulations (figure 6.7). Setting τ_{A1} equal to τ_{N1} is equivalent to removing the effect of adaptation entirely—the adaptation waveform is identical to the synaptic waveform and has no effect (since the amplitudes are adjusted to keep the gain constant). Decreasing τ_{A1} below τ_{N1} causes the network time constant to increase sharply; in fact, it becomes larger than it would be if no adaptation were present at all.

6.5.1 Approximations for τ_{net}

Since we are interested only in the smallest roots of equation 6.26, it is possible to find an expression for an approximate root. We simply discard the highest power of s in the polynomial and solve the resulting system. Numerically, this does not work well for the fourth degree polynomial in equation 6.26 as it stands; however, it does work well if we assume that $\tau_{N2} = \tau_{A2} = \tau_2$. In this

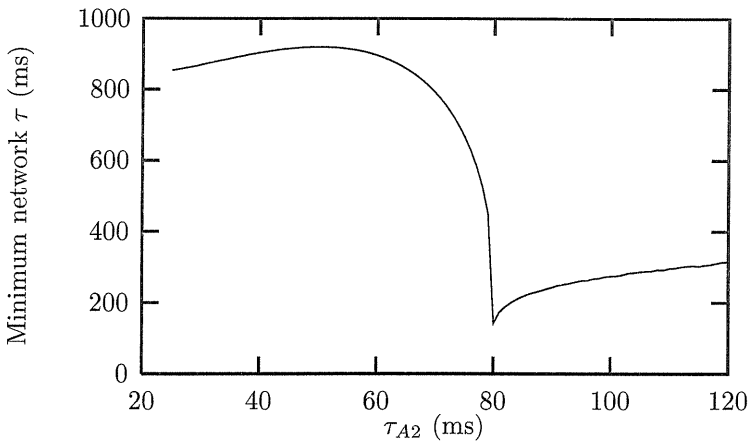

Figure 6.6: The effect of varying τ_{A2} on the minimum network time constant when τ_{A1} is fixed at 20 ms and the gain at 10. For each τ_{A2} value, the a for the collision point described above was computed; the time constant at the collision point is the minimum possible. With no adaptation at all, the network time constant would be 845 ms (what the curve reaches at the left edge).

case, we can cancel the term $(1+\tau_2 s)$ in both the numerator and the denominator and we have a third degree polynomial. Numerical studies show that discarding the s^3 term provides an approximation which seems to be good to within about 5% near the collision point for reasonable parameter values.

After cancelling $(1 + \tau_2 s)$ and simplifying, equation 6.26 reduces to

$$s^2(\tau_{A1}\tau_2 + \tau_{N1}\tau_2 + \tau_{A1}\tau_{N1}) + s(\tau_2 + \tau_{A1} + \tau_{N1}) - w\tau_{A1}(\tau_2 - \tau_{N1}) + a\tau_{N1}(\tau_2 - \tau_{A1}) + 1 - w(\tau_2 - \tau_{A1}) + a(\tau_2 - \tau_{N1}) = 0. \quad (6.27)$$

For convenience, we define

$$S_\tau = \tau_{A1} + \tau_{N1} + \tau_2 \quad (6.28)$$

$$S_{\tau\tau} = \tau_{A1}\tau_2 + \tau_{N1}\tau_2 + \tau_{A1}\tau_{N1} \quad (6.29)$$

$$\Omega = w\tau_{A1}(\tau_2 - \tau_{N1}) - a\tau_{N1}(\tau_2 - \tau_{A1}). \quad (6.30)$$

Also, the steady state gain of the system can be obtained from $\lim_{t\to\infty} f(t) = \lim_{s\to 0} sF(s)$:

$$G = \frac{1}{1 - w(\tau_2 - \tau_{A1}) + a(\tau_2 - \tau_{N1})}. \quad (6.31)$$

Making all these substitutions reduces the equation to

$$S_{\tau\tau}s^2 + (S_\tau - \Omega)s + \tfrac{1}{G} = 0$$

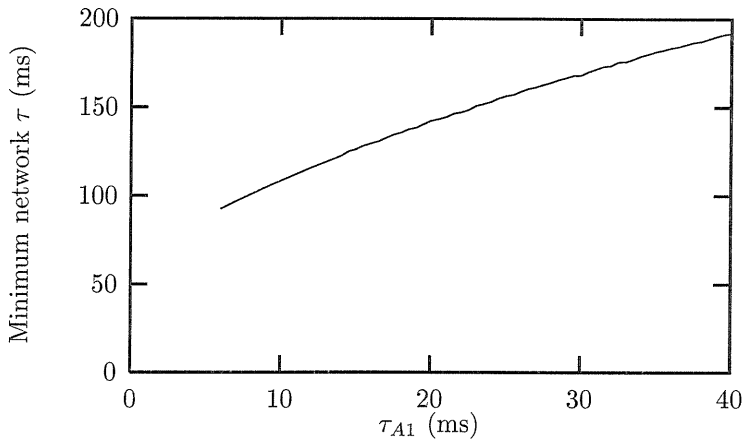

Figure 6.7: The effect of varying τ_{A1} on the minimum network time constant when τ_{A2} is fixed at 80 ms and the gain at 10. The smallest network time constant achievable in this framework is about 90 ms. For $\tau_{A1} \leq \tau_{N1}$ (5 ms), the minimum network τ jumps suddenly to almost a second. Note that in order to keep the gain constant, a and w approach infinity as $\tau_{A1} \rightarrow \tau_{N1}$. Thus the discontinuity in the root location as a function of τ_{A1} is not surprising, since the polynomial coefficients are discontinuous there.

for which the solution is

$$s = \frac{-(S_\tau - \Omega) \pm \sqrt{(S_\tau - \Omega)^2 - 4S_{\tau\tau}/G}}{2S_{\tau\tau}}. \tag{6.32}$$

We know that the shortest possible τ_{net} occurs when the two roots coincide, so we set the discriminant to 0:

$$\Omega^2 - 2S_\tau\Omega + S_\tau^2 - 4S_{\tau\tau}/G = 0$$
$$\Omega = S_\tau \pm 2\sqrt{\frac{S_{\tau\tau}}{G}}.$$

We choose the negative root so that $s < 0$ in equation 6.32:

$$s = -\frac{1}{\sqrt{GS_{\tau\tau}}} = -\frac{1}{\sqrt{G(\tau_{A1}\tau_2 + \tau_{N1}\tau_2 + \tau_{A1}\tau_{N1})}}$$
$$\tau_{net} = \sqrt{G(\tau_{A1}\tau_2 + \tau_{N1}\tau_2 + \tau_{A1}\tau_{N1})}. \tag{6.33}$$

Numerical studies show that this value of s is slightly closer to 0 than the roots of the cubic in equation 6.26, so this is apparently (at least for the numbers I tried) slightly greater than the minimum achievable τ_{net}.

This solution is only valid for $\tau_{A1} > \tau_{N1}$. Also, $w \neq a$ in general; for large τ_2, the solution for $w = a$ is better (see equation 6.13). This does not fall out of the approximation because the smallest root of the denominator cancels with a root in the numerator if $w = a$, so the smallest root of the denominator is not actually the relevant time constant.

In general, then, we have

$$\tau_{net} \approx \begin{cases} \dfrac{G(\tau_{A1} + \tau_{N1})}{2} & \text{for large } \tau_2 \\ \sqrt{G(\tau_{A1}\tau_2 + \tau_{N1}\tau_2 + \tau_{A1}\tau_{N1})} & \text{otherwise.} \end{cases} \tag{6.34}$$

This confirms that the best time course for adaptation is to set the rise time of adaptation as small as possible to match the rise time of the excitatory conductance. Note that adaptation can speed up the network even if the neither excitation nor adaptation has a finite rise time; see section 6.4.

6.6 Reducing the time constant further

When recurrent synaptic input has a slow time course typical of the NMDA receptor, the above analysis shows that no matter how the adaptation time constants are set the network time constant cannot be lowered below 90 ms if the gain is 10. This is still too high.

One possible solution to this problem, while still keeping the system linear, is to make i_{rec} faster, say by adding a conductance with an AMPA time course. For example, if

$$i_{rec} = w_{AMPA}(e^{-t/\tau_{AMPA2}} - e^{-t/\tau_{AMPA1}}) + w_{NMDA}(e^{-t/\tau_{N2}} - e^{-t/\tau_{N1}}), \tag{6.35}$$

then if we set $w_{AMPA} = w_{NMDA}$ and $\tau_{AMPA2} = \tau_{N1}$ (i.e., the fall time of the Q/K conductance equals the rise time of the NMDA conductance), then

$$i_{rec} = w(e^{-t/\tau_{N2}} - e^{-t/\tau_{QK1}}).$$

By doing so we have eliminated the 5 ms rise time of the NMDA conductance. Now we can tune the adaptation conductance to match the this new synaptic conductance with a much faster rise time. Numerical studies of the poles of $F(s)$ show that for $\tau_{AMPA1} = 0.5$ ms, the network time constant can be below 10 ms if τ_{AMPA1} is brought very close to τ_{AMPA1}.

Reducing the network time constant in this way may not be practical for several reasons:

1. The NMDA currents are voltage dependent and it may not be possible to cancel the slow components out exactly in the manner shown here. Inaccuracy in the cancellation will seriously affect the minimum achievable network time constant.

2. The smallest network time constants are obtained by bringing τ_{A1} close to the rise time of

i_{rec}. In order to do so and to keep the gain high, the synaptic weight w and the adaptation strength a become very large. Probably inaccuracies from slightly incorrect time courses will become more important as well.

6.7 Simplified network dynamics in the time domain

The time constants of course do not provide a complete description of network behavior, and in fact they can be somewhat misleading. For example, there is a double pole when the two roots collide, and the solution actually approaches its asymptote somewhat faster than a single exponential would predict (not shown).

We consider once again the simplified model, where both recurrent excitation and adaptation do not have a finite rise time (equation 6.14 on page 94). Figure 6.8 shows solutions for a few values of A. The theory predicts that the minimum network time constant is achieved at the collision point, and the simulations bear this out. The line for $A = 0.1351$ approaches its asymptote the quickest of all A values shown. However, this is hardly better than the network without any adaptation at all ($A = 0$); it turns out that the difference is much more noticeable for larger G (not shown). (The time constant without adaptation is $G = 5$, and with adaptation it is $\sqrt{\tau G} = 3.2$.)

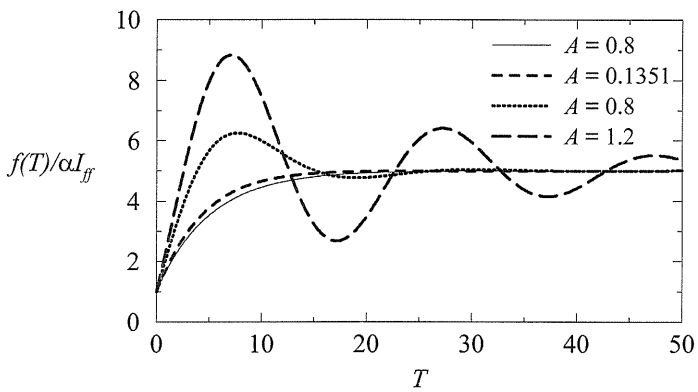

Figure 6.8: Response to step input for the simplified model. The gain is held constant at $G = 5$, and A and W are varied. At $A = 0$, the network responds with a time constant $G = 5$. $A = 0.1351$ corresponds to the collision point, the minimum network time constant, which is $\sqrt{\tau G} \approx 3.2$. (The difference between $A = 0$ and the solution at the collision point is much greater for larger G.) Theoretically, the network begins to ring for larger values of A, but we can increase A up to 0.8 without any perceptible ringing; there is only an overshooting response. For somewhat higher A, ringing becomes obvious. Parameters: $\tau = 2$, $G = 5$.

Although in theory ringing does set in for $A > 0.1351$, oscillations are not at all perceptible until A is much larger (> 0.8 here). Initially an overshooting response develops; subsequent cycles are not visible because of the damping. Intuitively, the overshooting response ($A = 0.8$) looks faster

than the response with minimum time constant ($A = 0.1351$)because the system comes close to its steady state firing rate much earlier. An overshooting response, while it technically lengthens the time constant, may actually be preferable; the time constant may not be a good measure of the response time.

It is possible to glean some more information on the shape of the response from a further analysis of equation 6.21. A difference of two exponentials can give several different shapes of responses, including an overshooting response, depending on the signs and magnitudes of the coefficients C_1 and C_2 (equation 6.22 on page 96).

If A is such that both poles are real, then $s > -1/\tau > -1$ (see above), and by definition $s_1 < s_2$. This implies that $C_1 > 0$ and $C_2 < 0$. Furthermore, since

$$\lim_{s\to\infty} s\hat{f}(s) = \lim_{T\to 0^+} f(T),$$

we see from equation 6.20 that $f(0) = I_{ff}$. Substituting this into equation 6.21 gives

$$C_1 + C_2 = -(G - 1) < 0.$$

Given that $C_1 > 0$ and $C_2 < 0$, it follows that $|C_1| < |C_2|$. Since the time constant associated with C_1 is also shorter than the time constant associated with C_2, it follows that the response in this simplified system cannot be overshooting unless there is ringing, regardless of the parameters.

6.8 Discussion

The effect of adaptation in a recurrent network may be qualitatively different from its effect in a feedforward network. In a recurrent network, it can very significantly speed up response time of the network.

Suarez (1994) found that in his network of spiking neurons, the network time constant was around 25 ms with adaptation present. It is difficult to compare this analysis with his work directly. He used an alpha function with a time constant of 20 ms for the synaptic time course, so his feedback conductance had a slower rise time but a much faster fall time. He found that when he sped up the dynamics of the calcium conductance, network time constants increased dramatically; perhaps this is because he reduced the rise time of adaptation below the rise time of feedback. His network is not entirely linear because the $f - I$ curves are not exactly straight, as assumed here, so other effects may also be important.

Since cortical neuronal responses are usually overshooting, it is not at all unlikely that the cortical network is set up to have an overshooting (slightly ringing) response. On the other hand, the overshooting may be due to nonlinear mechanisms such as synaptic depression.

This analysis is for mean-rate neurons, which under some circumstances behave differently from spiking neurons. If inhibition is very strong, networks of spiking neurons can very rapidly reach their steady state firing rates (Usher *et al.*, 1994; Tsodyks and Sejnowski, 1995; van Vreeswijk and Sompolinsky, 1996). However, these spiking networks tend to have very low gain and use only fast conductances, ignoring the slower NMDA and $GABA_B$ synapses. The "canonical" microcircuit network as we have simulated it so far appears to be fairly well described by equation 6.3 (Holt and Koch, manuscript in preparation).

Chapter 7 Steady state of circuits with dynamic synapses

7.1 Introduction

Multiplication and division are essential components of many models of cortical function (e.g., Heeger, 1993), and there is physiological evidence for divisive interactions between stimuli (Rose, 1977; Dean *et al.*, 1980; Reid *et al.*, 1987). However, the underlying biophysical mechanism responsible for this nonlinearity is not clear, and a number of different mechanisms are possible (Mel, 1994; Somers *et al.*, 1996; Salinas and Abbott, 1996). Shunting inhibition is a commonly proposed mechanism for division, but the conductance changes required have not been observed so far (Berman *et al.*, 1989; Ferster and Jagadeesh, 1992) and in fact shunting inhibition acts subtractively rather than divisively in spiking neurons (Holt and Koch, 1997; chapter 4). We suggest another possible mechanism based on the phenomena of paired pulse depression and facilitation.

In vitro in cortex, synaptic depression and facilitation have been observed at a variety of different synapses in olfactory cortex (e.g., Bower and Haberly, 1986), somatomotor areas (Thomson and West, 1993; Thomson *et al.*, 1993a, 1993b, 1995; Thomson and Deuchars, 1994) and in visual cortex (Stratford *et al.*, 1996; Markram and Tsodyks, 1996; Tsodyks and Markram, 1997; Abbott *et al.*, 1997). It is not yet clear how widespread the phenomena of depression and facilitation are *in vivo*. Recently Abbott *et al.* (1997) and Tsodyks and Markram (1997) have suggested a number of ways in which synaptic depression could be computationally useful. The steady-state synaptic current delivered by synapses from layer 4 to layers 2–3 and synapses between layer 5 cells is approximately independent of presynaptic firing rate when the presynaptic firing rate is above 20 Hz, making the postsynaptic cell sensitive to fractional changes in its input rather than the absolute level. However, the layer 4 to layer 4 synapses observed by Stratford *et al.* (1996) show considerably less synaptic depression; synaptic current is a slowly saturating function of the presynaptic firing rate rather than a constant. We suggest that the cortex uses this slowly saturating function as an approximation to a logarithm.

Thalamic afferents to visual cortex terminate primarily on layer 4 spiny stellate cells. Anatomically, however, the majority of the input to these cells comes from other cortical sources (Peters and Payne, 1993; Peters *et al.*, 1994). Most of this comes from cells with similar receptive fields. 40%of

the excitatory synapses onto spiny stellate cells come from other spiny stellate cells, and about 45% come from layer 6 pyramidal cells (Ahmed *et al.*, 1994; Anderson *et al.*, 1994a, 1994b). Since layer 4 cells have a strong projection to layer 6, and layer 4 is the primary cortical target of layer 6 cells, there is an important feedback loop between these two layers. Inactivation of layer 6 cells can affect the firing rate of layer 4 cells by a factor of two or more (Grieve and Sillito, 1991, 1995). The presence of strong layer 4 to layer 4 and layer 4 to layer 6 to layer 4 feedback loops suggests that a small thalamic current is amplified by recurrent cortical excitation (Douglas and Martin, 1991).

Models based on the idea of an amplifier (Suarez *et al.*, 1995; Somers *et al.*, 1995; Maex and Orban, 1996) can explain a variety of puzzling physiological results but so far have assumed that synapses are non-depressing or only very slowly depressing. However, layer 6 to layer 4 synapses *in vivo* show pronounced facilitation. Synapse strength can increase by a factor of two or more (Ferster and Lindström, 1985a, 1985b; Stratford *et al.*, 1996). This study suggests that the facilitation at synapses of layer 6 cell axons compensates for depression at synapses on layer 4 axons. By using a loop consisting of depressing and facilitating synapses instead of ordinary linear synapses, the cortex might be able to perform additional computations. The firing rate of layer 6 cells may be approximately the logarithm of the firing rate of layer 4 cells; additive and subtractive effects on the layer 6 cells will have approximately multiplicative and divisive effects on the layer 4 cells.

7.2 Synaptic depression model

Abbott *et al.* (1997)[1] use a simple mathematical model of depressing synapses:

$$\frac{dA}{dt} = \frac{A_\infty - A(t)}{\tau} - \gamma \sum_i \delta(t - t_i) A(t) \tag{7.1}$$

where $A(t)$ is the amplitude of the synapse if a presynaptic impulse occurs at time t. An incoming spike decreases the amplitude of the next impulse to $(1 - \gamma)A$, and then the amplitude decays exponentially back to A_∞. Replacing the sum of δ functions by a continuous firing rate[2] $f(t)$ gives

$$\frac{dA}{dt} = \frac{A_\infty - A(t)}{\tau} - \gamma f(t) A(t). \tag{7.2}$$

[1] Abbott *et al.* (1997) use a slightly different notation: their f is $1 - \gamma$ and their $r(t)$ is our $f(t)$.

[2] Abbott *et al.* (1997) work with continuous rates by assuming the interspike intervals are perfectly regular and then solving equation 7.1 for the steady state. The approach here gives a much more tractable expression which turns out to be slightly more accurate for spike trains from a Poisson process than their formulation (not shown).

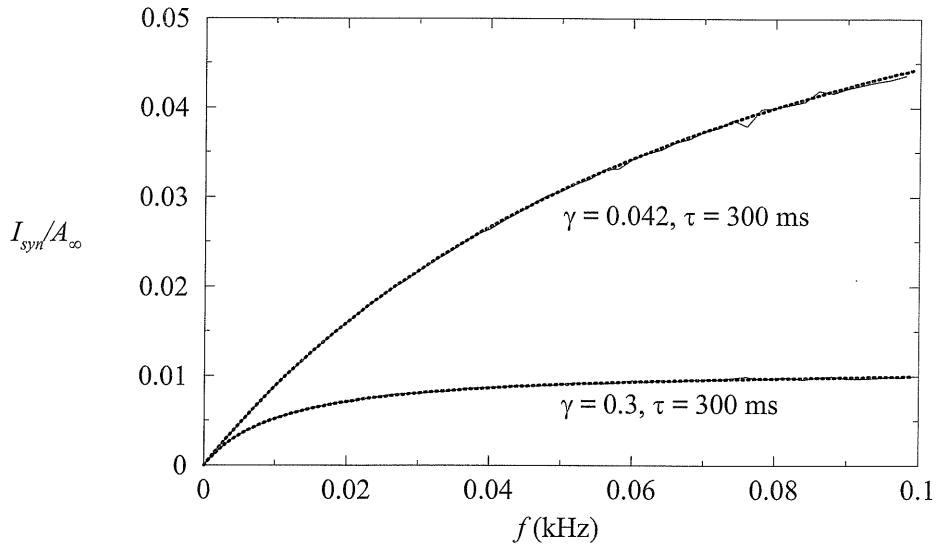

Figure 7.1: Synaptic current I_{syn} as a function of presynaptic firing rate. Solid lines are the mean EPSP amplitude of a synapse following equation 7.1 driven by a Poisson process for 5000 spikes at each input rate f, and the dotted lines are the prediction from equation 7.4. When $\gamma\tau = 12.5$ ms (upper curves), I_{syn} is a slowly saturating function over the relevant range of firing rates. When $\gamma\tau = 90$ ms (lower curves; Abbott *et al.*, 1997), I_{syn} is approximately constant for firing rates above 20 Hz (solid line).

At steady state, then,

$$A = \frac{A_\infty}{1 + f\gamma\tau}, \tag{7.3}$$

so the synaptic current delivered will be

$$I_{syn} = fA = \frac{fA_\infty}{1 + f\gamma\tau}. \tag{7.4}$$

This approximates the average synaptic current from a synapse driven by a Poisson process with rate f quite well (figure 7.1).

Abbott *et al.* (1997) measure $\gamma\tau$ values in the range of 28 to 210 ms for synapses from layer 4 to layers 2–3. However, Stratford *et al.* (1996) report that layer 4 to layer 4 synapses in their preparation do not show visible synaptic depression when the interspike firing rate is 20 Hz. When presynaptic firing rates are increased to 80 Hz the amplitude is a factor of two smaller (Stratford, personal communication), suggesting that for these synapses $f\tau \approx 1/80$ Hz or 12.5 ms. We examine the effect of both values.

7.3 Effect on simple recurrent networks

Douglas and Martin (1991) suggest that the recurrent cortical input to the layer 4 cells acts as an amplifier, so the firing rate of the layer 4 cells is approximately proportional to the LGN input current but is perhaps a factor of five or so larger than it would be if only the synapses from the LGN were present. In symbols,

$$f = \alpha(I_{ff} + I_{rec}), \tag{7.5}$$

where f is the firing rate of the layer 4 cells, I_{ff} is the feedforward thalamic input, I_{rec} is the recurrent cortical input, and α is the slope of the current–discharge curve for the cortical cells. For the moment we consider input only from other layer 4 cells, so

$$I_{rec} = Af, \tag{7.6}$$

where A is the synaptic weight from layer 4 cells to other layer 4 cells. Solving this system,

$$f = \frac{\alpha I_{ff}}{1 - \alpha A} = G\alpha I_{ff}, \tag{7.7}$$

where G is the gain (i.e., the ratio of the firing rate to what the firing rate would be in the absence of any cortical feedback). Douglas and Martin (1991) estimate that G is somewhere close to 5.

If synapses are non-depressing, then A is a constant, and therefore $G = 1/(1 - \alpha A)$ is a constant independent of the amount of input current. The system is a proportional amplifier. However, if A is not a constant, then the response of the system is no longer proportional to its input. If we use the parameters from Abbott *et al.* (1997), it would not at all be surprising to find that the system does not act as a proportional amplifier at firing rates above 20 Hz, since I_{rec} is approximately constant and therefore cannot be proportional to I_{ff}. However, it may be more surprising that the system ceases to be a proportional amplifier long before I_{rec} comes close to saturating.

With depressing synapses, equation 7.7 becomes

$$f = \frac{\alpha I_{ff}}{1 - \frac{\alpha A_\infty f}{1+\gamma\tau f}}. \tag{7.8}$$

Figure 7.2 shows the solution to this equation. Note that for $\gamma\tau = 12.5$ ms, I_{syn} does not saturate until about 150 Hz (figure 7.1), whereas there is very little amplification above even 20 Hz.

In fact, the gain $G = 1/(1 - \alpha A_\infty/(1 + \gamma\tau f))$ drops precipitously for $f > 2$ Hz for $\gamma\tau = 90$ ms and for $f > 10$ Hz for $\gamma\tau = 12.5$ ms (figure 7.3). The drop is even more severe if we consider the

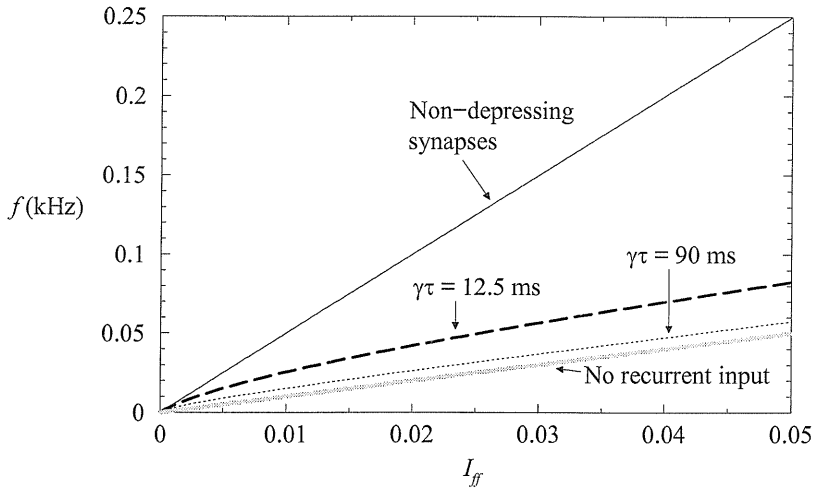

Figure 7.2: Synaptic depression dramatically reduces the output of the network, even at firing rates well before I_{syn} saturates. Solid line is the output if synapses are perfectly linear. For the top dotted line ($\gamma\tau$ = 12.5 ms), I_{syn} saturates at firing rates of 150 Hz; for the bottom] ($\gamma\tau$ = 90 ms), I_{syn} saturates at around 20 Hz (compare with figure 7.1). α was set to 1 so the gain is simply the ratio of the y to x coordinate and the small signal gain is the slope.

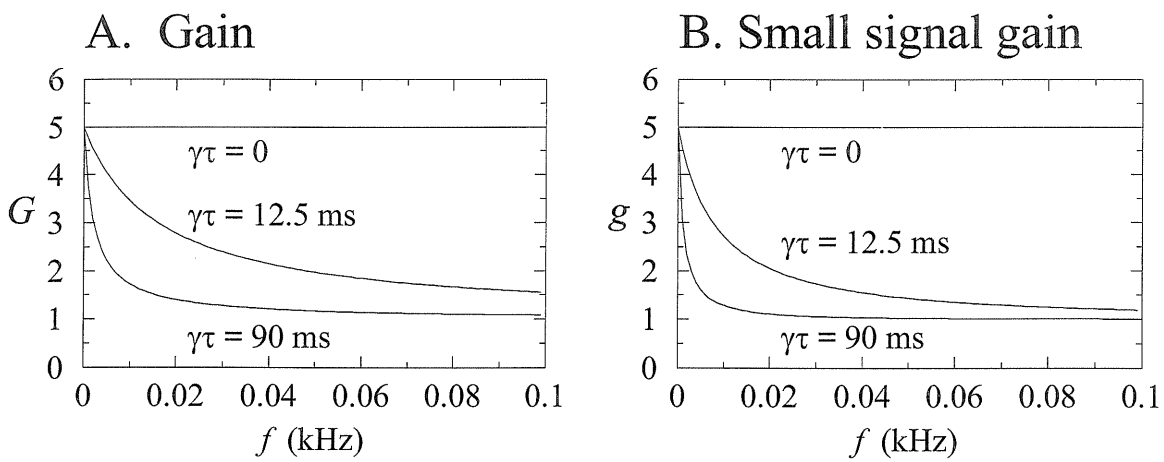

Figure 7.3: The gain G (panel A) and the small signal (or incremental) gain g (panel B) fall off much more steeply than one might naively expect based on the plot of I_{syn} vs. f (figure 7.1).

small signal or incremental gain, i.e., the ratio of the change in output to the change in input (the slope in figure 7.2):

$$\begin{aligned} g = \frac{1}{\alpha}\frac{df}{dI_{ff}} &= \frac{1}{\alpha}\frac{d}{dI_{ff}}\alpha(I_{ff} + I_{rec}) \\ &= 1 + \frac{dI_{rec}}{dI_{ff}} \\ &= 1 + \alpha\frac{dI_{rec}}{df}\left(\frac{1}{\alpha}\frac{df}{dI_{ff}}\right) \\ &= \frac{1}{1 - \alpha\frac{dI_{rec}}{df}}. \end{aligned} \tag{7.9}$$

Since $I_{rec} = fA_\infty/(1+\gamma\tau f)$,

$$g = \frac{1}{1 - \frac{\alpha A_\infty}{(1+\gamma\tau f)^2}}. \tag{7.10}$$

This depends on $(1+\gamma\tau f)^2$ rather than on $1+\gamma\tau f$. It falls off more steeply than the gain G (figure 7.3B).

7.3.1 Recurrence greatly amplifies deviations from linearity

Why is the effect of even a small nonlinearity in I_{syn} so dramatic? Suppose we start with a system with gain G_0, and then we perturb $I_{rec}(f) \to I_{rec}(f)[1+\epsilon(f)]$. From equations 7.6 and 7.7, the new gain will be

$$\begin{aligned} G_\epsilon &= \frac{1}{1 - \alpha A(1+\epsilon)} = \frac{1}{1 - \alpha A - \alpha A\epsilon} \\ &= \frac{1/(1-\alpha A)}{1 - \alpha A\epsilon/(1-\alpha A)} \\ &= \frac{G_0}{1 - G_0\epsilon\alpha A}, \end{aligned}$$

and since $\alpha A = 1 - 1/G_0$,

$$\begin{aligned} G_\epsilon &= \frac{G_0}{1 - \epsilon G_0(1 - 1/G_0)} \\ &= G_0(1 + (G_0 - 1)\epsilon + \cdots). \end{aligned} \tag{7.11}$$

Thus percent changes in the recurrent current have an effect proportional to the square of the gain. For example, if we change the recurrent current by 1% and the original gain is 5, there will be a change of about 20% in the output current.

The small signal gain is even more sensitive to perturbations. If the original small signal gain

was g_0, then from equation 7.9 on the preceding page, the new small signal gain will be

$$\begin{aligned} g_\epsilon &= \frac{1}{1-\alpha\frac{d}{df}I_{rec}(1+\epsilon)} \\ &= \frac{1}{1-\alpha\frac{dI_{rec}}{df}-\alpha\frac{d\epsilon I_{rec}}{df}} \\ &= \frac{1/(1-\alpha dI_{rec}/df)}{1-\frac{\alpha\frac{d\epsilon I_{rec}}{df}}{1-\alpha\frac{dI_{rec}}{df}}} \\ &= \frac{g_0}{1-g_0\alpha\frac{d\epsilon I_{rec}}{df}} \\ &= \frac{g_0}{1-g_0\alpha\epsilon\frac{dI_{rec}}{df}-\alpha I_{rec}\frac{d\epsilon}{df}}. \end{aligned}$$

Since $\alpha dI_{rec}/df = 1 - 1/g_0$ (equation 7.9) and $\alpha I_{rec} = f - \alpha I_{ff} = (1 - 1/G)f$,

$$\begin{aligned} g_0 &= \frac{g_0}{1-(g_0-1)\epsilon-g_0(1-\frac{1}{G})\frac{d\epsilon}{df}} \\ &= g_0\left[1+(g_0-1)\epsilon+g_0\left(1-\frac{1}{G}\right)\frac{d\epsilon}{d}f\right]. \end{aligned} \tag{7.12}$$

For small ϵ values, the change is proportional to $g_0^2\epsilon + g_0 f d\epsilon/df$. Thus g decreases more steeply than G (figure 7.3).

7.4 A possible role for layer 6

The analysis so far has ignored a number of important factors, among them the layer 6 input to layer 4. Blocking layer 6 with GABA iontophoresis causes a decrease in layer 4 response amplitudes by a factor of 2 or more, so the layer 6 input is clearly important. Furthermore, the layer 6 input to layer 4 has been known for many years to show strong facilitation rather than depression *in vivo* (Ferster and Lindström, 1985a, 1985b). It is possible that facilitation compensates for the synaptic depression.[3]

Using the more moderate synaptic depression observed by Stratford *et al.* (1996), the synaptic current I_{syn} is a slowly saturating function of the presynaptic firing rate (figure 7.1). This saturating function might be used as an approximation to a logarithm[4], and the facilitation observed in the synapses from layer 4 to layer 6 might be an approximation to an exponential. The resulting loop would have a linear input–output relationship, but subtractive inhibition in layer 6 would have a

[3]The layer 6 projection to the thalamus will have mathematically the same effect on layer 4 cells as the 16 projection to layer 4 if the thalamocortical synapses are non-depressing, since it merely adds an amount proportional to the layer 6 firing rate to the layer 4 input.

[4]See Tal and Schwartz (1997) for a similar approximation to a logarithm using the refractory period of a neuron.

divisive effect on layer 4.

7.4.1 A simplified example

To illustrate the mechanism, suppose fist that synaptic depression and facilitation exactly compute the logarithm and exponent:

$$\begin{aligned} A_4 &\approx A_{40} \log s_4 f_4 \quad \text{for } s_4 f_4 > 1 \\ A_6 &\approx A_{60} e^{s_6 f_6} \end{aligned} \tag{7.13}$$

where s_4 and s_6 are constants. The firing rates of the layer 4 and layer 6 cells are given by

$$\begin{aligned} f_4 &= \alpha_4 (I_{ff} + A_6 f_6) \\ f_6 &= \alpha_6 (A_4 f_4 - I_{inh}) \end{aligned} \tag{7.14}$$

where α is the slope of the current discharge curve, I_{ff} is the synaptic current from the thalamic afferents, A_4 and A_6 are the amplitudes of the synapses on the axons of the layer 4 and layer 6 cells, and I_{inh} is an inhibitory current onto layer 6 cells. Eliminating f_6,

$$f_4 = \alpha_4 I_{ff} + \alpha_4 A_{60} e^{s_6 \alpha_6 (A_{40} \log s_4 f_4 - I_{inh})} \tag{7.15}$$

Setting $s_6 \alpha_6 A_{40} = 1$ makes the feedback current proportional to f_4 with a proportionality constant governed by I_{inh}.[5] The system simplifies to

$$f_4 = \frac{\alpha_4 I_{ff}}{1 - \alpha_4 A_{60} s_4 e^{-I_{inh}/A_{40}}} \tag{7.16}$$

so the firing rate of layer 4 cells is proportional to their input times a function which depends on an inhibitory current. Inhibition in layer 6 therefore has a divisive effect on layer 4.

7.4.2 More realistic synapses

Although synaptic depression is only an approximation to a logarithm, it may be a sufficiently accurate approximation to support divisive interactions. Synaptic facilitation in layer 6 cells has not yet been quantitatively characterized; we first derive a form that makes the layer 4 to layer 6 to layer 4 loop into a linear amplifier, and then we analyze the effect of inhibition in layer 4.

[5] Note that other values of $s_6 \alpha_6 A_{40}$ will make the firing rate f_4 be a nonlinear function of I_{ff}. This could be used, for example, to compute an approximate square (Heeger, 1992b).

Equations 7.5 and 7.6 on page 109 can be modified to include layer 6:

$$f_4 = \alpha_4 \lfloor I_{ff} + A_6 f_6 + A_{44} f_4 \rfloor \tag{7.17}$$

$$f_6 = \alpha_6 \lfloor A_{46} f_4 - I_{inh} \rfloor \tag{7.18}$$

where $\lfloor x \rfloor = 0$ if $x < 0$ and x otherwise. A_{44} is the amplitude of the synapses from layer 4 to layer 4, which will depend on frequency f as described by equation 7.3 on page 108; A_{46}, the weight from layer 4 to layer 6, has the same frequency dependence but a possibly different amplitude. I_{inh} is inhibitory current supplied to layer 6.

We want to calculate what the form of A_6 is so that the system acts as a proportional amplifier when $I_{inh} = 0$. In a proportional amplifier, the total input current to layer 4 cells is proportional to the thalamic input:

$$I_{ff} + A_6 f_6 + A_{44} f_4 = G I_{ff}$$

where G is the gain of the network. Eliminating I_{ff} using equation 7.17,

$$I_{ff} = \frac{f_4 - \alpha_4 A_6 f_6 - \alpha_4 A_{44} f_4}{\alpha_4} = \frac{A_6 f_6 + A_{44} f_4}{G - 1}.$$

Following equation 7.3,

$$A_{44} = \frac{A_{44\infty}}{1 + \gamma_4 \tau_4} \qquad A_{46} = \frac{A_{46\infty}}{1 + \gamma_4 \tau_4}. \tag{7.19}$$

Using these expressions and equation 7.18, we can eliminate f_4. After some algebra,

$$A_6(f) = \left(\frac{G - 1}{G \alpha_4 \alpha_6 A_{46\infty}} \right) \left(\frac{1}{1 - \frac{\gamma_4 \tau_4}{\alpha_6 A_{46\infty}} f_6} \right) - \frac{A_{44\infty}}{\alpha_6 A_{46\infty}}. \tag{7.20}$$

Note that the description of facilitating synapses in equation 7.20 is similar in form to equation 7.3 on page 108 for depressing synapses; the sign of $\gamma\tau$ has been reversed, and a constant value subtracted.

If synaptic facilitation in layer 6 cells follows this equation, then layer 4 cells will respond linearly to their input. This expression has a pole for $f_6 = \alpha_6 A_{46\infty} / \gamma_4 \tau_4$, so facilitation cannot have exactly this form, but we will consider only layer 6 firing rates far from the pole.

Since depression is not exactly logarithmic and facilitation is not exactly exponential, this will not exactly implement the log-and-exponentiation transform described above. However, it performs remarkably well. Figure 7.4 shows simulations of the circuit.

The firing rate of layer 6 cells cannot be negative, so there is no divisive effect at very low firing

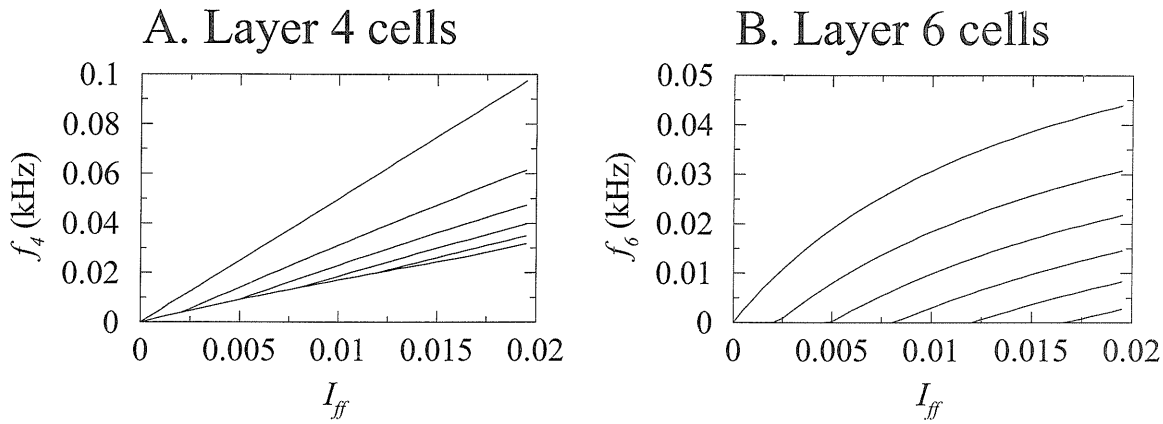

Figure 7.4: Inhibitory input to layer 6 has a divisive effect on layer 4 firing rates. **A**: Firing rate of layer 4 cells as a function of the input current I_{ff} for different values of I_{inh}. At higher firing rates, changing I_{inh} changes only the slope of the curve. **B**: Firing rate of layer 6 cells under the same conditions. The kinks in the curves in A are present because layer 6 firing rates cannot be negative; the bend occurs when the layer 6 firing rate becomes positive. Parameters: $\alpha_4 = \alpha_6 = 1$, $A_{44\infty} = 0.5$, $A_{46\infty} = 1$, $G = 5$, $\gamma_4\tau_4 = 12.5$ ms, I_{inh} ranged from 0 to 0.02 in steps of 0.004. Note that with these parameters, I_{ff} has the same units as f_4 so the gain can be read directly off the graph as the ratio of f to I_{ff}.

rates. The curve in panel A from which all the lines diverge is the input–output relationship when layer 6 cells are turned off; parameter values have been set so the system has a gain of about 1.5 under those circumstances. When layer 6 cells do begin firing, the system acts almost linear; it is not exactly linear but so close that it is not easy to see the deviations from linearity on the graph. In this range, changing I_{inh} primarily changes the slope of the curve rather than shifting it.

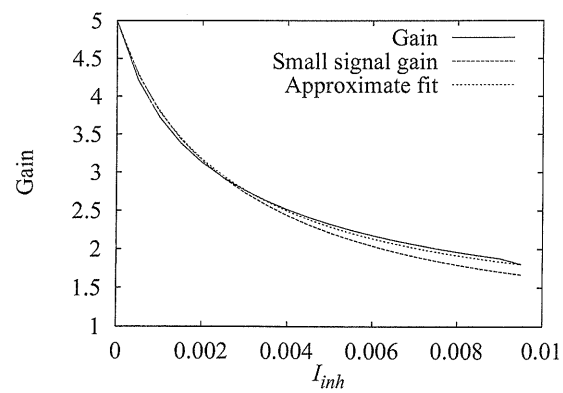

Figure 7.5: The gain G (equation 7.7) and the small signal gain g (equation 7.9) as a function of inhibitory current I_{inh} to the layer 6 cells. The approximate fit is the function $4/(1 + 420 * I_{inh}) + 1$.

7.4.3 What is the arithmetic operation?

Using this mechanism, subtractive inhibition in layer 6 has a divisive effect on layer 4, but so far we have not specified precisely what the divisor is. It is possible to work out the exact input–output relationship from equations 7.17 through 7.20, but the result is complicated and not useful. Instead, we resort to approximate solutions. Figure 7.5 shows the gain G and the small signal gain g as a function of inhibitory current to layer 6 cells. The gain turns out to be well described by a function of the form

$$G(I_{inh}) = \frac{G(0) - 1}{1 + \beta I_{inh}} + 1 \tag{7.21}$$

where $G(0)$ is the gain without any inhibition and β is a constant. Since the feedback is excitatory, the gain cannot be less than 1; that is the origin of the $+1$ term. A number of models require that the output be divided by a factor of $1 + g(x)$ (Heeger, 1992a; Heeger *et al.*, 1996) so this form may be quite useful. The precise expression for $g(x)$ depends on what sort of depression or facilitation the inhibitory synapses onto layer 6 show.

7.5 Conclusions

Synaptic depression has a profound effect on recurrent circuits because any deviation from linearity is amplified greatly by the recurrence. Even if the synapses depress only weakly, as measured by Stratford *et al.* (1996), the resulting network can hardly be called an "amplifier" at steady state. This effect cannot be counteracted simply by increasing the weight of the recurrent synapses. The gain will still fall off precipitously at higher firing rates, because of the $1/(1 + \gamma\tau f)$ term in the denominator of equation 7.8.

Synaptic depression could perform a useful function in an amplifier circuit if it is coupled with synaptic facilitation. If layer 4 to layer 6 synapses display weak synaptic depression, the current into layer 6 could be approximately the logarithm of the layer 4 firing rate. Facilitation in the synapses from layer 6 to layer 4 could approximately undo the effect of the depression. Subtractive inhibition in layer 6 would have an approximately divisive effect on layer 4.

Such a mechanism makes several testable predictions about responses in layer 4 and layer 6:

1. Layer 4 synapses onto layer 6 should show weak paired pulse depression as described by equation 7.19, and layer 6 cells should show facilitation with corresponding parameters given by equation 7.20 over the relevant range of firing rates. A considerable amount of variability in parameter values is most likely present in cortex, but facilitation in the layer 6 population as a whole should approximately compensate for depression in the population of layer 4 synapses.

2. Divisive interactions should not be visible immediately, in the transient response; it should take a few spikes for the layer 4 synapses to depress and the layer 6 synapses to facilitate to reach their steady state levels. Divisive interactions might be apparent only for slowly changing stimuli.

3. Divisive interactions should be visible only in layer 4, not layer 6.

4. Divisive effects should not be visible when the layer 6 cell population is silenced by GABA iontophoresis as in the experiments by Grieve and Sillito (1991, 1995).

5. Layer 6 cells should have a contrast response curve that saturates earlier than layer 4.

To my knowledge, no one examining divisive interactions or contrast response curves has reported what layers they recorded from.

Part IV

Appendices

Appendix A The homogenization approximation for parallel cables

A.1 Introduction

In order to be able to calculate the extracellular potential, I assumed that the extracellular space can be treated as approximately homogenous (assumption 3 on page 6). But the extracellular space is highly irregular; is this approximation fair?

Electron microscopic reconstructions of the extracellular space are unavailable so it is difficult to come up with an exact model of the extracellular space. However, for the molecular layer of the cerebellum, the extracellular space is fairly regular. I considered a dense set of parallel cables and estimated the magnitude of the effect of the action potential, comparing the potential when I explicitly simulated the extracellular space as broken up into thousands of compartments, and where I treated it as homogenous.

A.2 Hexagonal axon array

Conceptually, the simplest possible array of axons to study would be a rectangular array of cylinders, for which the bulk conductivity has been calculated (see Cole *et al.*, 1969). However, a rectangular array of cylinders has too much extracellular space; in most regions of the brain the extracellular space accounts for about 20% of the volume, and even when the cylinders in a rectangular array are touching, the extracellular volume fraction is larger. So I used a hexagonal array instead.

I also used hexagonal tubes instead of cylindrical tubes because the geometry is more regular. For a given extracellular volume fraction, the surface–to–volume ratio for the hexagonal tubes is only 5% greater than for cylindrical tubes, so distortion should be minimal. The resulting array is shown in figure A.1.

The hexagonal array has 12-fold symmetry, which means that we only need to compute the extracellular potential in the shaded wedge shown in figure A.1. Because of symmetry, no current flows across the upper and lower boundaries of the shaded region; this is equivalent to a Neumann boundary condition on the differential equation.

I used Y-shaped extracellular elements, as shown in figure A.1. At the boundaries of the shaded

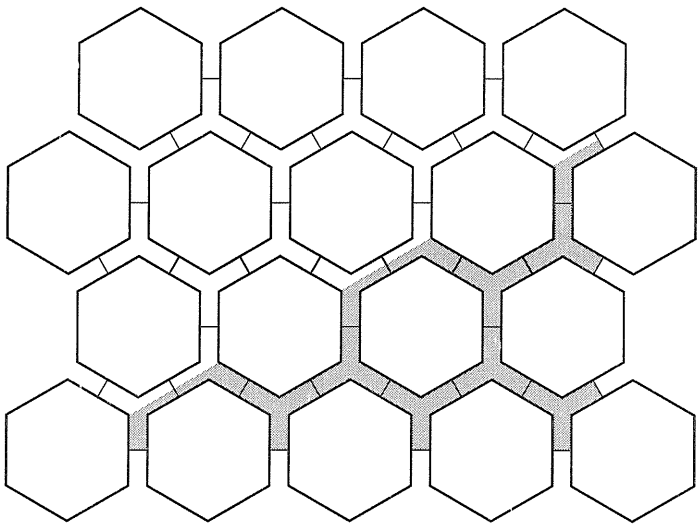

Figure A.1: A cross section perpendicular to the axis of the axons. The hexagonal array around a single hexagon (lower left) has a 12-fold symmetry, so only the shaded wedge is actually simulated.

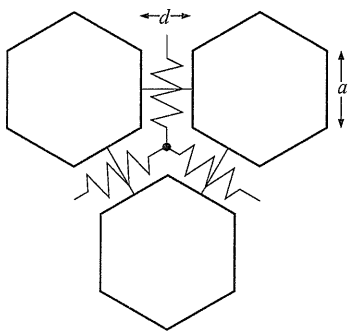

Figure A.2: The geometrical parameters for each element. d is the separation between adjacent hexagonal faces, and a is the side length of each face.

wedge, only half of the element is simulated because of symmetry. Elements were converted into an equivalent resistive grid (figure A.2). The resistances shown in the figure were assigned the value

$$G_{lateral} = \sigma_e \frac{\Delta z d}{a} \tag{A.1}$$

where Δz is the grid spacing in the z direction (coming out of the plane in figures A.1 and A.2). Resistances parallel to the axis of the axons are

$$G_{longitudinal} = \sigma_e \left(\frac{3ad}{2\Delta z} + \frac{\sqrt{3}}{2} \frac{d^2}{\Delta z} \right) \tag{A.2}$$

where the first term corresponds to the area in the arms of the Y and the second is the area of the central triangle.

At the right edge of the wedge, the extracellular potential was set to 0. This boundary condition is important, because the extracellular potentials can depend noticeably on how far away the ground is. Also Clark and Plonsey (1968) found that the extracellular potentials are significantly larger if there is a resistive sheath surrounding the cables; we do not currently simulate this situation, but we could.

Instead of setting up a complicated simulator to solve the Hodgkin–Huxley euqations explicitly for the central axon, I simply assumed a set of transmembrane currents at each point along the axon. I used my previous simulator to calculate the transmembrane currents for an axon with the same surface area. I then took 1/12 of the total current at each z value along the axon and injected that into the extracellular space at the tip of the wedge in figure A.1.

This approach is reasonable because we don't expect the extracellular potentials to be large, so they shouldn't have a significant effect. Even if they are noticeable, the effect on the transmembrane potential (and therefore the transmembrane current) will be small because the intracellular potential tends to move along with the extracellular potential. Clark and Plonsey (1968) used precisely the same procedure except they assumed a current distribution rather than taking a previously calculated one.

It has been known for some time that in the relevant frequency range (around 1 kHz) the capacitance of the membranes are essentially irrelevant to measurements of bulk impedance. Therefore I did not model the capacitance of the membranes. I also neglected current through the membranes, because I am interested in the largest possible extracellular effects. Therefore, for simplicity I assumed that the membranes of the inactive axons are completely non-conducting.

A.2.1 Parameter values for hexaongal array

There are several critical parameters in the simulations. a, the side length of the hexagons, can be easily determined from EM views of the tissue. I used $a = 2\pi \times 0.1/6$ μm so that the surface area of the hexagonal tube is the same as the surface area of a cylinder with a radius of 0.1 μm.

d, the distance between fibers, is determined by a if the volume fraction α of the tissue (the fraction of the volume that is extracellular space) is given. α is usually around 20% in most tissues, but in the parallel fiber system it is closer to 30% (see Nicholson, 1995). The extracellular volume fraction is simply the ratio of the area between the dotted hexagon and the inner solid hexagon in figure A.3 to the area of the dotted hexagon, which is

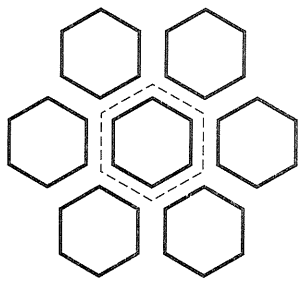

Figure A.3: Scheme used for calculation of volume fraction.

$$\alpha = 1 - \frac{1}{(1 + \frac{d}{2a})^2}. \tag{A.3}$$

Solving for d gives:

$$d = a\frac{\sqrt{\frac{1}{1-\alpha}} - 1}{2}. \tag{A.4}$$

I used a volume fraction of 0.2 (typical for the whole brain; see Nicholson, 1995), implying $d = 0.06a$. 0.3 would be more appropriate for the cerebellar molecular layer (see Nicholson, 1995); this would imply $d = 0.098a$. In this case the extracellular potentials will be even lower.

We use the bulk conductivity to constrain the resistivity of the extracellular fluid. In this hexagonal grid, the bulk conductivity varies depending on the direction of current flow. If current is flowing parallel to the axis of the axons, then the conductivity is the conductivity of the interstial fluid, σ_e, adjusted for the fraction α of the space which is extracellular:

$$\sigma_z = \sigma_e \alpha \tag{A.5}$$

The bulk conductivity in the horizontal direction on the grid in figure A.1 is slightly more complicated to calculate. The tissue is composed of a number of repeating blocks like that shown in figure A.4, joined together at their edges. The conductance between the left and right face of the block is

$$g_{block} = 2\frac{\Delta z d}{2a}\sigma_e. \tag{A.6}$$

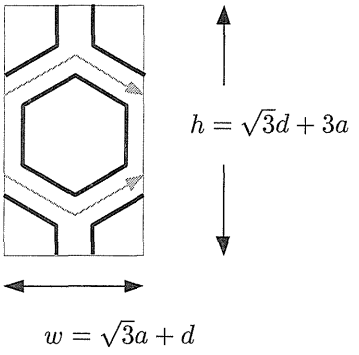

Figure A.4: The unit cell for a hexagonal array, showing the current path used to calculate conductivity in the left-right direction.

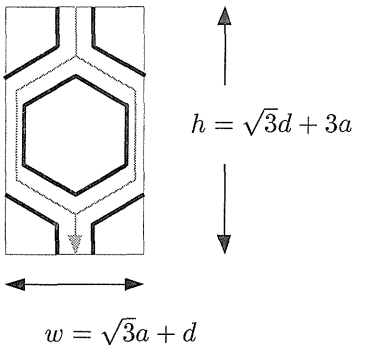

Figure A.5: The unit cell for a hexagonal array, showing the current path used to calculate conductivity in the vertical direction.

The bulk conductivity in the horizontal direction is

$$\begin{aligned}\sigma_x &= g_{block}\frac{w}{h\Delta z} \\ &= \sigma_e \frac{d}{a}\frac{\sqrt{3}a + d}{\sqrt{3}d + 3a}.\end{aligned}$$

The bulk conductivity in the vertical direction can be calculated similarly, using the same fundamental block but a different current path (figure A.5):

$$\begin{aligned}g_{block} &= \left[\left(\frac{a}{\sigma_e d\Delta z}\right) + \frac{1}{2}\left(\frac{2a}{\sigma_e d\Delta z} + \frac{a}{\sigma_e \frac{d}{2}\Delta z}\right)\right]^{-1} \\ &= \sigma_e \frac{d\Delta z}{3a},\end{aligned}$$

so the bulk conductivity in the vertical direction is

$$\begin{aligned}\sigma_y &= g_{block}\frac{h}{w\Delta z} \\ &= \sigma_e \frac{d}{3a}\frac{\sqrt{3}d + 3a}{\sqrt{3}a + d} \\ &= \sigma_e \frac{d}{a}\frac{\sqrt{3}a + d}{\sqrt{3}d + 3a} \\ &= \sigma_x.\end{aligned}$$

The conductivity in the various different directions is shown in table A.1. Note that σ_z/σ_x is 5 or 6: the conductivity is highly anisotropic. This is actually more anisotropic than *in vivo* among the cerebellar parallel fibers. The tortuosity λ varies from 1.44 to 1.95 in turtle cerebellum, and

since $\sigma = \sigma_e \alpha / \lambda^2$, the bulk conductivity varies by only a factor of 1.8 as a function of direction (see Nicholson, 1995). The difference is probably due to the presence of Purkinje cell dendrites, radial glia, and other inhomogeneities in the cerebellar molecular layer. These could lower σ_z and raise σ_x somewhat.

	$\alpha = 0.2$	$\alpha = 0.3$
σ_x	$0.034\sigma_e$	$0.056\sigma_e$
σ_y	$0.034\sigma_e$	$0.056\sigma_e$
σ_z	$0.2\sigma_e$	$0.3\sigma_e$

Table A.1: Bulk conductivity of the hexagonal array in different directions. σ_e is the conductivity of the interstitial medium by itself, and α is the extracellular volume fraction.

A.3 Homogenized extracellular space

For comparison, I computed extracellular potentials in a system where the hexagonal array of tubes has been replaced with a medium of the same bulk conductivity. Since the conductance is anisotropic, the equation which must be solved is

$$\nabla \cdot \left(\sigma_{xy} \frac{\partial \phi}{\partial x} \hat{\mathbf{i}} + \sigma_{xy} \frac{\partial \phi}{\partial y} \hat{\mathbf{j}} + \sigma_z \frac{\partial \phi}{\partial z} \hat{\mathbf{k}} \right) = 0 \tag{A.7}$$

where the boundary conditions are

$$\sigma_{xy} \nabla \phi \cdot \hat{\mathbf{n}} = J_m \tag{A.8}$$

where J_m is the current density through the membrane at that point. We also assume the tissue is grounded a distance r_{max} away.

The numerical methods for solving this equation are discussed in section C.2.2. Increasing the density of points in the u or z direction had essentially no effect. I used 70 $\Omega-$cm for the extracellular resistivity and computed σ_{xy} and σ_z using a volume fraction of 0.2 from table A.1.

A.4 Comparison of simulations

To obtain the transmembrane currents, I first simulated a single 5 mm axon with a diameter of 0.1 μm using the standard Hodgkin-Huxley formalism and parameters, assuming that the extracellular potential was everywhere at ground. When the action potential was close to the middle of the axon, I recorded the currents flowing through each compartment of the axon.

These currents were then used to set the boundary conditions for the hexagonal array simulation and the homogenized extracellular space simulation. The hexagonal axon array requires far larger matrices because the element sizes are specified by the hexagonal geometry and cannot be changed;

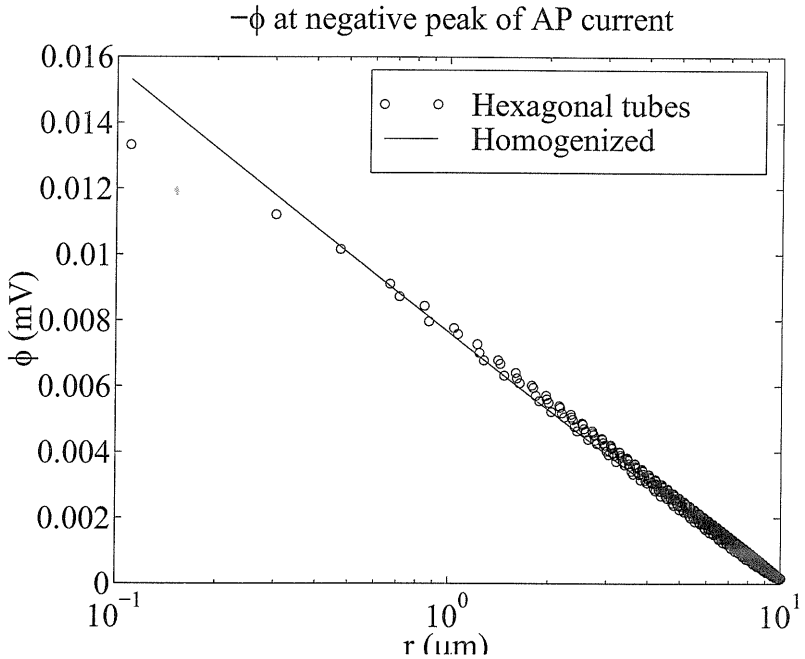

Figure A.6: $-\phi$ as a function of distance from the axon in both simulations at the z position where the maximum current is flowing into the axon. The hexagonal array results are shown as a scatterplot rather than a line because there is no natural ordering of all of the elements.

as a result, I could only solve for a wedge with 50 axons on the base (about 10 μm thick), even when I used only a small fraction of points along the z axis that I used in the other simulation. I also had to use a different technique that takes less memory (the biconjugate gradient method). It is possible to solve far larger problems easily using the homogenized extracellular space approximation.

To make the simulations comparable, both were solved with the extracellular ground placed 10 μm away from the axon in the r direction. (This extracellular ground is quite close but I was unable to do a larger hexagonal array simulation.) Each end of the axon was also grounded. The two simulation paradigms produce very similar results over the domain I was able to compare them in (figures A.6 and A.7). It is clear, therefore, that nothing is gained in this problem by modeling the extracellular space explicitly, and that the homogenization approximation should be used in subsequent work.

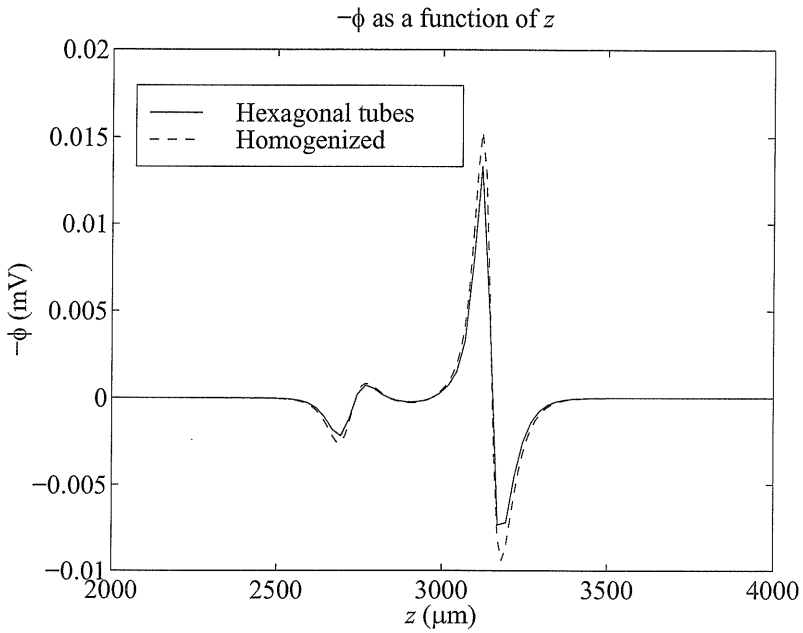

Figure A.7: $-\phi$ adjacent to the membrane as a function of distance along the axon in both simulations.

Appendix B Time average voltage

Koch *et al.* (1995) argue that to a surprisingly good approximation the time averaged voltage of a simulated cell above threshold depends logarithmically on the applied current and linearly on the firing frequency. This dependence suggests that the spiking mechanism be modeled by a diode, a circuit element with a logarithmic relationship between voltage and current—the *diode model.* However, this was only tested this for one particular model of a cell, the model described by Bernander *et al.* (1991, 1994). Since that compartmental model had only voltage-independent time constants for the conductances, it is possible that the relationship is an artifact of the model and does not apply to real cells.

I attempted to explore the validity of the logarithmic relationship for other systems. I looked at integrate and fire cells and the basic Hodgkin-Huxley equations; I also attempted to test real cells in slice as well.

B.1 Integrate–and–fire

For integrate and fire cells receiving constant input it is possible to compute the time averaged voltage analytically. Suppose we have a leaky integrator with a capacitance C, a membrane resistance R, and a threshold voltage V_{th}. Then the membrane potential between spikes is described by

$$C\frac{dV_m}{dt} = -\frac{V_m}{R} + I \tag{B.1}$$

where I is the input current. Let T be the interval between spikes not counting the refractory period; then

$$T = \begin{cases} -RC\ln\left(1 - \frac{V_{th}}{IR}\right) & \text{for a leaky integrator,} \\ \frac{CV_{th}}{I} & \text{for a perfect integrator.} \end{cases} \tag{B.2}$$

The time averaged membrane potential, averaging over the spike itself and the refractory period as well as the intervals between spikes, will be

$$\langle V_m \rangle = ft_r V_{spike} + (1 - ft_r)V_{ISI}, \tag{B.3}$$

where f is the firing rate and t_r is the length of the spike and the refractory period. V_{spike} is the average voltage during the whole period t_r, including both the spike and the refractory period. This is an arbitrary constant in the integrate-and-fire model. V_{ISI} is the average voltage between spikes (during all the time not counted in the refractory period t_r).

V_{ISI} can be computed from

$$V_{ISI} = \frac{1}{T}\int_0^T V_m(t)\,dt, \tag{B.4}$$

where (as above) T is the length of the period between spikes, not including the refractory period. For a perfect integrator, since the voltage increases linearly, this works out to be $V_{ISI} = V_{th}/2$. After some rearrangements,

$$\begin{aligned}\langle V_m\rangle &= \frac{V_{th}}{2} + \frac{t_r}{t_r + \frac{CV_{th}}{I}}\left(V_{spike} - \frac{V_{th}}{2}\right) \\ &= \frac{V_{th}}{2} + ft_r\left(V_{spike} - \frac{V_{th}}{2}\right).\end{aligned} \tag{B.5}$$

Thus $\langle V_m\rangle$ depends linearly on the firing frequency f and sub-linearly (not exactly logarithmically) on I. If there were no refractory period ($t_r = 0$) then $\langle V_m\rangle = V_{th}/2$, regardless of the value of f and I.

For a leaky integrator, the time averaged membrane potential is linear in I if $I < I_{th}$, where $I_{th} = V_{th}/R$ is the current threshold. For $I > I_{th}$,

$$\begin{aligned}\langle V_m\rangle = &\left(1 - \frac{t_r}{t_r - \tau\ln\left(1 - \frac{I_{th}}{I}\right)}\right)\left(\frac{I}{I_{th}} + \frac{1}{\ln\left(1 - \frac{I_{th}}{I}\right)}\right)V_{th} + \\ &\frac{V_{spike}t_r}{t_r - \tau\ln\left(1 - \frac{I_{th}}{I}\right)} \\ = &(1 - ft_r)\left(\frac{1}{1 - e^{-\left(\frac{1}{f} - t_r\right)/\tau}} + \frac{\tau}{\frac{1}{f} - t_r}\right)V_{th} + ft_rV_{spike}\end{aligned} \tag{B.6}$$

where $\tau = RC$. This function is non-monotonic because for just subthreshold currents, $\langle V_m\rangle \approx V_{th}$; when spiking begins, the spike reset mechanism reduces the potential back to zero, thus lowering $\langle V_m\rangle$. For high I the curve approaches that of the perfect integrator but always remains a distance away; the leak is like subtracting a constant current (chapter 4).

These results for one particular set of numerical parameters are shown in figure B.1. Membrane potential is approximately a logarithmic function of current, but not a linear function of firing frequency except when the interspike interval is comparable to the time constant.

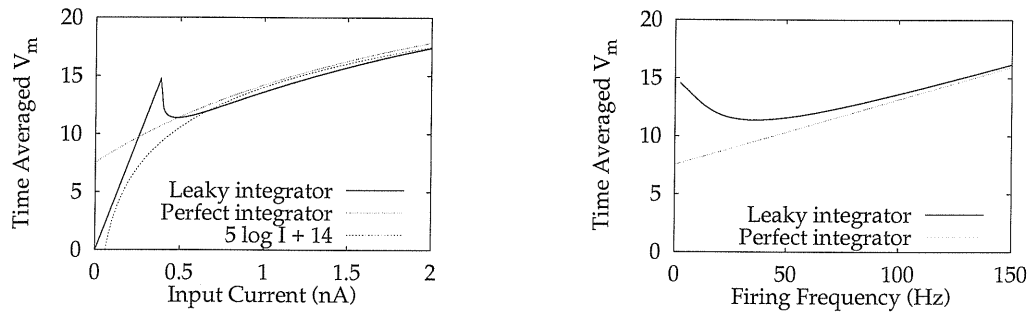

Figure B.1: $\langle V_m \rangle$ is approximately a logarithmic function of input current and a linear function of firing rate for both leaky and perfect integrators. Parameters: $V_{spike} = 30$ mV, $V_{th} = 15$ mV, $R = 38.1$ MΩ, $C = 0.393$ pC, $t_r = 2.5$ ms, $I_{th} = 0.393$ nA, $\tau = 15$ ms. These parameters were set so that the leaky integrator would have a firing rate of 100 Hz with a 1 nA current injection. The logarithmic fit was done by eye.

B.2 Hodgkin-Huxley equations

Simulation of the raw Hodgkin-Huxley equations using the defaults in the NEURON program produce similar looking plots (figure B.2). $\langle V_m \rangle$ is not exactly logarithmic (not as impressively logarithmic as the model discussed by Koch *et al.*, 1995) but can be approximated by a logarithm. Above threshold, $\langle V_m \rangle$ is approximately linear in f.

B.3 Cortical cells in slice

Although conceptually simple, it is sometimes difficult to determine $\langle V_m \rangle$ for cells in response to current injection. If bridge circuitry is used, as in the case of the many recordings I examined from the laboratory of Kevan Martin and Rodney Douglas, often the bridge is not exactly balanced. Also, in some cases electrode polarization causes a slower change in the membrane potential which can be significant for higher currents. Since the shift is dependent on the current (often proportional to it for low currents), this can give seriously misleading results.

I analyzed data collected from cat area 17 slices by Berman (1991). In only one experiment (s98) were the current injections long enough (320 ms) for averaging over time. Most of the 36 cells from this experiment do not appear to have a stable enough membrane potential when current is being injected to be useful in this analysis[1], since we expect that the time averaged membrane potential changes very slowly as a function of current; systematic differences of $1-2$ mV may seriously affect the results.

[1] Many of them probably could be compensated by subtracting a linear function of the current from the membrane voltage, but I did not want to introduce any more assumptions.

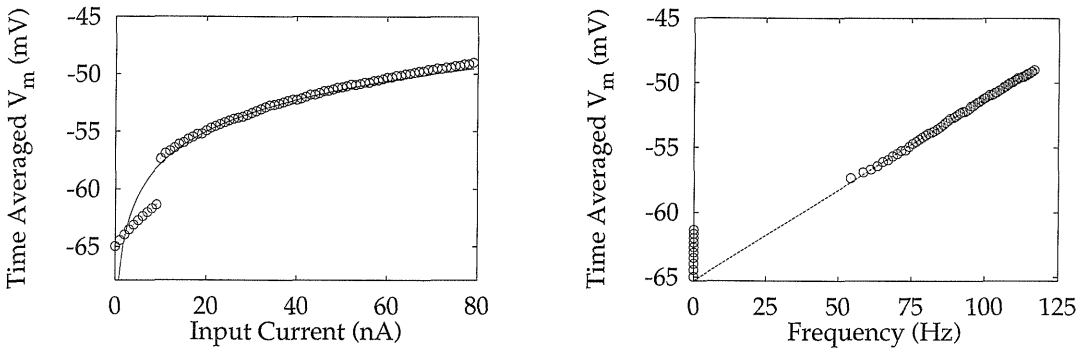

Figure B.2: Time averaged membrane potential for the Hodgkin-Huxley equations in a single compartment. Simulations were for the parameters measured for the squid at 6.3°C. Parameters: cell body was a cylindrical compartment with a diameter of 500 μm and a length of 100 μm, with a capacitance of 1 μF/cm^2. $\bar{g}_{\mathrm{Na}} = 0.12$ S/cm^2, $\bar{g}_{\mathrm{K}} = 0.036$ S/cm^2, $g_{leak} = 0.0003$ S/cm^2, $E_{leak} = -54.3$ mV, $E_{\mathrm{Na}} = 50$ mV, $E_{\mathrm{K}} = -77$ mV. The logarithmic fit ($\langle V_m \rangle = 4.0 \ln I - 67$) was done by eye; the linear fit ($\langle V_m \rangle = 0.14f - 65.3$) was done with linear regression on the points above threshold.

It is difficult to determine with any precision whether there is an artifactual shift in the DC potential since there is no clear reference point. The peak amplitude of a spike does not seem to be a good indicator because the spikes are slightly shorter when the current is higher. Instead, I determined by eye whether the spike thresholds appeared to be constant as a function of current and time. I found that I was able to discriminate differences of about 1 mV by eye.

This means we can only discuss the average membrane voltage *relative to threshold.* However, it is reasonable to expect from biophysical models that the voltage threshold should not change much as a function of current (Koch *et al.*, 1995). The threshold is determined to a large extent by the sodium conductance, and the sodium conductance will not be affected by the amount of current injected unless the firing rate is sufficiently high that the current has not recovered from inactivation during the previous spike. At low firing rates, then, we expect the threshold to be relatively constant, while at very high firing rates it may vary more significantly.

An example of the procedure is shown in figure B.3. The last 10 spikes in each trial are aligned at the point where they cross a threshold (I used -20 mV). Trials are arranged along the x axis in order of increasing current. In this case, the threshold is roughly constant until the trace at roughly 350 ms; this trace corresponds to a current of 1.8 nA. So trials from this cell for which the current is less than 1.8 nA are accepted.

With this analysis, there were 6 cells that had stable enough threshold levels to be useful for determining $\langle V_m \rangle$. Current was injected for only 320 ms, and adaptation was not complete until about 100 ms into the trace. That leaves only 200 ms to average over, or typically 2-5 spikes. Such

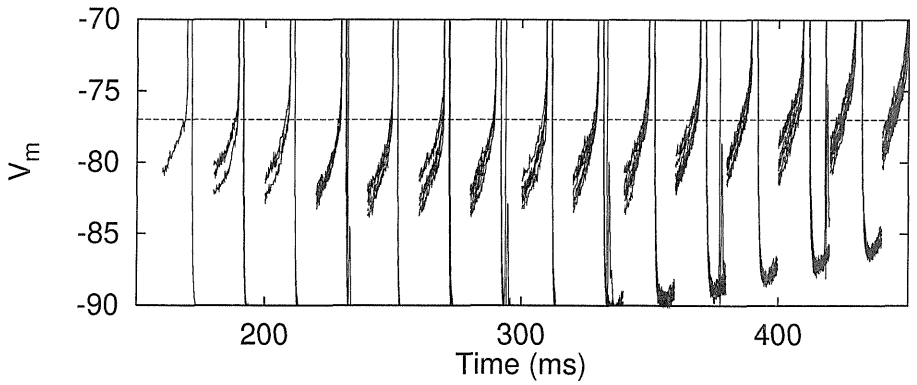

Figure B.3: Example of procedure for determining variations in baseline. For each trial of the cell at a different current level, 20 ms surrounding each of the last 10 spikes are extracted and aligned on the trace. Different groups of aligned spikes correspond to trials with different current levels. As the current increases (from left to right), the spike thresholds are roughly constant up until about 350 ms on the x axis; this means that the DC level is roughly stable until 1.8 nA (the trace which is around 350 ms).

a small number of spikes can lead to artifacts. For example, suppose there are only two spikes in the region we average over, but for a very slightly larger current there would be 3 spikes. This means that our average will be artifactually low. To avoid problems like this, the average started 3 ms before a spike and ended 3 ms before the last spike, so there was always an integral number of interspike intervals. When the current was below threshold, the last 100 ms or so (depending on the trace) was used for averaging. Each trace was examined by eye to validate the range of times to compute $\langle V_m \rangle$.

Results from these cells are shown in figure B.4. In general, the membrane potential above threshold appears to increase slowly, but there is no good way of deciding between a logarithmic fit and a linear fit. A logarithmic fit to the above threshold data does not even come close to the subthreshold data (not shown), unlike the model considered by Koch *et al.* (1995).

B.4 Conclusions

In addition to the equations simulated by Koch *et al.* (1995), both the integrate-and-fire and the Hodgkin-Huxley equations for the squid giant axon show an approximately logarithmic relationship between the time averaged membrane potential and the input current, and a linear relationship between membrane potential and firing frequency. The logarithmic fit of these simpler models is not nearly as impressive as for the detailed pyramidal cell model, but it is nevertheless approximately valid. Thus the diode model is not merely an artifact of one particular set of simulated currents.

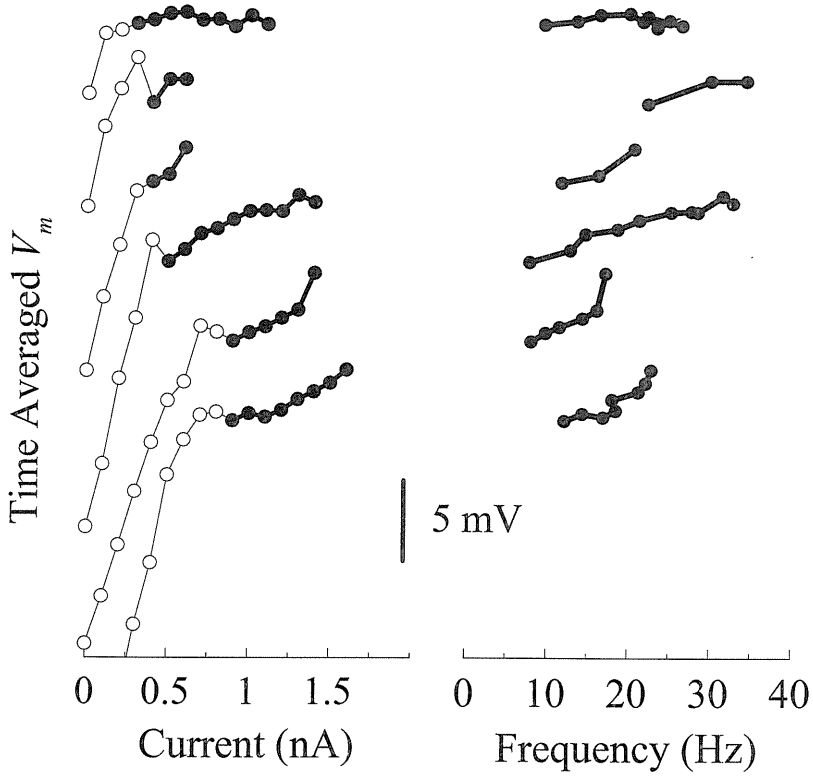

Figure B.4: Above threshold, the time average membrane potential does not change much with input current, while below threshold V_m changes dramatically with current. Filled circles are for trials when the cell was above threshold and open circles are subthreshold. Data from separate cells have been offset for clarity. The data are fit equally well by linear or logarithmic fits above threshold (not shown) so it is not possible to support or deny the diode model.

With the data I have available, it does not seem possible to confirm or deny a logarithmic relationship between $\langle V_m \rangle$ and input current. Better quality recordings are needed.

Nevertheless, the basic phenomena observed by Koch *et al.* (1995) is supported: the spiking mechanism acts like a kind of voltage clamp. Over a wide range of input currents and firing rates, the time average voltage at the soma does not vary much (only a few mV). This is a generic property of a spiking mechanism, and not a peculiarity of any particular model. This has strong implications for the effects of conductance changes (chapter 4 on page 63).

Appendix C Numerical methods

C.1 Software

Much of the numerical work was done in C++. It is often more convenient to display and analyze the results using graphics from a program like Matlab, so I made my C++ code callable from Matlab. I developed an automatic wrapper generator that takes only the function prototypes and the class definitions and generates all of the code necessary to link the C++ code with Matlab or other matrix-manipulation languages. Type checking is automatically performed; structure pointers and inheritance are handled properly. Functions are automatically vectorized. The wrapper generator is available from `http://www.klab.caltech.edu/~holt/matwrap/`.

C.2 Methods for chapter 2: Ephaptic interactions

C.2.1 Action potential in an axon

An action potential propagating down an axon was simulated in two different ways, both of which yielded numerically identical answers. First, the NEURON simulation program (Hines, 1989, 1993a, 1993b) with the default parameters for the Hodgkin-Huxley equations. I also wrote my own axon simulator in C++ which can take into account the extracellular potential naturally, in order to be able to simulate situations where the extracellular potential produced by a cell is not negligible compared to the transmembrane potential. (Results from such simulations are not included in this thesis.) The numerical techniques for this are straightforward and essentially identical to those NEURON uses except that there was an additional term corresponding to the ephaptic current (equation 2.19 on page 36), so I will not describe them here.

C.2.2 Potential around an axon

It is relatively straightforward to compute the potential around an axon because the geometry is fairly simple, as long as the extracellular potential is small enough that the transmembrane potential can be calculated assuming the extracellular potential is 0. The line-source approximation (section 2.2.1 on page 18) is quite good for this situation because the transmembrane currents change only slowly as a function of z. However, I also wanted to investigate the effect of sheath diameter, and as far as

I know the line-source approximation with a sheath cannot be expressed in a simple form. Instead, I discretized Laplace's equation,

$$\nabla^2\phi = 0 \tag{C.1}$$

with the boundary conditions that

$$\phi = 0 \qquad \text{for } r = \sqrt{x^2+y^2} = \infty \tag{C.2}$$

$$\phi = 0 \qquad \text{for } z = z_{min} \text{ or } z = z_{max} \tag{C.3}$$

$$\sigma_e \nabla\phi \cdot \mathbf{n} = J_m \qquad \text{for } r = a. \tag{C.4}$$

where J_m is the transmembrane current density and a is the radius of the axon. (For the simulations in appendix A, we simulate a nearby ground rather than a ground at infinity; equation C.2 is applied at a finite, relatively small radius.)

The axon is a circular cylinder along the z axis. We assume the potential is independent of angle on the $x-y$ plane, i.e., it only depends on $\sqrt{x^2+y^2}$ and z. One could use cylindrical polar coordinates, setting $\partial\phi/\partial\theta = 0$:

$$\frac{\partial^2\phi}{\partial r^2} + \frac{1}{r}\frac{\partial\phi}{\partial r} + \frac{\partial^2\phi}{\partial z^2} = 0. \tag{C.5}$$

However, this equation has a first-order derivative in it, and discretization yields a non-symmetric matrix. Solving a system with a non-symmetric matrix is somewhat slower and more difficult.

Instead, I used a conformal map. An analytic function $u+iv = w(x+iy)$ defines a conformal map between the $x-y$ and the $u-v$ planes. It can be shown that Laplace's equation is transformed under this map into:

$$\frac{\partial^2\phi}{\partial x^2} + \frac{\partial^2\phi}{\partial y^2} + \frac{\partial^2\phi}{\partial z^2} = |w'(x+iy)|^2 \left(\frac{\partial^2\phi}{\partial u^2} + \frac{\partial^2\phi}{\partial v^2}\right) + \frac{\partial^2\phi}{\partial z^2} = 0, \tag{C.6}$$

where w' denotes the derivative of the analytic function with respect to its complex argument. Numerically, the equation in $u-v-z$ space is as almost easy to solve as it is in $x-y-z$ space, provided χ' is not zero. Also, because v is the angle and we are assuming cylindrical symmetry, we drop the terms involving v.

A conformal map also transforms the boundary conditions in a simple way. The Dirichlet conditions, equations C.2 and C.3, are unaltered. The Neumann condition (C.4) transforms simply

into:

$$|w'|\sigma_e \frac{\partial \phi}{\partial u} = J_m. \tag{C.7}$$

These equations can be discretized in a number of different ways. The finite difference method does not yield a symmetric matrix. The box method applied directly to equation C.6 does not yield a symmetric matrix either because of the presence of the $|w'|$ term. However, dividing through by $|w'|$ and applying the box method does yield a symmetric matrix:

$$\frac{\partial^2 \phi}{\partial u^2} + \frac{1}{|w'|^2}\frac{\partial^2 \phi}{\partial z^2} = 0. \tag{C.8}$$

Integrating over the area shown in figure C.1 gives

$$\begin{aligned} 0 &= \iiint \nabla \cdot \left(\frac{\partial^2 \phi}{\partial u^2}\mathbf{i} + \frac{1}{|w'|^2}\frac{\partial^2 \phi}{\partial z^2}\mathbf{k} \right) \\ &= \iint \left(\frac{\partial \phi}{\partial u}\mathbf{i} + \frac{1}{|w'|}\frac{\partial \phi}{\partial z} \right) \cdot \mathbf{dS} \end{aligned} \tag{C.9}$$

from the divergence theorem. We evaluate the first derivatives on all four faces of the box using a centered difference formula:

$$\begin{aligned} &\left(\frac{\phi_{i+1,k} - \phi_i k}{h_{i+1}} + \frac{\phi_{i-1,k} - \phi_i k}{h_i} \right) \frac{h_k + h_{k+1}}{2} + \\ &\quad \frac{1}{|w'|_i} \left(\frac{\phi_{i,k+1} - \phi_{ik}}{h_{k+1}} + \frac{\phi_{i,k-1} - \phi_{ik}}{h_k} \right) \frac{h_i + h_{k+1}}{2} = 0. \end{aligned} \tag{C.10}$$

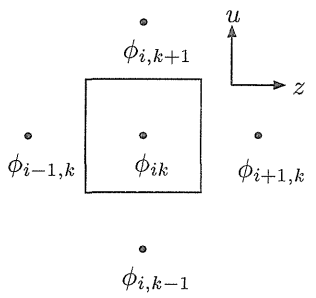

Figure C.1: The box method and discretization scheme.

where

$$\begin{aligned} h_i &= u_i - u_{i-1}, & h_{i+1} &= u_{i+1} - u_i \\ h_k &= z_k - z_{k-1}, & h_{k+1} &= z_{k+1} - z_k \\ |w'|_i &= e^{-u_i}. \end{aligned}$$

For simplicity, the grid was uniformly spaced in the u variable ($\Delta u = 0.4$ for chapter 2 and 0.2 for appendix A) and the z variable ($\Delta z = 6.25$ μm for chapter 2 and 12.5 for appendix A). The boundary condition (C.7) is applied by substituting the expression from (C.7) for $\partial\phi/\partial u$ in (C.9). The smallest u value is one half step beyond the membrane ($u_0 = 0.2$). $\sigma_e = 0.3$ μS/μm (330 Ω-cm).

The resulting matrix was solved using a sparse matrix solver built into Matlab.

C.2.3 Potential around a cell

To calculate the potential around a cell, with dendrites branching in every direction, it was no longer possible to use a conformal map to simplify the extracellular geometry. I tried several different techniques for solving for the potential.

First, I attempted to use a volume source formulation, as described in section 2.2.3 on page 25. This formulation has the advantage that a standard Poisson's equation solver can be used without modification; one merely calculates the total current source in each volume element and calls the solver. The theory and code for such solvers is well-developed; in particular, I used the code from Holst (1993) and Holst and Saied (1993).

The chief difficulty with this formulation is that there have to be too many volume elements for easy computation. The boundary conditions at infinity imply that there must be elements a large distance away from the cell (1 mm or more in all directions). I used a nonuniform grid so I could have much higher element density in the center, but even so I was unable to have volume elements smaller than 20 μm around the soma. This is unacceptably large, because the potential drops several mV in that distance. Even at this resolution, it was taking hours to compute the extracellular potential for a single timestep.

Computation using line source model

Instead, I resorted back to the line source model. The potential at any point in space is approximately the sum of the potentials from each of the segments of the dendrite and axon, calculated as if the segment were the only thing in the space. The potential from each segment can be written as a simple analytic function of its current and coordinates. This formulation has the enormous advantage over the Poisson solver formulation that the potential only needs to be calculated where we want to know it; the calculation of potential at one point is in no way dependent on the calculation at another point. This technique is orders of magnitude faster for my purposes and requires far less memory than solving Poisson's equation, making it possible to obtain detailed potential maps with a 2 μm resolution near the soma in a minute or so on ordinary workstations. Furthermore, the algorithm is trivially parallelizable, requiring virtually no communication between processors. A similar approach was used by Wilson and Bower (1992).

The dendrites and axon were broken up into straight line segments based on the geometry of the neuron; each compartment in the NEURON compartmental model usually corresponded to many segments, since the dendrites did not run straight. The potential from each line segment was

calculated using the line-source model, where the symbols are defined in figure C.2:

$$\phi = \frac{1}{4\pi\sigma_e}\int_{-\Delta s}^{0} \frac{I}{\Delta s}\frac{ds}{\sqrt{(h-s)^2+r^2}} \tag{C.11}$$

where I is the current from just that compartment. After some manipulation,

$$\phi = \frac{I}{4\pi\sigma_e \Delta s}\log\left|\frac{\sqrt{h^2+r^2}-h}{\sqrt{l^2+r^2}-l}\right| \tag{C.12}$$

where $\sigma_e = 0.3\ \mu\text{S}/\mu\text{m}$ (330 Ω-cm).

As written, this formulation involves subtraction of almost-equal large numbers when $h > 0$ and $l > 0$. This leads to large roundoff error. In these cases, I multiplied numerator and denominator by $\sqrt{h^2+r^2}+h$ and $\sqrt{l^2+r^2}+l$ to obtain:

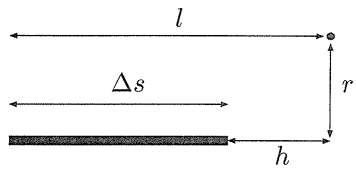

Figure C.2: Symbols used in calculating ϕ from a straight line source. Note that $l = h + \Delta s$.

$$\phi = \frac{I}{4\pi\sigma_e\Delta s}\begin{cases}\log\frac{\sqrt{h^2+r^2}-h}{\sqrt{l^2+r^2}-l} & \text{for } h<0,\ l<0\\ \log\frac{(\sqrt{h^2+r^2}-h)(l+\sqrt{l^2+r^2})}{r^2} & \text{for } h<0,\ l>0\\ \log\frac{l+\sqrt{l^2+r^2}}{\sqrt{h^2+r^2}+h} & \text{for } h>0,\ l>0.\end{cases} \tag{C.13}$$

Since all of the line segments are at different orientations, h and r must be determined from the orientation of the line segment. If (x_1, y_1, z_1) and (x_2, y_2, z_2) are the beginning and ending points of the line segment in three-dimensional space, and (x, y, z) is the coordinates of the point we are trying to calculate the potential at, then

$$h = \frac{1}{\Delta s}(x-x_2, y-y_2, z-z_2)\cdot(x_2-x_1, y_2-y_1, z_2-z_1) \tag{C.14}$$

$$r^2 = (x-x_1)^2 + (y-y_1)^2 + (z-z_1)^2 - h^2 \tag{C.15}$$

$$l = h + \Delta s. \tag{C.16}$$

The soma was treated as a sphere; the potential from it is simply:

$$\phi = \frac{I_{soma}}{4\pi\sigma_e r} \tag{C.17}$$

where r is the distance away.

Points which lie inside dendrites (i.e., $r < a$, where a is the radius of the dendrite at that point) or inside the soma were excluded from the calculation. I also excluded points in a small volume at

each tip of each line segment ($0 < h < a, r < a$ or $-a < l < 0, r < a$) to account for the space occupied by the junction of two line segments.

The currents from each compartment were calculated using the NEURON simulation of Mainen and Sejnowski (1996).[1] In the original model, the neuron was activated by an electrode in the soma. I removed the electrode and substituted synaptic input scattered uniformly throughout the dendrites. I used the same approximation as Bernander *et al.* (1991): synapses were not explicitly modeled, but the leak resistance and reversal potential was changed to reflect the time-averaged synaptic conductance. I found that a synaptic conductance of 0.2 times the leak conductance in every compartment supplied enough current to make the cell fire after 35 ms.[2]

At specified times, the total current (capacitive + ionic) in each segment was dumped to disk and loaded into Matlab to calculate ϕ. I sampled the action potential at 0.05 ms during its steep rising phase, and at larger intervals elsewhere. I found that I had to drop the timestep in NEURON considerably (to $dt = 0.01$ ms from 0.05 ms); otherwise the total current through the neuron was significantly different from 0. I believe this is because of the way NEURON computes the capacitive and ionic currents; ionic currents are correct at times $t + dt/2$ while capacitive currents are correct at times t.

This technique for calculating the extracellular potential involves two main assumptions:

1. The extracellular potential is small enough that the transmembrane currents can be computed by assuming $V_e = 0$.

2. The potential from a given line segment is not influenced much by the presence of other processes from the same neuron.

Assumption 2 could be a problem very near the soma, where the somatic sphere occupies a substantial solid angle. To avoid this problem, one could use a boundary-element method: boundary elements at the soma have a fictional current equal and opposite to the current that would flow through them if the soma were not present. This allows one to calculate the extracellular potential when the somatic current is exactly what is specified by the NEURON model. However, the somatic current will not be exactly as specified by the NEURON model, even if it were 100% right in the numerical values of the conductances, because the current will be affected by the extracellular potential. Violations of assumption 1 tend to cancel out violations of assumption 2. Since the magnitude of the channel conductances could be off by orders of magnitude (compare measurements of Stuart and Sakmann,

[1] Note that some of the published equations and parameters are inaccurate in the article. I used their source code directly, obtaining it from `http://www.cnl.salk.edu/~zach/patdemo.html`.

[2] I did not attempt to distribute the synapses according to an anatomically realistic distribution, as Bernander *et al.* (1991) did. The purpose of the synapses was to get the model to fire without using an electrode; the extracellular potential due to synaptic currents is miniscule compared to the potential from the spike, so I do not expect the details of synaptic localization to matter much.

1994 with Colbert and Johnston, 1996), it does not seem worth the enormous complexity of adding boundary elements: we cannot take the values that seriously anyway.

The electrical field can be calculated numerically by subtracting adjacent values of ϕ. However, I actually calculated the electrical field directly. Differentiating equation C.12 and simplifying gives the components of the electrical field parallel to the segment (the h direction) and perpendicular (the r direction):

$$E_h = \frac{I}{4\pi\sigma_e} \frac{l+h}{\sqrt{l^2+r^2}\sqrt{h^2+r^2}(\sqrt{l^2+r^2}+\sqrt{h^2+r^2})} \tag{C.18}$$

$$E_y = -\frac{Ir}{4\pi\sigma_e} \begin{cases} \left(h+l-\frac{h^3+h^2l+hl^2+l^3+r^2h+r^2l}{(h+l)\sqrt{h^2+l^2}}\right)\left(\frac{1}{\sqrt{h^2+r^2}(\sqrt{h^2+r^2}-h)\sqrt{l^2+r^2}(\sqrt{l^2+r^2}-l)}\right) & \text{for } h<0,\ l<0 \\ \left(h+l+\frac{h\sqrt{h^2+r^2}-l\sqrt{l^2+r^2}}{\Delta s}\right)\left(\frac{1}{\sqrt{h^2+r^2}(\sqrt{h^2+r^2}-h)}\frac{\sqrt{l^2+r^2}+l}{r^2\sqrt{l^2+r^2}}\right) & \text{for } h<0<l \\ \left(h+l-\frac{h^3+h^2l+hl^2+l^3+r^2h+r^2l}{(h+l)\sqrt{h^2+l^2}}\right)\left(\frac{\sqrt{h^2+r^2}+h}{r^2\sqrt{h^2+r^2}}\frac{\sqrt{l^2+r^2}+l}{r^2\sqrt{l^2+r^2}}\right) & \text{for } h>0,\ l>0. \end{cases} \tag{C.19}$$

This vector then has to be rotated to calculate the contribution to E_x, E_y, and E_z from this cable segment.

Accuracy of the line source model

Since we compute potentials very close to neural elements, it is reasonable to ask whether the line source model is sufficiently dependable at the membrane. To evaluate its accuracy, I compare it with the solution for a cylinder with a finite radius. The solution for a cylindrical geometry can be obtained numerically using the techniques in section C.2.2, or by separation of variables from the original equation.

If we set $phi(z,r) = Z(z)R(r)$, then Laplace's equation can be separated as

$$Z'' + k^2 Z = 0 \tag{C.20}$$

$$rR'' + R' - k^2 rR = 0 \tag{C.21}$$

to which the solutions are

$$Z = e^{ikz} \tag{C.22}$$

$$R = AI_0(|k|r) + BK_0(|k|r) \tag{C.23}$$

where A and B are constants and I_0 and K_0 are modified Bessel functions. Since eigenfunctions in the z direction are just sines and cosines, we are doing a spatial Fourier transform in space using k

as the angular frequency. We can write

$$\phi = \mathcal{F}^{-1}\left[R_k(r)\right]. \tag{C.24}$$

Next we apply the boundary conditions. Since ϕ at infinity is 0, $R(\infty) = 0$ and $A = 0$. The boundary condition at the neural membrane ($r = a$) is

$$\frac{J_m}{\sigma_e} = \left.\frac{\partial \phi}{\partial r}\right|_{r=a} \tag{C.25}$$

or expressed in terms of the current density per length,

$$\frac{i_m}{2\pi a \sigma_e} = \left.\frac{\partial \phi}{\partial r}\right|_{r=a}. \tag{C.26}$$

Switching to the Fourier domain,

$$R_k'(a) = -|k|K_1(|k|a) = \frac{\hat{\imath}_m(k)}{2\pi a \sigma_e} \tag{C.27}$$

where $\hat{\imath}_m(k)$ is the Fourier transform of $i_m(z)$. Therefore

$$\phi = \mathcal{F}^{-1}\left[\frac{\hat{\imath}_m(k)}{2\pi a \sigma_e}\frac{K_0(|k|r)}{|k|K_1(|k|a)}\right]. \tag{C.28}$$

A Fourier formulation for the line-source model can be obtained by letting $a \to 0$ in equation C.28:

$$\phi = \mathcal{F}^{-1}\left[\frac{\hat{\imath}_m(k)}{2\pi\sigma_e}K_0(|k|r)\right]. \tag{C.29}$$

I evaluated the line and cylinder source models for a 10 μm cable emitting a constant current per unit length. Figure C.3 shows the extracellular potential along the line $r = a$, i.e., at the neural membrane, and extending on both sides of the cable. The Fourier transforms were evaluated numerically with an FFT using Matlab with 4096 points separated by 0.05 μm. The results are virtually indistinguishable (figure C.3); the line source model is definitely sufficiently accurate for computation, even close to the membranes.

Using different simulations, others have also found the line source model to be very accurate under these conditions (Rosenfalck, 1969, appendix 1; Trayanova and Henriquez, 1991).

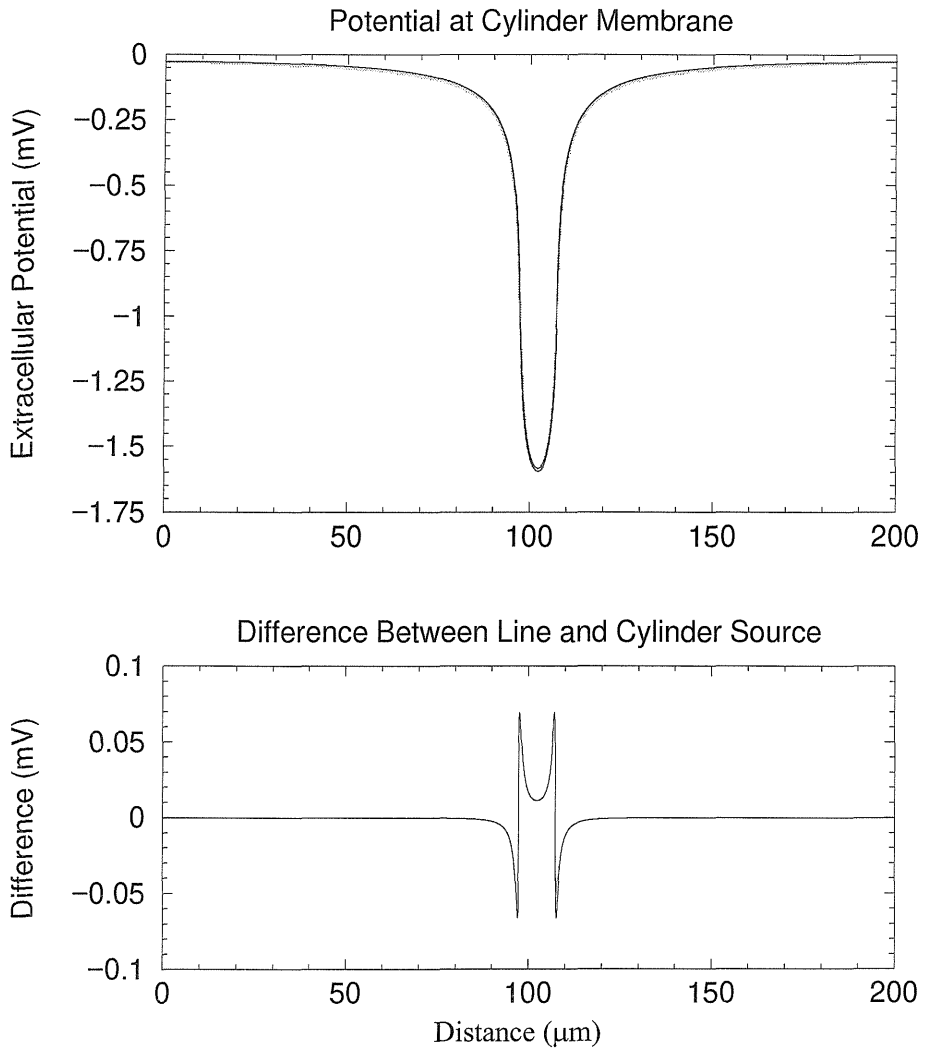

Figure C.3: A comparison of three ways of computing the extracellular potential at the membrane of a cylinder. *Top:* Potential calculated using the three different techniques. There are actually three lines on the figure; the results are indistinguishable. A uniform current is following into a cylinder of radius $a = 0.5$ in the central 10 μm of the plot. The potential is shown at $r = a = 0.5$ μm. Potential was calculated using the formulation of the line source model in section C.2.3, a cylinder model (equation C.28) and a Fourier version of the line source model (equations C.29). *Bottom:* The difference between calculated potential from the line source method (equation C.29) and cylinder source method (equation C.28).

Bibliography

Numbers in brackets are the page numbers where the article is referenced.

Abbott, L. F. 1991. Realistic synaptic inputs for model neural networks. *Network* 2:245–258. [69, 75, 87]

Abbott, L. F. 1994. Decoding neuronal firing and modelling neural networks. *Q. Rev. Biophys.* 3:291–331. [86]

Abbott, L. F., Varela, J. A., Sen, K., and Nelson, S. B. 1997. Synaptic depression and cortical gain control. *Science* 275:220–224. [16, 86, 106, 107, 108, 109]

Abeles, M. 1982. Role of cortical neuron: Integrator or coincidence detector? *Israeli Journal of Medical Sciences* 18:83–92. [2, 14]

Agmon-Snir, H., and Segev, I. 1993. Signal delay and input synchronization in passive dendritic structures. *J. Neurophysiol.* 70:2066–2085. [83, 84]

Ahmed, B., Anderson, J. C., Douglas, R. J., Martin, K. A. C., and Whitteridge, D. 1993. A method of estimating net somatic input current from the action potential discharge of neurons in the visual cortex of the anesthetized cat. *J. Physiol.* 459:134P. [77, 85]

Ahmed, B., Anderson, J. C., Douglas, R. J., Martin, K. A. C., and Nelson, J. C. 1994. Polyneuronal innervation of spiny stellate neurons in cat visual cortex. *J. Comp. Neurol.* 341:39–49. [107]

Albrecht, D. G., and Geisler, W. S. 1991. Motion selectivity and the contrast-response function of simple cells in the visual cortex. *Vis. Neurosci.* 7:531–546. [71]

Altman, K. W., and Plonsey, R. 1990. Point source nerve bundle stimulation: Effects of fiber diameter and depth on simulated excitation. *IEEE Trans. Biomed. Eng.* 37:688–698. [38]

Amit, D. J., and Brunel, N. 1993. Adequate input for learning in attractor neural networks. *Network* 4:177–194. [85]

Amit, D. J., and Tsodyks, M. V. 1991a. Quantitative study of attractor neural network retrieving at low spike rates: I. Substrate–spikes, rates, and neuronal gain. *Network* 2:259–273. [86, 87]

Amit, D. J., and Tsodyks, M. V. 1991b. Quantitative study of attractor neural network retrieving at low spike rates: I. Low rate retrieval in symmetric networks. *Network* 2:275–294. [85]

Amit, D. J., and Tsodyks, M. V. 1992. Effective neurons and attractor neural networks in cortical environment. *Network* 3:121–137. [85, 86, 87]

Andersen, P., Silfvenius, H., Sundberg, S., and Sveen, O. 1980. A comparison of distal and proximal dendritic synapses on CA1 pyramids in guinea pig hippocampal slices *in vitro*. *J. Physiol.* 307:273–300. [84]

Anderson, J. C., Douglas, R. J., Martin, K. A. C., and Nelson, J. C. 1994a. Synaptic output of physiologically identified spiny stellate neurons in cat visual cortex. *J. Comp. Neurol.* 341:16–24. [107]

Anderson, J. C., Douglas, R. J., Martin, K. A. C., and Nelson, J. C. 1994b. Map of the synapses formed with the dendrites of spiny stellate neurons of cat visual cortex. *J. Comp. Neurol.* 341:25–38. [107]

Angelides, K. J., Elmer, L. W., Loftus, D., and Elson, E. 1988. Distribution and lateral mobility of voltage-dependent sodium channels in neurons. *J. Cell. Biol.* 106:1911–1925. [29]

Armstrong-James, M., Welker, E., and Callahan, C. A. 1993. The contribution of NMDA and non-NMDA receptors to fast and slow transmission of sensory information in the rat SI barrel cortex. *J. Neurosci.* 13:2149–2160. [90]

Arvanitaki, A. 1942. Effects evoked in an axon by the activity of a contiguous one. *J. Neurophysiol.* 5:89–108. [17, 34, 44]

Attwell, D., Barbour, B., and Szatkowski, M. 1993. Nonvesicular release of neurotransmitter. *Neuron* 11:401–407. [49]

Barr, R. C., and Plonsey, R. 1992. Electrophysiological interaction through the interstitial space between adjacent unmyelinated parallel fibers. *Biophys. J.* 61:1164–1175. [37, 38]

Ben-Yishai, R., Bar-Or, R. L., and Sompolinsky, H. 1995. Theory of orientation tuning in visual cortex. *Proc. Natl. Acad. Sci. USA* 92:3844–3848. [14, 15]

Berman, N. J. 1991. Aspects of inhibition in the visual cortex. Ph. D. thesis, Lincoln College, University of Oxford. [129]

Berman, N. J., Douglas, R. J., and Martin, K. A. C. 1989. The conductances associated with inhibitory postsynaptic potentials are larger in visual cortical neurones in vitro than in similar neurones in intact, anesthetized rats. *J. Physiol.* 418:107P. [106]

Berman, N. J., Douglas, R. J., Martin, K. A. C., and Whitteridge, D. 1991. Mechanisms of inhibition in cat visual cortex. *J. Physiol.* 440:697–722. [14]

Berman, N. J., Douglas, R. J., and Martin, K. A. C. 1992. GABA-mediated inhibition in the neural networks of visual cortex. *Prog. Brain Res.* 90:443–476. [14, 72]

Bernander, Ö. 1993. Synaptic integration and its control in neocortical pyramidal cells. Ph. D. thesis, California Institute of Technology. [64]

Bernander, Ö., Douglas, R., Martin, K., and Koch, C. 1991. Synaptic background activity determines spatio-temporal integration in single pyramidal cells. *Proc. Natl. Acad. Sci. USA* 88:1569–1573. [13, 64, 65, 72, 74, 77, 85, 127, 138]

Bernander, Ö., Koch, C., and Douglas, R. J. 1994. Amplification and linearization of distal synaptic input to cortical pyramidal cells. *J. Neurophysiol.* 72:2743–2753. [64, 87, 127]

Bishop, G. H., and O'Leary, J. L. 1942. The polarity of potentials recorded from the superior colliculus. *J. Cell. Comp. Physiol.* 19:289–300. [26]

Blomfield, S. 1974. Arithmetical operations performed by nerve cells. *Brain Res.* 69:114–124. [71]

Borg-Graham, L., Monier, C., and Frégnac, Y. 1996. Voltage-clamp measurement of visually-evoked conductances with whole-cell patch recordings in primary visual cortex. *J. Physiol. (Paris)* 90:185–188. [15]

Bose, A., and Jones, C. K. R. T. 1995. Stability of the in-phase travelling wave solution in a pair of coupled nerve fibers. *Indiana Univ. Math. J.* 14:189–220. [38]

Bower, J. M., and Haberly, L. B. 1986. Facilitating and nonfacilitating synapses on pyramidal cells: A correlation between physiology and morphol-

ogy. *Proc. Natl. Acad. Sci. USA* 83:1115–1119. [106]

Brunel, N. 1996. Dynamics of an attractor neural network converting temporal into spatial correlations. *Network: Comp. Neural Sys.* 5:449–470. [85]

Buanomano, D. V., and Merzenich, M. M. 1995. Temporal information transformed into a spatial code by a neural network with realistic properties. *Science* 267:1028–1030. [85]

Bullock, T. H. 1997. Signals and signs in the nervous system: The dynamic anatomy of electrical activity is probably information-rich. *Proc. Natl. Acad. Sci. USA* 94:1–6. [28]

Burkitt, A. N. 1994. Attractor neural networks with excitatory neurons and fast inhibitory interneurons at low spike rates. *Network: Comp. Neural. Sys.* 4:437–448. [85]

Buzsáki, G., Penttonen, M., Nádasdy, Z., and Bragin, A. 1996. Pattern and inhibition-dependent invasion of pyramidal cell dendrites by fast spikes in the hippocampus *in vitro*. *Proc. Natl. Acad. Sci. USA* 93:9921–9925. [28, 32, 34]

Carandini, M., Heeger, D. J., and Movshon, J. A. 1996a. Linearity and gain control in V1 simple cells. In: *Cerebral Cortex vol. 10: Cortical Models.* New York: Plenum Press. [75]

Carandini, M., Mechler, F., Leonard, C. S., and Movshon, J. A. 1996b. Spike train encoding in regular-spiking cells of the visual cortex. *J. Neurophysiol.* 76:3425–3441. [2, 4, 12, 13, 75, 87]

Carandini, M., Heeger, D. J., and Movshon, J. A. 1997. Linearity and normalization in simple cells of the macaque primary visual cortex. *J. Neurosci.* 17:in press. [12, 13, 75]

Carandini, M., and Heeger, D. J. 1994. Summation and division by neurons in primate visual cortex. *Science* 264:1333–1335. [12, 13, 14, 63, 71, 74, 75, 79]

Carslaw, H. S., and Jaeger, J. C. 1959. *Conduction of Heat in Solids.* Oxford: Clarendon Press. [55]

Celebrini, S., Thorpe, S., Trotter, Y., and Imbert, M. 1993. Dynamics of orientation coding in area V1 of the awake primate. *Vis. Neurosci.* 10:811–825. [15]

Chow, C. C., and White, J. A. 1996. Spontaneous action potentials due to channel fluctuations. *Biophys. J.* 71:3013–3021. [5]

Clare, M. H., and Bishop, G. H. 1955. Properties of dendrites: Apical dendrites of the cat cortex. *Electroencephalog. Clin. Neurophysiol.* 7:85–98. [28]

Clark, J., and Plonsey, R. 1966. A mathematical evaluation of the core conductor model. *Biophys. J.* 6:95–112. [7]

Clark, J., and Plonsey, R. 1968. The extracellular potential field of the single active nerve fiber in a volume conductor. *Biophys. J.* 8:842–864. [22, 121]

Clark, J. W., and Plonsey, R. 1971. Fiber interaction in a nerve trunk. *Biophys. J.* 11:281–294. [35, 36, 37]

Cohen, L. B., and De Weer, P. 1977. Structural and metabolic processes directly related to action potential propagation. In: *Handbook of Physiology. I. The Nervous System, vol. I: Cellular Biology of Neurons.* Kandel, E. R., ed., pp. 137-159. Bethesda, Maryland: American Physiological Society. [53]

Colbert, C. M., and Johnston, D. 1996. Axonal action-potential initiation and Na^+ channel densities in the soma and axon initial segment of subicular neurons. *J. Neurosci.* 16:6676–6686. [5, 29, 34, 45, 139]

Cole, K. S., Li, C. L., and Bak, A. F. 1969. Electrical analogues for tissues. *Exp. Neurol.* 24:459–473.

[119]

Connors, B. W., Malenka, R. C., and Silva, L. R. 1988. Two inhibitory postsynaptic potentials, and $GABA_A$ and $GABA_B$ receptor-mediated responses in neocortex of rat and cat. *J. Physiol.* 406:443–468. [72]

Coombs, J. S., Curtis, D. R., and Eccles, J. C. 1957a. The interpretation of spike potentials of motoneurons. *J. Physiol.* 139:198–231. [10, 45]

Coombs, J. S., Curtis, D. R., and Eccles, J. C. 1957b. The generation of impulses in motoneurons. *J. Physiol.* 139:232–249. [10, 45]

Cordingley, G. E., and Somjen, G. G. 1978. The clearing of excess potassium from extracellular space in spinal cord and cerebral cortex. *Brain Res.* 151:291–306. [52, 54, 55]

Creutzfeld, O., and Houchin, J. 1974. Neuronal basis of EEG-waves. In: *Handbook of Electroencephalography and Clinical Neurophysiology. II. Electrical Activity from the Neuron to the EEG and EMG.* Creutzfeld, O., ed., pp. 2C-5–2C-55. Amsterdam: Elsevier Scientific. [18]

Cull-Candy, S. 1995. NMDA receptors: Do glia hold the key? *Curr. Biol.* 5:841–843. [49]

Dalkara, T., Krnjević, K., Ropert, N., and Yim, C. Y. 1986. Chemical modulation of ephaptic activation of CA3 hippocampal pyramids. *Neurosci.* 17:361–370. [44, 45]

Dalva, M. B., Weliky, M., and Katz, L. C. 1997. Relationships between local synaptic connections and orientation domains in primary visual cortex. *Neuron* 19:871–880. [15]

Davenport, R. W., and McCaig, C. D. 1993. Hippocampal growth cone responses to focally applied electric fields. *J. Neurobiol.* 24:89–100. [46]

Dean, A. F., Hess, R. F., and Tolhurst, D. J. 1980. Divisive inhibition involved in direction selectivity. *J. Physiol.* 308:84–85P. [106]

Debanne, D., Guérineau, N. C., Gähwiler, B. H., and Thompson, S. M. 1997. Action-potential propagaion gated by an axonal I_A-like K^+ conductance in hippocampus. *Nature* 389:286–289. [46]

Dehay, C., Douglas, R. J., Martin, K. A. C., and Nelson, C. 1991. Excitation by geniculocortical synapses is not 'vetoed' at the level of dendritic spines in cat visual cortex. *J. Physiol.* 440:723–734. [14]

Dermietzel, R., and Spray, D. C. 1993. Gap junctions in the brain: Where, what type, how many, and why? *Trends Neurosci.* 16:186–192. [46]

Dodge, F. A., and Cooley, J. W. 1973. Action potential of the motorneuron. *IBM J. Res. Develop.* 17:219–229. [45]

Douglas, R. J., Martin, K. A. C., and Whitteridge, D. 1991. An intracellular analysis of the visual responses of neurones in cat visual cortex. *J. Physiol.* 440:659–696. [14, 65]

Douglas, R. J., Koch, C., Mahowald, M., Martin, K., and Suarez, H. 1995. Recurrent excitation in neocortical circuits. *Science* 269:981–985. [14, 15, 72]

Douglas, R. J., and Martin, K. A. C. 1990. Control of neuronal output by inhibition at the axon initial segment. *Neural Comp.* 2:283–292. [72]

Douglas, R. J., and Martin, K. A. C. 1991. A functional microcircuit for cat visual cortex. *J. Physiol.* 440:735–769. [4, 14, 15, 107, 109]

Eccles, J. C. 1964. *The Physiology of Synapses.* New York: Academic Press. [17]

Eccles, J. C., Llinás, R., and Sasaki, K. 1966. The excitatory synaptic action of climbing fibres on the Purkinje cells of the cerebellum. *J. Physiol.* 182:268–296. [28]

Eilbeck, J. C., Luzader, S. D., and Scott, A. C. 1981.

Pulse evolution on coupled nerve fibers. *Bull. Math. Biol.* 43:389–400. [38]

Erecińska, M., and Silver, I. A. 1994. Ions and energy in mammalian brain. *Prog. Neurobiol.* 43:37–71. [50, 52]

Erulkar, S. D., and Weight, F. F. 1979. Ionic environment and the modulation of transmitter release. *Trends Neurosci.* 2:298–301. [50]

Faber, D. S., and Korn, H. 1989. Electrical field effects: Their relevance in central neural networks. *Physiol. Rev.* 69:821–863. [17, 18, 44, 46]

Fatt, P. 1957. Electric potentials occuring around a neurone during its antidromic activation. *J. Neurophysiol.* 20:27–60. [28, 32]

Ferster, D. 1986. Orientation selectivity of synaptic potentials in neurons of cat primary visual cortex. *J. Neurosci.* 6:1284–1301. [14]

Ferster, D. 1987. Origin of orientation-selective EPSPs in simple cells of cat visual cortex. *J. Neurosci.* 7:1780–1791. [14]

Ferster, D., and Jagadeesh, B. 1992. EPSP-IPSP interactions in cat visual cortex studied with *in vivo* whole-cell patch recording. *J. Neurosci.* 12:1262–1274. [14, 106]

Ferster, D., and Lindström, S. 1985a. Augmenting responses evoked in area 17 of the cat by intracortical axon collaterals of cortico-geniculate cells. *J. Physiol.* 367:217–232. [107, 112]

Ferster, D., and Lindström, S. 1985b. Synaptic excitation of neurones in area 17 of the cat by intracortical axon collaterals of cortico-geniculate cells. *J. Physiol.* 367:233–252. [107, 112]

Fox, K., Sato, H., and Daw, N. 1989. The location and function of NMDA receptors in cat and kitten visual cortex. *J. Neurosci.* 9:2443–2454. [90]

Franciolini, F. 1987. Spontaneous firing and myelination of very small axons. *J. Theor. Biol.* 128:127–134. [5]

Freygang, W. H. 1958. An analysis of extracellular potentials from single neurons in the lateral geniculate nucleus of the cat. *J. Gen. Physiol.* 41:543–564. [25, 28]

Freygang, W. H., and Frank, K. 1959. Extracellular potentials from single spinal motoneurons. *J. Gen. Physiol.* 42:749–760. [25, 28]

Frolov, A. A., and Medvedev, A. V. 1986. Substantiation of the point approximation for describing the total electrical activity of the brain with use of a simulation model. *Biophysics* 31:332–337. [85, 86]

Fuortes, M. G. F. 1959. Initiation of impulses in visual cells of *Limulus*. *J. Physiol.* 148:14–28. [72]

Fuortes, M. G. F., Frank, K., and Becker, M. C. 1957. Steps in the production of motoneuron spikes. *J. Gen. Physiol.* 40:735–752. [10, 29, 45]

Fuxe, K., and Agnati, L. F. 1991. *Volume Transmission in the Brain.* New York: Raven Press, Ltd. [49]

Ganapathy, N., and Clark, J. W. 1987. Extracellular currents and potentials of the active myelinated nerve fiber. *Biophys. J.* 52:749–761. [25]

Gardner-Medwin, A. R. 1983a. A study of the mechanisms by which potassium moves through brain tissue in the rat. *J. Physiol.* 335:353–374. [50, 53]

Gardner-Medwin, A. R. 1983b. Analysis of potassium dynamics in mammalian brain tissue. *J. Physiol.* 335:393–426. [50, 53, 54]

Gardner-Medwin, A. R., and Nicholson, C. 1983. Changes of extracellular potassium activity induced by electric current through brain tissue in the rat. *J. Physiol.* 335:375–392. [50, 53]

Geselowitz, D. B. 1966. Comment on the core conductor model. *Biophys. J.* 6:691–692. [19]

Goldberg, J. M. 1996a. Theoretical analysis of intercellular communication between the vestibular type I hair cell and its calyx ending. *J. Neurophysiol.* 76:1942–1957. [51]

Goldberg, J. M. 1996b. Transmission between the type I hair cell and its calyx ending. *Ann. N. Y. Acad. Sci.* 781:474–488. [51]

Granit, R. 1947. *Sensory Mechanisms of the Retina.* Oxford University Press. [11]

Granit, R. 1955. *Receptors and Sensory Perception.* Yale University Press. [11]

Granit, R., Kernell, D., and Shortess, G. K. 1963. Quantitative aspects of repetitive firing of mammalian motoneurons, caused by injected currents. *J. Physiol.* 168:911–931. [11, 85]

Granit, R., Kernell, D., and Lamarre, Y. 1966. Algebraical summation in synaptic activation of motoneurons firing within the 'primary range' to injected currents. *J. Physiol.* 187:379–399. [72]

Green, H. S., and Triffet, T. 1985. Extracellular fields within the cortex. *J. Theor. Biol.* 115:43–64. [52]

Grieve, K. L., and Sillito, A. M. 1991. A re-appraisal of the role of layer VI of the visual cortex in the generation of cortical end inhibition. *Exp. Brain Res.* 87:521–529. [107, 117]

Grieve, K. L., and Sillito, A. M. 1995. Non-length-tuned cells in layers II/III and IV of the visual cortex: The effect of blockade of layer VI on responses to stimuli of different lengths. *Exp. Brain Res.* 104:12–20. [107, 117]

Griffith, J. S. 1963. A field theory of neural nets: I. Derivation of field equations. *Bull. Math. Biophys.* 25:111–120. [85]

Heeger, D. J. 1992a. Normalization of cell responses in cat striate cortex. *Vis. Neurosci.* 9:181–197. [71, 116]

Heeger, D. J. 1992b. Half-squaring in responses of cat striate cells. *Vis. Neurosci..* [113]

Heeger, D. J. 1993. Modeling simple-cell direction selectivity with normalized, half-squared, linear operators. *J. Neurophysiol.* 70:1885–1898. [106]

Heeger, D. J., Simoncelli, E. P., and Movshon, J. A. 1996. Computational models of cortical visual processing. *Proc. Natl. Acad. Sci. USA* 93:623–627. [71, 116]

Hille, B. 1977. Ionic basis of resting and action potentials. In: *Handbook of Physiology. I. The Nervous System, vol. I: Cellular Biology of Neurons.* Kandel, E. R., ed., pp. 99-136. Bethesda, Maryland: American Physiological Society. [5]

Hines, M. 1989. A program for simulation of nerve equations with branching geometries. *Int. J. Biomed. Comp.* 24:55–68. [65, 133]

Hines, M. 1993a. The NEURON simulation program. In: *Neural Network Simulation Environments.* Skrzypek, J., ed. Kluwer Academic Publishers. [65, 133]

Hines, M. 1993b. NEURON—a program for simulation of nerve equations. In: *Neural Systems: Analysis and Modeling.* Eeckman, F., ed., pp. 127-136. Kluwer Academic Publishers. [133]

Hodgkin, A. L., and Huxley, A. F. 1952. A quantitative description of membrane current and its application to conduction and excitation in nerve. *J. Physiol. (Lond.)* 117:500–544. [20]

Hoffman, D. A., Magee, J. C., Colbert, C. M., and Johnston, D. 1997. K^+ channel regulation of signal propagation in dendrites of hippocampal pyramidal neurons. *Nature* 387:869–875. [28, 29, 46, 48]

Holst, M. 1993. Multilevel methods for the Poisson–Boltzmann equation. Ph. D. thesis, University of Illinois at Urbana-Champaign. [136]

Holst, M., and Saied, F. 1993. Multigrid solution of

the Poisson–Boltzmann equation. *J. Comput. Chem.* 14:103–113. [136]

Holt, G. R., Douglas, R. J., and Koch, C. 1996. A cortical amplifier model of direction selectivity. *Soc. Neurosci. Abstr.* 22:632.4. [14, 15]

Holt, G. R., and Koch, C. 1997. Shunting inhibition does not have a divisive effect on firing rates. *Neural Comp.* 9:1001–1013. [63, 87, 106]

Hopfield, J. J. 1984. Neurons with graded response have collective computational properties like those of two-state neurons. *Proc. Natl. Acad. Sci. USA* 81:3088–3092. [2, 4, 13, 63, 74, 75, 76]

Hoppe, D., Chvatal, A., Kettenmann, H., Orkand, R. K., and Ransom, B. R. 1991. Characteristics of activity–dependent potassium accumulation in mammalian peripheral nerve *in vitro*. *Brain Res.* 552:106–112. [50]

Hubbard, J. I., Llinás, R., and Quastel, D. M. J. 1969. *Electrophysiological Analysis of Synaptic Transmission.* Baltimore: Williams & Wilkins. [18, 25]

Jack, J. J. B., Noble, D., and Tsien, R. W. 1983. *Electric Current Flow in Excitable Cells.* Oxford University Press. [20]

Jaeger, J. C. 1942. Heat flow in the region bounded internally by a circular cylinder. *Proc. Roy. Soc. Edinburgh A* 61:223–228. [55]

Jefferys, J. G. R. 1995. Nonsynaptic modulation of neuronal activity in the brain: Electric current and extracellular ions. *Physiol. Rev.* 75:689–723. [17, 18, 44, 50]

Johnston, D., Magee, J., Colbert, C., and Christie, B. 1996. Active properties of neuronal dendrites. *Ann. Rev. Neurosci.* 19:165–186. [84]

Karwoski, C. J., and Proenza, L. M. 1987. Sources and sinks of light-evoked $\Delta[K^+]_o$ in the vertebrate retina. *Can. J. Physiol. Pharmacol.* 65:1009–1017. [50, 61]

Katz, B. 1950. Depolarization of sensory terminals and the initiation of impulses in the muscle spindle. *J. Physiol.* 111:261–282. [10, 11]

Katz, B., and Schmitt, O. H. 1940. Electrical interaction between two adjacent nerve fibres. *J. Physiol.* 97:471–488. [17, 35, 44]

Katz, B., and Schmitt, O. H. 1942. A note on interaction between nerve fibers. *J. Physiol.* 100:369–371. [17, 35, 37, 44]

Keener, J. P. 1989. Frequency dependent decoupling of parallel excitable fibers. *SIAM J. Appl. Math.* 49:210–230. [38]

Kernell, D. 1969. Synaptic conductance changes and the repetitive impulse discharge of spinal motoneurons. *Brain Res.* 15:291–294. [72]

Kisvárday, Z. F., Tóth, É., Rausch, M., and Eysel, U. T. 1997. Orientation-specific relationship between populations of excitatory and inhibitory lateral connections in the visual cortex of the cat. *Cereb. Cort.* 7:605–618. [15]

Klee, M., and Rall, W. 1977. Computed potentials of cortically arranged populations of neurons. *J. Neurophysiol.* 40:647–666. [18, 26]

Kleinfeld, D. 1986. Sequential state generation by model neural networks. *Proc. Natl. Acad. Sci. USA* 83:9469–9473. [75]

Knight, B. W. 1972. Dynamics of encoding in a population of neurons. *J. Gen. Physiol.* 59:734–766. [79, 81, 83]

Koch, C., Poggio, T., and Torre, V. 1982. Retinal ganglion cells: A functional interpretation of dendritic morphology. *Proc. R. Soc. Lond. B* 298:227–264. [71]

Koch, C., Poggio, T., and Torre, V. 1983. Nonlinear interaction in a dendritic tree: Localization timing and role in information processing. *Proc. Natl. Acad. Sci. USA* 80:2799–2802. [13, 71]

Koch, C., Bernander, Ö., and Douglas, R. J. 1995.

Do neurons have a voltage or a current threshold for action potential initiation? *J. Comp. Neurosci.* 2:63–82. [64, 65, 67, 69, 83, 127, 129, 130, 131, 132]

Koch, C., Rapp, M., and Segev, I. 1996. A brief history of time (constants). *Cereb. Cortex* 6:93–101. [84]

Kocsis, J. D., Ruiz, J. A., and Cummins, K. L. 1982. Modulation of axonal excitability mediated by surround electrical activity: An intra-axonal study. *Exp. Brain Res.* 47:151–153. [35, 44]

Kocsis, J. D., Malenka, R. C., and Waxman, S. G. 1983. Effect of extracellular potassium concentration on the excitability of the parallel fibres of the rat cerebellum. *J. Physiol.* 334:225–244. [60]

Korn, H., and Axelrad, H. 1980. Electrical inhibition of Purkinje cells in the cerebellum of the rat. *Proc. Natl. Acad. Sci. USA* 77:6244–6247. [44]

Korn, H., and Faber, D. S. 1980. Electrical field effect interactions in the vertebrate brain. *Trends Neurosci.* 3:6–9. [44]

Lapicque, L. 1907. Recherches quantitatifs sur l'excitation electrique des nerfs traitée comme une polarisation. *J. Physiol (Paris)* 9:620–635. [4, 76]

Lebovitz, R. M. 1996. Quantitative examination of dynamic interneuronal coupling via single-spike extracellular potassium ion transients. *J. Theor. Biol.* 180:11–25. [57, 60]

Lorente de Nó, R. 1947a. Analysis of the distribution of action currents of nerve in volume conductors. *Studies from the Rockefeller Institute for Medical Research* 132:384–477. [19]

Lorente de Nó, R. 1947b. Action potential of the motoneurons of the hypoglossus nucleus. *J. Cell. Comp. Physiol.* 29:207–287. [10, 26, 27, 28, 34]

Lorente de Nó, R. 1953. Conduction of impulses in the neurons of the oculomotor nucleus. In: *The Spinal Cord.* Malcolm, J. L., Gray, J. A. B., eds., pp. 132-173. CIBA Foundation Symposium. [27]

Low, F. N. 1976. The perineurium and connective tissue of peripheral nerve. In: *The Peripheral Nerve.* Landon, D. N., ed., pp. 159-187. London: Chapman and Hall, Ltd. [22, 25]

Lux, H. D. 1976. Change of potassium activity associated with membrane current flow. *Fed. Proc.* 35:1248–1253. [51]

MacNeal, D. R. 1976. Analysis of a model for excitation of myelinated nerve. *IEEE Trans. Biomed. Eng.* BME-33:329–337. [38]

MacVicar, B. A., and Dudek, F. E. 1981. Electrotonic coupling between pyramidal cells: A direct demonstration in rat hippocampal slices. *Science* 213:782–785. [45, 46]

Maeda, K., Yagi, T., and Noguchi, A. 1980. Induced excitation and synchronization of nerve impulses in two parallel unmyelinated fibers. *IEEE Trans. Biomed. Eng.* BME-27:139–145. [37, 38]

Maex, R., and Orban, G. A. 1992. A model circuit for cortical temporal low-pass filtering. *Neural Comp.* 4:932–945. [14, 15, 90]

Maex, R., and Orban, G. A. 1996. Model circuit of spiking neurons generating directional selectivity in simple cells. *J. Neurophysiol.* 75:1515–1545. [14, 15, 107]

Magherini, P. C., Precht, W., and Schwindt, P. C. 1976. Evidence for electrotonic coupling between frog motoneurons in the in situ spinal cord. *J. Neurophysiol.* 39:474–483. [44, 46]

Mainen, Z. F., Joerges, J., Huguenard, J. R., and Sejnowski, T. J. 1995. A model of spike initia-

tion in neocortical pyramidal neurons. *Neuron* 15:1427–1439. [28]

Mainen, Z. F., and Sejnowski, T. J. 1996. Influence of dendritic structure on firing pattern in model neocortical neurons. *Nature* 382:363–366. [28, 29, 34, 138]

Malcolm, J. L., and Gray, J. A. B. 1953. *The Spinal Cord.* Boston: Little, Brown, and Company. [28]

Malmivuo, J., and Plonsey, R. 1995. *Bioelectromagnetism: Principles and Applications of Bioelectric and Biomagnetic Fields.* Oxford University Press. [18]

Markin, V. S. 1970a. Electrical interaction of parallel non-myelinated nerve fibers. I. Change in excitability of the adjacent fiber. *Biofizika* 15:120–128. [38]

Markin, V. S. 1970b. Electrical interaction of parallel non-myelinated nerve fibers. II. Collective conduction of impulses. *Biofizika* 15:681–689. [38]

Markin, V. S. 1973a. Electrical interaction of parallel non-myelinated nerve fibers. III. Interaction in bundles. *Biofizika* 18:314–321. [38]

Markin, V. S. 1973b. Electrical interaction of parallel non-myelinated nerve fibers. IV. Role of anatomical inhomogeneities of nerve trunks. *Biofizika* 18:512–518. [38, 40]

Markram, H., and Tsodyks, M. 1996. Redistribution of synaptic efficacy between neocortical pyramidal neurons. *Nature* 382:807–810. [16, 86, 106]

Marks, W. B., and Loeb, G. E. 1976. Action currents, internodal potentials, and extracellular records of myelinated mammalian nerve fibers derived from node potentials. *Biophys. J.* 16:655–668. [25]

Matthews, M. A., Willis, W. D., and Williams, V. 1971. Dendrite bundles in lamina IX of cat spinal cord: A possible source for electrical interaction between motoneurons? *Anat. Rec.* 171:313–328. [46]

McCaig, C. D. 1988. Nerve guidance: A role for bio-electric fields? *Prog. Neurobiol.* 30:449–468. [46]

McCaig, C. D., and Zhao, M. 1997. Physiological electrical fields modify cell behaviour. *Bioessays* 19:819–826. [47]

McCulloch, W. S., and Pitts, W. 1943. A logical calculus of the ideas immanent in nervous activity. *Bull. Math. Biophys.* 5:115–133. [2]

Mel, B. W. 1994. Information processing in dendritic trees. *Neural Comp.* 6:1031–1085. [86, 106]

Miller, K. D., Chapman, B., and Stryker, M. P. 1989. Visual responses in adult cat visual cortex depend on *N*-Methyl-D-Aspartate receptors. *Proc. Natl. Acad. Sci. USA* 83:5183–5187. [90]

Mitzdorf, U. 1985. Current source-density method and application in cat cerebral cortex: Investigation of evoked potentials and EEG phenomena. *Physiol. Rev.* 65:37–100. [18, 28]

Nelson, M. E. 1994. A mechanism for neuronal gain control by descending pathways. *Neural Comp.* 6:242–254. [13, 63, 71]

Nelson, P. G. 1966. Interaction between spinal motoneurons of the cat. *J. Neurophysiol.* 29:275–287. [44]

Nelson, P. G., and Frank, K. 1964. Extracellular potential fields of single spinal motoneurons. *J. Neurophysiol.* 27:913–927. [28, 32]

Nelson, S., Toth, L., Sheth, B., and Sur, M. 1994. Orientation selectivity of cortical neurons during intracellular blockade of inhibition. *Science* 265:774–777. [14]

Nicholson, C. 1980. Dynamics of the brain cell microenvironment. *Neurosci. Res. Prog. Bull.* 18:177–322. [54]

Nicholson, C. 1995. Extracellular space as the pathway for neuron-glial cell interaction. In: *Neuroglia.* Kettenmann, H., Ransom, B. R., eds., pp. 387-397. Oxford University Press. [3, 54, 122, 124]

Nicholson, C., and Llinás, R. 1971. Field potentials in the alligator cerebellum and theory of their relationship to purkinje cell dendritic spikes. *J. Neurophysiol.* 34:509–531. [28]

Nicholson, C., and Phillips, J. M. 1981. Ion diffusion modified by tortuosity and volume fraction in the extracellular microenvironment of the rat cerebellum. *J. Physiol.* 321:225–257. [54, 55]

Nicholson, C., and Rice, M. E. 1986. The migration of substances in the neuronal microenvironment. *Ann. NY Acad. Sci.* 481:55–71. [54]

Nicholson, C., and Rice, M. E. 1991. Diffusion of ions and transmitters in the brain cell microenvironment. In: *Volume Transmission in the Brain: Novel Mechanisms for Neural Transmission.* Fuxe, K., Agnati, L. F., eds., pp. 279-336. New York: Raven Press, Ltd. [50, 54]

Nicoll, A., Larkman, A., and Blakemore, C. 1993. Modulation of EPSP shape and efficacy by intrinsic membrane conductances in rat neocortical pyramidal neurons in vitro. *J. Physiol.* 468:693–710. [84]

Özişik, M. N. 1993. *Heat Conduction.* New York: Wiley. [55]

Panzeri, S., Biella, G., Rolls, E. T., Skaggs, W. E., and Treves, A. 1996. Speed, noise, information and the graded nature of neuronal responses. *Network: Comp. Neural. Sys.* 7:365–370. [81]

Patel, N. B., and Poo, M. M. 1984. Perturbation of the direction of neurite growth by pulsed and focal electric fields. *J. Neurosci.* 4:2939–2947. [47]

Payne, J. R., and Nelson, M. E. 1996. Neuronal gain control by regulation of membrane conductance in two classes of spiking neuron models. In: *Fifth Annual Computational Neuroscience Meeting Abstracts.* Bower, J. M., ed., p. 147. [64]

Pei, X., Vidyasagar, T. R., Vogulshev, M., and Creutzfeldt, O. D. 1994. Receptive field analysis and orientation selectivity of postsynaptic potentials of simple cells in cat visual cortex. *J. Neurosci.* 14:7130–7140. [14]

Peinado, A., Yuste, R., and Katz, L. C. 1993. Gap junctional communication and the development of local circuits in neocortex. *Cerebral Cortex* 3:488–498. [46]

Peters, A., Palay, S. L., and deF. Webster, H. 1991. *The Fine Structure of the Nervous System: The Neurons and Supporting Cells.* Philadelphia: W. B. Saunders Company. [22, 25, 29, 49]

Peters, A., Payne, B. R., and Budd, J. 1994. A numerical analysis of the geniculocortical input to strate cortex in the monkey. *Cereb. Cortex* 4:215–229. [15, 106]

Peters, A., and Payne, B. R. 1993. Numerical relationships between geniculocortical afferents and pyramidal cell modules in cat primary visual cortex. *Cereb. Cortex* 3:69–78. [15, 106]

Pfrieger, F. W., and Barres, B. A. 1996. New views on synapse–glia interactions. *Curr. Opin. Neurobiol.* 6:615–621. [49]

Plonsey, R. 1969. *Bioelectric Phenomena.* New York: McGraw-Hill. [7]

Plonsey, R. 1977. Action potential sources and their volume conductor fields. *Proc. IEEE* 65:601–611. [19, 22]

Plonsey, R. 1988. Bioelectric sources arising in excitable fibers (Alza lecture). *Ann. Biomed. Eng.* 16:519–546. [18]

Plonsey, R., and Barr, R. C. 1995. Electric field

stimulation of excitable tissue. *IEEE Trans. Biomed. Eng.* 42:329–336. [35]

Qian, N., and Sejnowski, T. J. 1989. An electrodiffusion model for computing membrane potentials and ionic concentrations in branching dendrites, spines and axons. *Biol. Cybern.* 62:1–15. [6, 50, 54]

Qian, N., and Sejnowski, T. J. 1990. When is an inhibitory synapse effective? *Proc. Natl. Acad. Sci. USA* 87:8145–8149. [6, 50]

Rall, W. 1962. Electrophysiology of a dendritic neuron model. *Biophys. J.* 2:145–167. [26, 27, 35, 75]

Rall, W. 1967. Distinguishing theoretical synaptic potentials computed for different soma-dendritic distributions of synapic input. *J. Neurophysiol.* 30:1138–1168. [84]

Rall, W. 1969. Distributions of potential in cylindrical coordinates and time constants for a membrane cylinder. *Biophys. J.* 9:1509–1541. [7, 75]

Rall, W. 1977. Core conductor theory and cable properties of neurons. In: *The Nervous System, Vol. I: Cellular Biology of Neurons, Part 1.* Kandel, E. R., ed., pp. 39-97. Bethesda: American Physiological Society. [4, 10, 83]

Rall, W. 1989. Cable theory for dendritic neurons. In: *Methods in Neuronal Modeling.* Koch, C., Segev, I., eds., pp. 9-61. MIT press. [84]

Rall, W., and Shepherd, G. M. 1968. Theoretical reconstruction of field potentials and dendrodendritic synaptic interactions in olfactory bulb. *J. Neurophysiol.* 31:884–915. [18]

Ramón, F., and Moore, J. W. 1978. Ephaptic transmission in squid giant axons. *Am. J. Physiol.* 234:C162–C169. [34, 44]

Ranck, J. B. 1963. Specific impedance of rabbit cerebral cortex. *Exp. Neurol.* 7:144–152. [7, 29]

Ranck, J. B. 1975. Which elements are excited in electrical stimulation of mammalian central nervous system: A review. *Brain Res.* 98:417–440. [38]

Rapp, M., Yarom, Y., and Segev, I. 1992. The impact of parallel fiber background activity on the cable properties of cerebellar Purkinje cells. *Neural Comp.* 4:518–533. [13, 72, 74, 85]

Rattay, F. 1987. Ways to approximate current–distance relations for electrically stimulated fibers. *J. Theor. Biol.* 125:339–349. [38]

Regehr, W. G., and Armstrong, C. M. 1994. Where does it all begin? *Current Biol.* 4:436–439. [45]

Reid, R. C., Soodak, R. E., and Shapley, R. M. 1987. Linear mechanisms of directional selectivity in simple cells of cat striate cortex. *Proc. Natl. Acad. Sci. USA* 84:8740–8744. [106]

Reid, R. C., and Alonso, J. M. 1995. Specificity of monosynaptic connections from thalamus to visual cortex. *Nature* 378:281–284. [14]

Roney, K. J., Scheibel, A. B., and Shaw, G. L. 1979. Dendritic bundles: Survey of anatomical experiments and physiological theories. *Brain Res. Rev.* 1:225–271. [46]

Rose, D. 1977. On the arithmetical operation performed by inhibitory synapses onto the neuronal soma. *Exp. Brain Res.* 28:221–223. [72, 106]

Rosenfalck, P. 1969. Intra- and extracellular potential fields of active nerve and muscle fibers. *Acta Physiol. Scand. Suppl.* 321:1–168. [5, 7, 18, 19, 22, 23, 140]

Rosenthal, F. 1972. Extracellular fields of single PT-neurons. *Brain Res.* 36:251–263. [25, 28, 32]

Rubinstein, J. T. 1991. Analytical theory for extracellular electrical stimulation of nerve with focal electrodes. II. Passive myelinated axon. *Biophys. J.* 60:538–555. [38]

Rubinstein, J. T., and Spelman, F. A. 1988. Analytical theory for extracellular electrical stimu-

lation of nerve with focal electrodes. *Biophys. J.* 54:975–981. [36]

Salinas, E., and Abbott, L. F. 1996. A model of multiplicative neural responses in parietal cortex. *Proc. Natl. Acad. Sci. USA* 93:11956–11961. [106]

Schmitt, F. O., Dev, P., and Smith, B. H. 1976. Electrotonic processing of information by brain cells. *Science* 193:114–120. [46]

Scott, A. C. 1977. *Neurophysics.* New York: John Wiley and Sons. [38]

Scott, A. C., and Luzader, S. D. 1979. Coupled solitary waves in neurophysics. *Physica Scripta* 20:395–401. [38]

Sejnowski, T. J. 1977. Storing covariance with nonlinearly interacting neurons. *J. Math. Biol.* 4:303–321. [13]

Shadlen, M. N., and Newsome, W. T. 1994. Noise, neural codes and cortical organization. *Curr. Opin. Neurobiol.* 4:569–579. [14]

Shell, M. J., Molliver, M. E., and Snyder, S. H. 1995. D-serine, an endogenous synaptic modulator: Localization to astrocytes and glutamate-stimulated release. *Proc. Natl. Acad. Sci. USA* 92:3948–3952. [49]

Sillito, A. M. 1975. The contribution of inhibitory mechanisms to the receptive field properties of neurones in the striate cortex of the cortex of the cat. *J. Physiol.* 250:305–329. [14]

Sillito, A. M. 1977. Inhibitory processes underlying the directional specificity of simple, complex and hypercomplex cells in the cat's visual cortex. *J. Physiol.* 271:699–720. [14]

Singer, W., and Lux, H. D. 1975. Extracellular potassium gradients and visual receptive fields in the cat striate cortex. *Brain Res.* 96:378–383. [51, 61]

Snow, R. W., and Dudek, F. E. 1984. Electrical fields directly contribute to action potential synchronization during convulsant-induced epileptiform bursts. *Brain Res.* 323:114–118. [45, 47]

Softky, W. R. 1995. Simple codes versus efficient codes. *Current Opin. Neurobiol.* 5:239–247. [2, 14]

Somers, D. C., Nelson, S. B., and Sur, M. 1995. An emergent model of orientation selectivity in cat visual cortical simple cells. *J. Neurosci.* 15:5448–5465. [14, 15, 107]

Somers, D. C., Todorov, E. V., Siapas, A. G., and Nelson, S. B. 1996. Contrast adaptation effects modeled as thalamocortical and intracortical synaptic transmission changes. *Soc. Neurosci. Abstr.*. [106]

Somjen, G. G. 1979. Extracellular potassium in the mammalian central nervous system. *Ann. Rev. Physiol.* 41:159–177. [50, 61]

Sperti, L., Gessi, T., and Volta, F. 1967. Extracellular potential field of antidromically activated CA1 neurons. *Brain Res.* 3:343–361. [28, 32]

Spira, M. E., Yarom, Y., and Zeldes, D. 1984. Neuronal interactions mediated by neurally evoked changes in the extracellular potassium concentration. *J. Exp. Biol.* 112:179–?? [51]

Spruston, N., Schiller, Y., Stuart, G., and Sakmann, B. 1995. Activity–dependent action potential invasion and calcium influx into hippocampal CA1 dendrites. *Science* 268:297–300. [28, 48]

Stein, R. B. 1967. The frequency of nerve action potentials generated by applied currents. *Proc. R. Soc. Lond. B* 167:64–86. [67]

Stein, R. B., and Oğuztöreli, M. N. 1978. The radial decline of nerve impulses in a restricted cylindrical extracellular space. *Biol. Cybern.* 28:159–165. [23]

Stein, R. B., and Pearson, K. G. 1971. Predicted amplitude and form of action potentials recorded

from unmyelinated nerve fibres. *J. Theor. Biol.* 32:539–558. [22, 23]

Stephanova, D., Traynova, N., Gydikov, A., and Kossev, A. 1989. Extracellular potentials of a single myelinated nerve fiber in an unbounded volume conductor. *Biol. Cyern.* 61:205–210. [25]

Stevens, C. F. 1966. *Neurophysiology: A Primer.* New York: John Wiley & Sons. [11]

Stone, J., Makarov, F., and Holländer, H. 1995. The glial ensheathment of the soma and axon hillock of retinal ganglion cells. *Vis. Neurosci.* 12:273–279. [29]

Strassberg, A. F., and DeFelice, L. J. 1993. Limitations of the Hodgkin–Huxley formalism—effects of single-channel kinetics on transmembrane voltage dynamics. *Neural Comp.* 5:843–855. [5]

Stratford, K. J., Tarczy-Hornoch, K., Martin, K. A. C., Bannister, N. J., and Jack, J. J. B. 1996. Excitatory synaptic inptus to spiny stellate cells in cat visual cortex. *Nature* 382:258–261. [16, 106, 107, 108, 112, 116]

Struijk, J. J. 1997. The extracellular potential of a myelinated nerve fiber in an unbounded medium and in nerve cuff models. *Biophys. J.* 72:2457–2469. [25]

Stuart, G., and Sakmann, B. 1994. Active propagation of somatic action potentials into neocortical pyramidal cell dendrites. *Nature* 367:69–72. [29, 45, 84, 138]

Suarez, H. H. 1994. Direction selectivity and the canonical microcircuit. Ph. D. thesis, California Institute of Technology. [92, 104]

Suarez, H., Koch, C., and Douglas, R. J. 1995. Modeling direction selectivity of simple cells in striate visual cortex using the canonical microcircuit. *J. Neurosci.* 15:6700–6719. [14, 15, 84, 107]

Swadlow, H. A. 1983. Efferent systems of primary visual cortex: A review of structure and function. *Brain Res. Rev.* 6:1–24. [85]

Swadlow, H. A., Kocsis, J. D., and Waxman, S. G. 1980. Modulation of impulse conduction along the axonal tree. *Ann. Rev. Biophys. Bioeng.* 9:143–179. [46]

Swadlow, H. A., and Weyand, T. G. 1981. Efferent systems of the rabbit visual cortex: Laminar distribution of the cells of origin, axonal conduction velcities, and identification of axonal branches. *J. Comp. Neurol.* 203:799–822. [85]

Syková, E. 1983. Extracellular K^+ accumulation in the central nervous system. *Prog. Biophys. Molec. Biol.* 42:135–189. [50, 61]

Syková, E. 1987. Modulation of spinal cord transmission by changes in extracellular K^+ activity and extracellular volume. *Can. J. Physiol. Pharmacol.* 65:1045–1066. [61]

Syková, E. 1991. Activity-related ionic and volume changes in neuronal microenvironment. In: *Volume Transmission in the Brain: Novel Mechanisms for Neural Transmission.* Fuxe, K., Agnati, L. F., eds., pp. 317-336. New York: Raven Press. [49, 50, 51]

Syková, E. 1997. The extracellular space in the CNS: Its regulation, volume and geomtry in normal and pathological neuronal function. *The Neuroscientist* 3:28–41. [3, 50, 54]

Tabata, T. 1990. Ephaptic transmission and conduction velocity of an action potential in *Chara* internodal cells placed in parallel and in contact with one another. *Plant Cell Physiol.* 31:575–579. [17, 35, 37, 44]

Tal, D., and Schwartz, E. L. 1997. Computing with the leaky integrate-and-fire neuron: Logarithmic computation and multiplication. *Neural Comp.* 9:305–318. [112]

Terzuolo, C. A., and Araki, T. 1961. An analysis of intra- versus extracellular potential changes associated with activity of single spinal motoneurons. *Ann. NY Acad. Sci.* 94:547–558. [25, 28, 32]

Thomson, A. M., Deuchars, J., and West, D. C. 1993a. Single axon excitatory postsynaptic potentials in neocortical interneurons exhibit pronounced paired pulse facilitation. *Neurosci.* 54:346–360. [106]

Thomson, A. M., Deuchars, J., and West, D. C. 1993b. Large, deep layer pyramid-pyramid single axon EPSPs in slices of rat motor cortex display paired pulse and frequency-dependent depression, mediated presynaptically and self-facilitation, mediated postsynaptically. *J. Neurophysiol.* 70:2354–2396. [16, 106]

Thomson, A. M., West, D. C., and Deuchars, J. 1995. Properties of single axon excitatory postsynaptic potentials elicted in spiny interneurons by action potentials in pyramidal neurons in slices of rat neocortex. *Neurosci.* 69:727–738. [106]

Thomson, A. M., and Deuchars, J. 1994. Temporal and spatial properties of local circuits in neocortex. *Trends Neurosci.* 17:119–126. [16, 106]

Thomson, A. M., and West, D. C. 1993. Fluctuations in pyramid–pyramid excitatory postsynaptic potentials modified by presynaptic firing pattern and postsynaptic membrane potential using paired intracellular recordings in rat neocortex. *Neurosci.* 54:329–346. [16, 106]

Torre, V., and Poggio, T. 1978. A synaptic mechanism possibly underlying directional selectivity to motion. *Proc. R. Soc. Lond. B* 202:409–416. [71]

Towe, A. L. 1973. Sampling single neuron activity. In: *Bioelectric Recording Techniques. Part A. Cellular Processes and Brain Potentials.* Thompson, R. F., Patterson, M. M., eds., pp. 79-93. Academic Press. [25]

Tranchina, D., and Nicholson, C. 1986. A model for the polarization of neurons by extrinsically applied electric fields. *Biophys. J.* 50:1139–1156. [38, 40, 44]

Traub, R. D., Dudek, F. E., Snow, R. W., and Knowles, W. D. 1985a. Computer simulations indicate that electrical field effects contribute to the shape of the epileptiform field potential. *Neurosci.* 15:947–958. [35, 45]

Traub, R. D., Dudek, F. E., Taylor, C. P., and Knowles, W. D. 1985b. Simulation of hippocampal afterdischarges synchronized by electrical interaction. *Neurosci.* 14:1033–1038. [35, 45]

Trayanova, N., Henriquez, C. S., and Plonsey, R. 1990. Extracellular potentials and currents of a single active fiber in a restricted volume conductor. *Ann. Biomed. Eng.* 18:219–238. [23]

Trayanova, N., and Henriquez, C. S. 1991. Examination of the choice of models for computing the extracellular potential of a single fibre in a restricted volume conductor. *Med. & Biol. Eng. & Comput.* 29:580–584. [23, 140]

Treves, A. 1992. Local neocortical processing: A time for recognition. *Int. J. Neural Sys.* 3 (suppl):115–119. [85]

Treves, A. 1993. Mean field analysis of neuronal spike dynamics. *Network Comp. Neural Sys.* 4:259–284. [85]

Troyer, T. W., and Miller, K. D. 1996. Physiological gain leads to high ISI variability in a simple model of a cortical regular spiking cell. *Neural Comp.* in press. [72]

Tsodyks, M. V., and Markram, H. 1997. The neural code between neocortical pyramidal neurons depends on neurotransmitter release probabil-

ity. *Proc. Natl. Acad. Sci. USA* 94:719–723. [16, 106]

Tsodyks, M. V., and Sejnowski, T. 1995. Rapid state switching in balanced cortical network models. *Network Comm. Neural Sys.* 6:111–124. [72, 85, 105]

Tsumoto, T., Creutzfeldt, O. D., and Legeéndy, C. R. 1978. Functional organization of the corticofugal system from visual cortex to lateral geniculate nucleus in the cat (with an appendix on geniculo-cortical mono-synaptic connections). *Exp. Brain Res.* 32:345–364. [85]

Tsumoto, T., and Suda, K. 1980. Three groups of cortico-geniculate neurons and their distribution in binocular and monocular segments of cat striate cortex. *J. Comp. Neurol.* 193:223–236. [85]

Turner, D. A. 1988. Waveform and amplitude characteristics of evoked responses to dendritic stimulation of CA1 guinea-pig pyramidal cells. *J. Physiol.* 395:419–439. [84]

Turner, R. W., and Richardson, T. L. 1991. Apical dendritic depolarizations and field interactions evoked by stimulation of afferent inputs to rat hippocampal CA1 pyramidal cells. *Neurosci.* 42:125–135. [44, 45]

Usher, M., Stemmler, M., Zeev, O., and Koch, C. 1994. Network amplification of local fluctuations causes high spike rate variability, fractal firing patterns and oscillatory local field potentials. *Neural Comp.* 6:795–836. [105]

Van Harreveld, A. 1966. *Brain Tissue Electrolytes.* Washington, DC: Butterworth. [3]

Van Harreveld, A. 1972. The extracellular space in the vertebrate central nervous system. In: *The STructure and Function of Nervous Tissue.* Bourne, G. H., ed., pp. 447-511. Academic Press. [3]

van Vreeswijk, C., and Sompolinsky, H. 1996. Chaos in neuronal networks with balanced excitatory and inhibitory activity. *Science* 274:1724–1726. [105]

Vern, B. A., Schuette, W. H., and Thibault, L. E. 1977. $[K^+]$ clearance in cortex: A new analytical model. *J. Neurophysiol.* 40:1015–1023. [52, 54, 55]

Vidyasagar, T. R., Pei, X., and Vogulshev, M. 1996. Multiple mechanisms underlying the orientation selectivity of visual cortical neurones. *Trends Neurosci.* 19:272–277. [14]

Wilson, H. R., and Cowan, J. D. 1972. Excitatory and inhibitory interactions in localized populations of model neurons. *Biophys. J.* 12:1–24. [85, 86]

Wilson, H. R., and Cowan, J. D. 1973. A mathematical theory of the functional dynamics of cortical and thalamic nervous tissue. *Kybernetik* 13:55–80. [86]

Wilson, M. A., and Bower, J. M. 1989. The simulation of large-scale neural networks. In: *Methods in Neuronal Modeling: From Synapses to Networks.* Koch, C., Segev, I., eds., pp. 291-333. MIT Press. [18, 75]

Wilson, M., and Bower, J. M. 1992. Cortical oscillations and temporal interactions in a computer simulation of piriform cortex. *J. Neurophysiol.* 67:981–995. [85, 136]

Wörgötter, F., and Holt, G. 1991. Spatiotemporal mechanisms in receptive fields of visual cortical cells—a model. *J. Neurophysiol.* 65:494–510. [75]

Yarom, Y., and Spira, M. E. 1982. Extracellular potassium ions mediate specific neuronal interaction. *Science* 216:80–82. [51]

Zador, A. M., Agmon-Snir, H., and Segev, I. 1995. The morphoelectrotonic transform: A graphi-

cal approach to dendritic function. *J. Neurosci.* 15:1669–1682. [83]

Zonneveld, J. A., and Berghuis, J. 1955. *The Asymptotic Expansion of a Special Function and some Relations with Bessel Functions.* Amsterdam: Mathematisch Centrum. [55]

Zucker, R. S. 1989. Short-term synaptic plasticity. *Ann. Rev. Neurosci.* 12:13–31. [16]

Zupanc, G. K. H. 1991. Clustering of cell bodies, bundling of dendrites, and gap junctions: Morphological substrate for electrical coupling in the prepacemaker nucleus. *Neurosci. Lett.* 129:29–34. [46]